Design and Control of Fully Flexible Valve Actuation Systems for Camless Engines

A DISSERTATION
SUBMITTED TO THE FACULTY OF THE GRADUATE SCHOOL
OF THE UNIVERSITY OF MINNESOTA
BY

Pradeep Kumar Gillella

IN PARTIAL FULFILLMENT OF THE REQUIREMENTS
FOR THE DEGREE OF
Doctor of Philosophy

Prof Zongxuan Sun, Advisor

December, 2012

Acknowledgements

I would like to express my sincere gratitude to Prof Zongxuan Sun for introducing me to this exciting field, providing all the resources and guiding me over the past 5 years. His commitment to helping me develop the technical and interpersonal skills has been my greatest asset during my entire educational experience up to this point.

Prof Rajesh Rajamani, Prof Perry Li, Prof Mihailo Jovanovich, Prof Kim Stelson and Prof James Van de Ven for the valuable experiences gained as part of the coursework and being their teaching assistant which has directly helped me with various research problems. Special thanks to Prof Stelson, Prof Rajamani and Prof Mihailo for agreeing to serve as my examining committee.

Fellow lab mates Xingyong, Adam, Yu, Chien-shin, Ke, Zhen, Ali, Vivek, Azrin, Virinchi, Yongsoon, Venkat, Haink, Rachel and Henry for all the discussions, help and fun times.

Peter Zimmerman, Robin Russell, Mark Erickson and Dave Hultmann for their help at the machine shop.

I would like to acknowledge MSI and MENET for the computational resources.

Dedication

To my family, members of zoogang, bunboys, shadowz, dopy2k, k5boys, pongalboys and howitzers.

Abstract

The motivation to improve the fuel efficiency and reduce emissions of the internal combustion engine comes from the dwindling oil reserves and the increased concerns about climate change. A key step towards realizing these improvements is to introduce flexibilities into the mechanisms used for air and fuel management by replacing the mechanical devices with mechatronic systems. The introduction of fuel injection systems in place of the carburetors resulted in significant improvements due to the additional flexibilities in fuel management. The traditional air management systems use camshaft based mechanisms to actuate the intake/exhaust valves. The benefits offered by fully flexible valve actuation and the limitations of the camshaft based systems motivate the development of a *"Camless valve actuation system"*. Research in this area during the past two decades has led to the development of several concepts. However, the stringent performance requirements to ensure reliable operation and the shortcomings of the previously developed concepts has impeded the widespread deployment of these systems. In this research, we propose to address the problem from two perspectives. A design based solution capable of achieving fully flexible operation using inexpensive components while requiring simplified controllers is first introduced. It is followed by the development of a systematic procedure for optimizing the design of a key component in this system to improve it performance and robustness. The second topic focuses on the implementation aspects of a new control algorithm to enable precise tracking of the engine valve reference profile. The effectiveness of the linear time invariant controllers based on the internal model principle for steady state operation of the engine is leveraged to enable tracking control during engine speed transients by extending the control framework to the time-varying setting. The challenges associated with the time-varying nature of the controller are revealed and the developed solutions help its implementation and validation on experimental hardware. The proposed framework can easily be extended to other engine subsystems as well as other general rotational machinery.

Contents

List of Tables

List of Figures

Chapter 1

Introduction

This research focuses on the design and control aspects of camless fully flexible valve actuation systems for internal combustion engines. A review of the benefits of variable valve actuation and the current state of the art i.e., camshaft based variable valve actuation motivates the concept of camless valve actuation. The stringent performance requirements and the performance characteristics of the existing camless actuation systems prevent the wide spread deployment of such systems. By systematically identifying the various challenges associated with camless engine valve actuation, this chapter lays the foundation for the research topics presented in this thesis.

1.1 Motivation

The internal combustion engine continues to be the preferred power source for automotive applications. This can be attributed to the desirable properties of fossil fuels such as high power density, high energy density and the ease of refueling. From the time of its invention, the internal combustion engine has been continuously refined during the last century. However, until recently, there was very little change in the fundamental subsystems used for the delivery of air and fuel to the combustion chamber.

Recent issues like depleting oil reserves, increasing fuel prices, stricter emission standards and the increased use of alternative fuels have all motivated the development of advanced power-train subsystems. The use of fuel injectors in place of the carburetor introduced flexibility in the control of fuel delivery. This helped optimize the engine operation for different load and speed conditions and hence led to significant improvements in the efficiency and the reduction in the emissions of the engine.

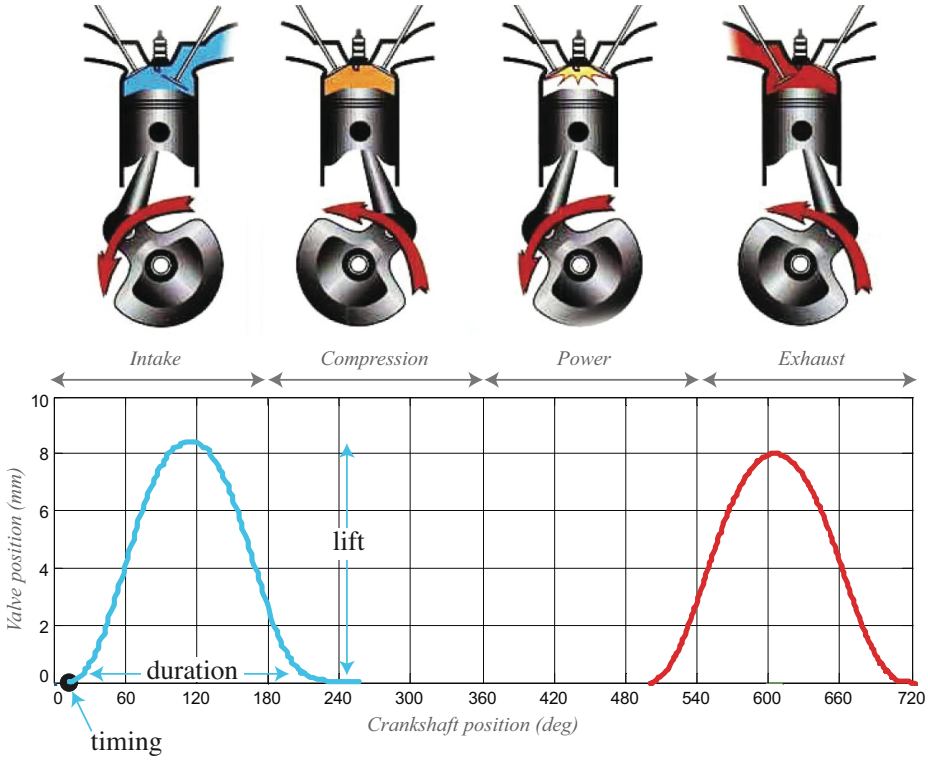

Figure 1.1: A typical trajectory of the intake and exhaust valves over one cycle of a four stroke engine

The traditional mechanisms for actuating the engine valves are based on the use of a camshaft which is mechanically linked to the crankshaft. Fig. 1.1 shows a typical 4-stroke combustion cycle and the corresponding displacement profiles for the intake and exhaust valves during the 720° i.e., 2 revolutions of the crankshaft. The valve profiles can be parametrized as follows,

- *Timing* - The crank angle (CAD) at valve opening with respect to the top/bottom dead center (the crankshaft positions corresponding to the piston at the end points of its stroke).
- *Duration* - The crank angle (CAD) at valve closing with respect to the opening CAD.
- *Lift* - The maximum displacement of the engine valve (mm).

Internal combustion engines in automotive applications operate over speed and load ranges covering an order of magnitude in each variable. This wide range of operating conditions results in conflicting demands for the shape of the displacement profiles for the intake / exhaust valves. However, with systems based purely on the camshaft, the motion of the engine valves is determined by the mechanical design of various components in the valve-train and thus offers no flexibility. It is typically designed to be a tradeoff between various operating conditions. Studies conducted by

various researchers has shown that an actuation system with the flexibility of varying the valve timing, duration, lift or a combination of these can increase the performance and efficiency of the engine by optimizing the delivery of gases to/from the cylinders for a wide range of operating conditions [1, 2, 3] .

1.2 Benefits of Variable Valve Actuation

The following section outlines the benefits that can be realized using the various flexibilities in valve actuation and their combinations i.e., variable lift, timing and duration. The articles relevant to the discussed topics are listed at the end of each subsection.

Throttle-less load control

In a conventional gasoline engine, the torque production is varied by controlling the fuel delivered to the cylinders. Maintaining the air/fuel ratio at the stoichiometric point is essential for reducing the emissions and this is achieved by restricting the air flow to the cylinders using a throttle. The combustion chamber is forced to draw the fresh charge at a pressure lower than ambient. This creates a significant amount of pumping losses during the cycle due to the imbalance in pressure on both sides of the piston. In a system with variable valve actuation, the amount of air intake can be controlled by varying the duration for which the intake valve is open. This strategy helps to eliminate the throttle and thus reduce the pumping losses by always drawing in air at ambient pressure. [1], [2], [4].

Volumetric efficiency

The duration during which the intake and exhaust valves are both open i.e., from end of exhaust → beginning of intake stroke is called the valve overlap. During high speed operation, a large overlap can increase the volumetric efficiency by improving the scavenging of the exhaust gases and thus improve the torque output. However, a large overlap at low speed and low load cannot sustain stable combustion due to excessive amounts of residual gases. Hence a decrease in overlap can lead to stable combustion at low speeds which can reduce the idle speeds of the engine and therefore lead to better fuel economy. In conventional engines, the valve overlap is chosen as a compromise between the requirements of the different operating conditions. With variable valve actuation, it would be possible to adjust this parameter in real-time to ensure that the torque output is optimal for each operating condition. [2], [4], [5], [6].

Cylinder charge mixing

The use of a throttle for load control has a secondary benefit. During part load operation, the low pressure in the intake manifold leads to better mixing of the air and fuel and thus offsets the effect of the decreased in-cylinder turbulence due to a reduced gas inlet velocity. The elimination of the throttle necessitates a supplementary method for improving the mixing by increasing the gas intake velocity. This is achieved by deactivating one of the two intake valves and/or by controlling the lift of the other intake valve. Another option is to retard the intake valve opening time to ensure that the piston is traveling at a certain velocity when the valve begins to open. [1], [4], [6].

Variable engine displacement

Although most engines are sized for peak acceleration, they rarely operate at the maximum load condition and the efficiency of the engine typically decreases during part load operation. By deactivating the intake/exhaust valves and the fuel injectors on certain cylinders, they function as gas springs with minimal energy losses. This increases the load on the remaining cylinders and shifts them to a more optimal operating condition and thus leads to an overall improvement in the efficiency of the engine. [4], [7].

Internal exhaust gas recirculation

Retaining a fraction of the residual burnt gas from the previous cycle can drastically affect the combustion for the current cycle and reduce the amount of Nitrous oxides (NOx) and hydrocarbons significantly. The reduction of NOx is due to the overall reduction in combustion temperature due to a decrease in the amount of combustible fresh charge. The reduction of the hydrocarbons is due to the re-combustion of the residual gas. Existing engines use dedicated subsystems to realize the Exhaust Gas Recirculation (EGR). Fully flexible valve actuation systems can realize the same in the following ways. Early intake valve opening forces some of the burnt gas into the intake manifold which is then drawn back along with the fresh charge during the intake stroke. Late exhaust valve closing results in the re-induction of the burnt gas from the exhaust manifold during the intake stroke. A negative overlap i.e., both intake and exhaust are closed for some duration before and after the top dead center leads to the entrapment of the burnt gases in the cylinder for the next cycle. These strategies are considered to be the fundamental enablers for advanced combustion concepts such as Homogenous Charge Compression Ignition. [1], [5], [8].

Pneumatic-hybridization

The independence of the valve operation with respect to crankshaft enables the utilization of the IC engine for other functions. It is possible to have a "charge valve" in addition to the 2 intake and exhaust valves, which connects the cylinders to a reservoir. It is capable of operating as a normal four stroke engine by deactivating the charge valve and operating the intake/exhaust valves in the conventional mode. By opening the intake valves during the downstroke and opening the charge valve during the upward stroke of the piston, the engine becomes an air pump and thus charges the reservoir. By opening the charge during the downward stroke and enabling the exhaust valves during the upward stroke, it becomes an air motor and can thus provide power. For normal 4 stroke operation, supercharging can be achieved by opening of the charge valve during the intake stroke. Hence in theory, optimizing this system on an individual cylinder basis can realize all the functions of a conventional hybrid drivetrain such as regenerative braking, downsizing and engine cycle optimization. [2], [7], [9].

Two/four stroke operation

By doubling the frequency of operation of the fuel injector and using appropriate timing of the engine valves, it is possible to realize two-stroke operation. To be specific, opening the exhaust valve during the later part of expansion stroke will expel the burnt gases. Opening the intake valves, after a certain delay will induct fresh air and also assist in the scavenging process. Closing the intake and exhaust valves during the upward stroke leads to compression which can be followed by the injection of fuel. The combustion can then be initiated close to the top dead center after allowing sufficient time for air-fuel mixing. Hence all the events of a normal four stroke cycle happen within two strokes of the piston. The advantage of two-stroke operation is the high power output for the same speed and engine displacement. However, it is characterized by higher fuel consumption and poor emissions. Hence, the flexibility to switch between the two modes can help leverage the advantages of both the modes and possibly lead to engine downsizing. [4], [7].

1.3 Camshaft-based Variable Valve Actuation

Camshaft based mechanical variable valve actuation systems have been researched extensively and are currently offered by a number of automobile manufacturers. [10] presents a 3-dimensional cam which can vary the valve profile by axially shifting the camshaft. The multistep cam mechanism shown in [6] can switch between a low lift, short duration cam and a high lift, long duration cam

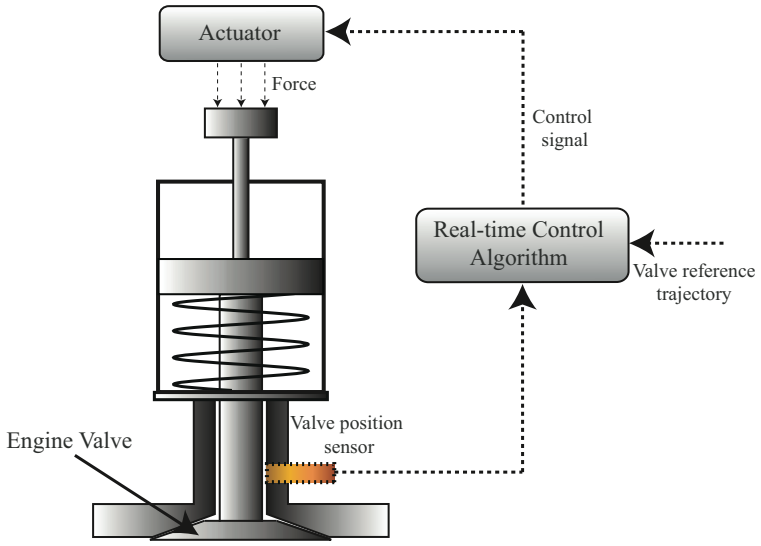

Figure 1.2: The schematic of a general camless engine valve actuation system

depending on the engine speed. The cam-phaser mechanisms described in [5], [11] and [12] have the capability of continuously varying the valve timing. [13] and [14] present system which can achieve 2 discrete lifts while being capable of continuously varying the timing. The mechanisms shown in [15], [16] and [17] have the capability of continuously varying the valve lift/duration together and with additional sub-systems, the flexibility of valve timing has also been incorporated. One fact that becomes evident is that the camshaft based systems either have limited flexibility or become mechanically complicated and expensive with the increase in flexibility. The mechanical complexity also raises concerns about power consumption due to friction losses.

1.4 Camless Engine Valve Actuation

One possibility of increasing the flexibility of the valve event without increasing the associated mechanical complexity is to use the so called "Camless Valve Actuation Systems" which eliminate the camshaft and use electronically controlled systems for actuating the engine valves. A general schematic which is able to capture the most basic ideas associated with camless valve actuation is shown in Fig. 1.2. Since each valve is actuated independently, it is possible to integrate all the flexibilities into one system i.e., vary the lift, timing and duration of the valve event on a cycle to cycle basis.

With the wide spread use of cam-based variable valve actuation systems, there is an increase in the available degrees of freedom during the design process of a new engine. Research oriented fully flexible valve actuation systems with all the flexibilities such as variable lift, duration and timing

can also serve as a platform for exploratory combustion research. They can help in simulating and evaluating the effect of different valve strategies and thus play a crucial part in the selection and design of the camshaft based valve-trains.

1.4.1 Requirements

In order to be viable for widespread application, the engine valve actuation system needs to address the following requirements outlined in [18]. Most of these requirements are automatically guaranteed for cam-based systems due to their mechanical design. However, the removal of the mechanical link between the crankshaft and the engine valve necessitates the active control of the entire actuation system to ensure the desired performance.

1. ***Robust valve motion control*** - Robust position control is required to enable repeatable valve profiles in the presence of disturbances such as varying gas forces and other engine operating conditions. Avoiding collisions between the valves and the pistons is an absolute requirement.

2. ***Soft seating*** - During valve closing, the speed at which the valve impacts its seat is termed as seating velocity. Excessive seating velocities result in increased valve-train noise and accelerated wear & tear and hence need to be minimized.

3. ***Energy consumption*** - The removal of the camshaft greatly reduces the frictional losses in the valve-train. However, the energy consumption of the valve actuator contributes to the overall efficiency of the engine. It needs to be minimized to levels that are comparable to the cam-based systems to justify the modification.

4. ***System cost*** - The requirement of high precision/complex components for sensing, actuation & control can result in a drastic increase in the overall system cost due to the multiplicity of engine valves which typically ranges from $16 \rightarrow 32$. Hence it is desirable to develop actuators based on inexpensive subsystems.

5. ***Control simplicity & calibration effort*** - The algorithms for the control of the actuators greatly depend on the system characteristics which are influenced by the system architecture and the design parameters. Issues such as non-linearity, limitations in control authority, parameter variation/uncertainties can all lead to the requirement of complicated control strategies and require extensive calibrations which are challenging to implement during mass production.

6. ***System size*** - The power density of the actuation system and the size of the sensing elements determine the overall size of the camless valve-train system, which should again

be comparable to the conventional camshaft based systems to enable implementation with minimal modifications to existing infrastructure.

1.4.2 Current State of the Art

This section outlines the characteristics of the various existing camless valve actuation systems. All of these systems can be broadly classified based on the energy source used for actuation.

Electro-mechanical systems

The most common electro-mechanical systems [19], [20], [21] are based on the use of solenoids or linear DC motors. The systems described in [22] and [23] rotational DC motor with very fast response to precisely control the position of the engine valve via a mechanical linkage. For the typical linear type electro-mechanical systems, the energy consumption is minimized by using springs to capture the kinetic energy of the moving valve and using it to move the valve in the opposite direction. The electro-magnetic force is only needed to supply the additional energy to overcome the friction and to hold the valve at the end positions. The nonlinearity of the electromechanical force and the time delay due to the inductance in the coils make it difficult to control the valve at the two ends of its trajectory. Complicated control strategies such as those described in [19] and [20] are required to ensure soft seating and variable lift operation. For the systems with rotational type actuators [23, 22] , the requirement of a relatively large motor to provide the required actuation force and bandwidth can significantly increase the size of the entire system.

Electro-hydraulic systems

The electro-hydraulic systems [4, 24, 25, 26, 27, 28] use pressurized hydraulic fluid to provide the actuation force. They have good control authority over the entire range of motion, are capable of variable lift operation and have superior power density which leads to compact system designs. The production oriented electro-hydraulic systems based on inexpensive valves have challenges associated with ensuring precise valve motion and effective seating velocity control. Research oriented laboratory systems use precision servo valves to achieve accurate valve motion. The high cost of the servo valves and the high power consumption due to the throttling of hydraulic fluid during a major portion of the valve operation makes it unsuitable for mass production.

Electro-pneumatic systems

The electro-pneumatic systems such as those presented in [29, 30, 31, 32] use pressurized air to generate the force required to control the position of the actuators. These systems are constrained

by the low power density and compressibility of air. This leads to bulky designs and also raises difficulties in achieving precise valve motion control and seating velocity control at high engine speeds. In addition to this, energy losses due to throttling of the working fluid is still a concern.

1.4.3 Summary of the Challenges

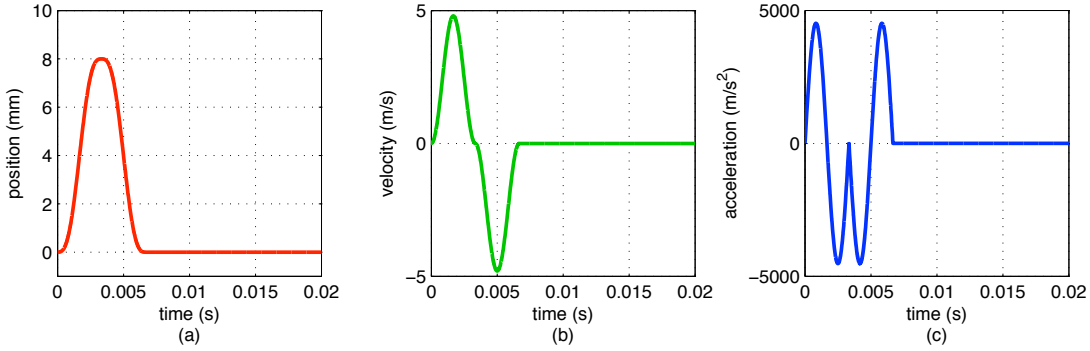

Figure 1.3: Typical characteristics of the valve reference trajectory corresponding to an aggressive operating condition (a) position, (b) velocity and (c) acceleration

For a camless actuation system to enable fully flexible operation, it needs to ensure robust and precise tracking of the desired valve reference trajectory even at the most demanding operating conditions such as the one shown in Fig. 1.3 which corresponds to an engine speed of 6000 RPM. The acceleration profile of the valve indicates that the actuation system needs to deliver forces with large magnitude, high precision and high bandwidth. Such demanding performance requirements along with the constraints on cost, power consumption and system size make the design of the actuators, sensors and real-time controllers extremely difficult and has impeded the large scale deployment of these systems.

1.5 Overview of Research Topics

The research presented in this thesis focuses on two topics aimed at addressing some of the challenges presented earlier. The electro-hydraulic architecture is chosen for both the investigations due to its superior power density and control authority over the entire range of operation.

1.5.1 Design based approach

The first topic focuses on a specific actuator design introduced in [33, 18], which overcomes most of the challenges of electro-hydraulic systems by combining the performance advantages of infinite

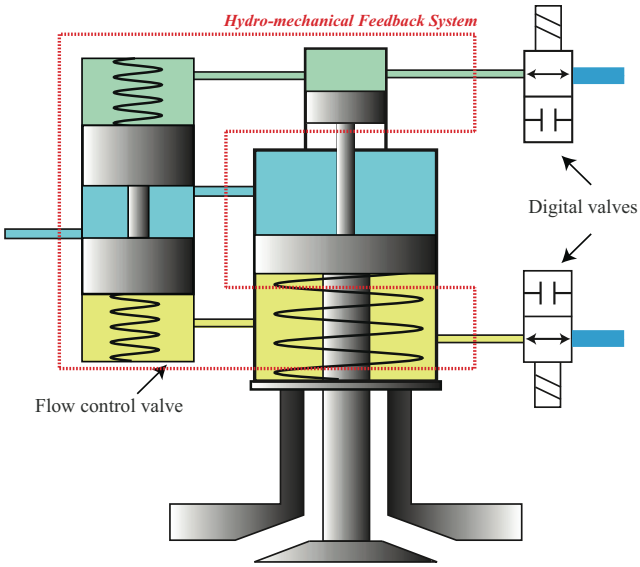

Figure 1.4: The new electro-hydraulic actuation system with internal feedback mechanism

position flow control valves and the simplicity of digital valves into the same architecture. The traditional feedback loop (position sensor, real-time controller and electro-mechanically actuated flow control valve) is replaced with a hydro-mechanical system as shown in Fig. 1.4. The digital valves shown in the figure are used only to activate/de-activate the feedback loop i.e., to couple/de-couple the motion of the actuator with the motion of the flow control valve's spool.

The inherently stiff nature of the hydro-mechanical systems makes it possible to achieve a high bandwidth using relatively simple and inexpensive components. An external feedback system is used only to evaluate the valve event characteristics and control the system on a cycle to cycle basis to ensure the desired performance such as the tracking of lift, timing and duration and minimization of the seating velocity. This greatly simplifies the external feedback loop by reducing the requirements on the sensor and real-time controller.

Extensive testing of a prototype system based on this concept reveals that the physical design of hydro-mechanical loop directly influences certain metrics associated with the performance and robustness of the system. Hence, this work [34] aims to develop of a systematic model based design procedure to optimize the performance of the hydromechanical loop to improve the overall performance of the system.

1.5.2 Control based approach

This topic focuses on the development and validation of an advanced motion control algorithm for tracking cyclic but aperiodic reference signals. The main application is to enable precise motion

control of the camless valve actuation system during engine speed transients. Although an electro-hydraulic actuation system is used for validating the proposed control framework, it can be easily adapted to other actuator architectures which satisfy the underlying assumptions.

Since there is no mechanical link between the engine valve and crankshaft, the capability of precisely controlling the actuation system to track a predetermined trajectory is a critical requirement for the camless systems. There has been extensive research in the area of control design for fully flexible valve actuation systems. Some notable contributions based on the actuation architecture are as follows, electro-mechanical systems [35, 20], electro-hydraulic systems [36, 24] and electro-pneumatic systems [31, 30]. The controllers predominantly started off with systems with limited flexibilities and were designed to extend the capabilities of a given architecture and to maintain the desired valve event characteristics under disturbances such as varying gas forces in the combustion chamber. Certain actuation architectures are capable of fully flexible actuation i.e., complete control of the overall shape of the valve profile as opposed to just the maximum lift and duration. The control design of such systems is challenging and has not yet been solved and hence is the focus of this research. It is motivated by the precise valve profile tracking achieved using the Linear time invariant repetitive control [37, 28] for electro-hydraulic systems under constant engine speed operation.

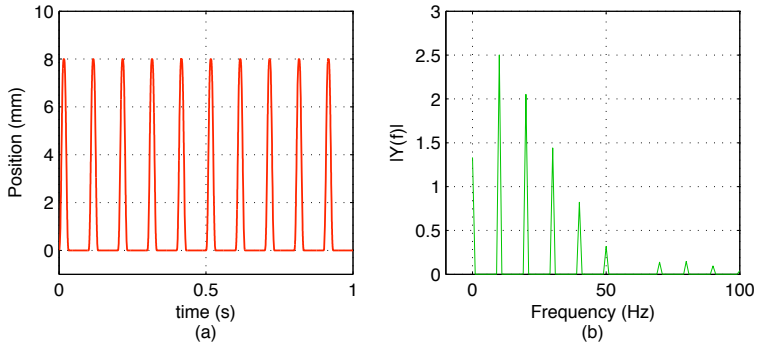

Figure 1.5: Valve reference trajectory corresponding to constant engine speed (1200 RPM) and fixed valve event (8mm lift and 240 CAD duration), (b) the corresponding frequency content

A typical trace of the valve displacement for a four stroke engine when its speed is constant is shown in Fig. 1.5(a). The signal is periodic and can be described using the expression $r(t) = r(t - N\Delta t)$, where Δt is the discrete sampling time and N is the period of the reference signal in number of samples. The key features that enabled the LTI repetitive control to achieve precise tracking performance are as follows,

1. It utilizes the periodicity to obtain the discrete time domain dynamics of the signal as $r(k) =$

$r(k-N)$, which enables a specialized implementation of the more general internal model based control.

2. The frequency domain representation of the reference signal as shown in Fig. 1.5(b) indicates that the magnitudes are concentrated at discrete locations which are integer multiples of the fundamental frequency. The closed-loop system using the repetitive controller has small sensitivities at these exact frequencies.

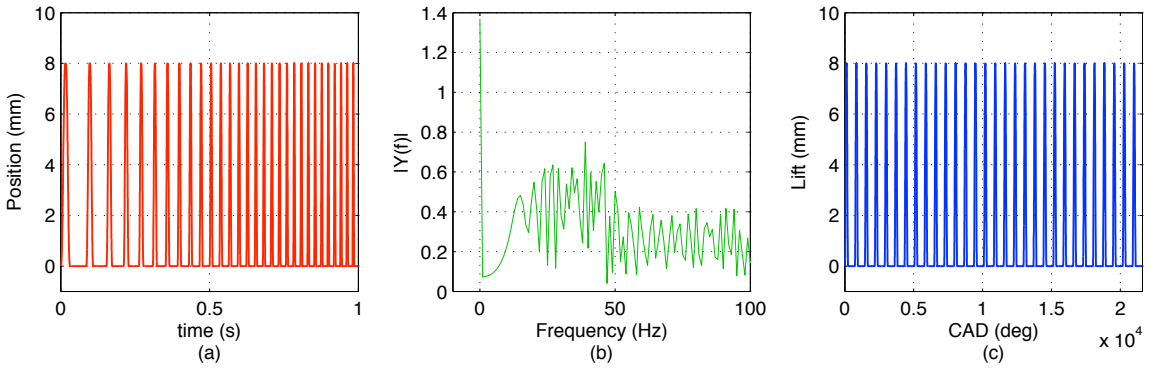

Figure 1.6: Valve reference trajectory corresponding to an engine speed transient (1200 to 3600 RPM) and fixed valve event (8mm lift and 240 CAD duration), (b) the corresponding frequency content, (c) representation of the signal in the rotational angle domain

However, during engine speed transients, the valve reference trajectory becomes aperiodic in time and both the characteristics described earlier are longer true as shown in Fig. 1.6(a) and (b). Two methods which are loosely tied to the ideas discussed earlier for obtaining the models for the reference signal during engine speed transients and later used in the design of controllers based on the internal model principle. The first method is to model the aperiodic reference signal as a combination of frequency varying sinusoids as shown in Eqn. 1.1. The frequency of the various harmonics are given by $[\omega_1(t), \omega_2(t), ..\omega_\rho(t)] = [1, 2, \cdots, \rho] \times \omega(t)$, where $\omega(t)$, the fundamental harmonic is related to the engine speed W [RPM] by $\omega(t) = W(t) \times \pi/60$. The details of all the terms are presented later on, the key issue to be noted at this point is that the model for the reference signal is time-varying.

$$r(t) = \gamma_0 + \sum_{i=1}^{\rho} \gamma_i \sin\left(\int \omega_i(t)dt + \phi_i\right) \tag{1.1}$$

The second method is based on the design and implementation of the controller in the rotational angle domain to leverage the dependance of the valve profile on the crankshaft position. The valve reference trajectory (for a fixed valve event) is thus periodic in the rotational angle domain as shown in Fig. 1.6(c). By sampling the entire system in the rotational angle domain, the signal can be

represented using $r(\theta) = r(\theta - N\Delta\theta)$, where N is the number of samples in one cycle and $\Delta\theta$ is the angular sampling resolution. Hence, the reference signal in the rotational angle domain can once again be written as $r(k) = r(k - N)$ which enables the use of a repetitive controller. However, the time interval between successive sampling instants i.e., $\Delta t(k) = \Delta\theta(k)/(6W(k))$ changes as the rotational speed changes in real time. Hence the model of the plant (valve actuator) with time-invariant dynamics becomes time(parameter)-varying in the rotational angle domain.

For both these methods, the models for the reference signal are known and thus makes it ideally suited for designing controllers based on the internal model principle. Based on the above observations, it is clear that either the plant (valve actuator) or the reference signal model is time-varying and thus makes the recently developed time-varying internal model based controller [38] ideally suited for this application. The details associated with various aspects of the design and implementation of this control framework are presented along with experimental data to validate the proposed approach.

1.6 Expected Contributions

Systematic design optimization for the VVA system with internal feedback

The inherent advantages of the new engine valve actuation system based on the internal feedback makes it ideally suitable for mass production. However, the complex dynamics of the hydro-mechanical feedback loop make the design of the overall system non-intuitive. By providing a systematic procedure for optimizing the design a key component in the feedback loop, the entire process of designing the actuation system for a wide variety of requirements can be streamlined.

Design of spool valves with arbitrary "area-schedules"

The "stroke vs effective orifice area" relationship of a spool valve is termed as the area-schedule. The area-schedules of most conventional spool valves is either linear, quadratic or other simple mathematical relationships. A recent trend is to modify the spool to address various performance requirements of the systems that they are part of. The systematic analysis and synthesis techniques developed as part of this research are expected to simplify the process of designing the spool valves.

Semi-automated process for the design and implementation of the time-varying internal model based controllers

The calculation of the controller coefficients requires the solution of very high order diophantine equations during each step. The process of deriving the symbolic expressions for their solution manually or by using the symbolic toolboxes in commercial packages becomes extremely tedious even for plants and signals with moderate complexity. A program for automating this process based only on the knowledge of the plant and signal orders has been developed. The program also generates a matlab code that can be readily integrated into the existing control design frameworks and implemented on real-time hardware. The simplification of the control design and implementation process for high order systems has enabled the rapid development and testing of controllers for a variety of cases which has helped uncover various characteristics of the proposed control framework.

A comprehensive framework for the transient control of FFVA systems and general periodic systems

The final objective of the control based approach will be to develop a comprehensive framework for applying the time-varying internal model based control to camless valve actuation systems. The details regarding the control implementation have been presented and validated experimentally. This framework can also serve as a template that can be readily extended to FFVA systems based on any architecture. The developed controller will also be applicable to the transient control of more general rotational and other spatially periodic systems.

1.7 Organization of the Thesis

The rest of the document is organized as follows. Chapter 2 presents a detailed overview of the modeling and design optimization of the actuation system with the internal feedback mechanism. The test results from a prototype experimental setup help identify key issues that need to be addressed. A mathematical model of the system helps identify the spool in the flow control valve as the most critical component from a control perspective. The design of this component is formulated as an optimization problem and solved using dynamic programming. Case studies using simulations are conducted to study the effectiveness of the proposed methodology to improve the overall system performance and robustness.

Chapter 3 presents a systematic method for redesigning the spool based on the results from the model based optimization procedure. An analysis method based on the use of computation fluid dynamics is used to study the effect of the design features on the spool. A simplified procedure based

on analysis of the geometry is then developed to accelerate the analysis procedure. Experimental investigations using the spool from the prototype system help validate the analysis procedures. The rapid turn around time of the geometry based procedure is then used to develop an iterative procedure for synthesizing the design of the spool.

Chapter 4 introduces the design aspects of the proposed framework by summarizing the information from existing literature and also introducing additional details associated with various components of the time-varying internal model based controller.

Chapter 5 aims to guide the practical implementation by documenting various implementation aspects of the control framework. The benefits/issues associated with various methods of implementing the controllers are presented. The challenges arising due to the time-varying nature of the controller are revealed and solutions are proposed. Finally, results from both simulations and experiments on a prototype actuation system are presented to highlight the effectiveness of the proposed approach.

Chapter 2

Design Optimization for the Actuator With Internal Feedback

The overall objective of this research topic is to develop a model based design optimization procedure for the valve actuation system with internal feedback. Experimental data from a prototype setup helps to uncover potential performance issues that need to be addressed. The representation of the mechanical system using a traditional control block diagram along with the mathematical model of the system helps identify the spool in the flow control valve as the key component whose design influences the overall behavior of the entire system. This chapter focuses on the details of the first step i.e., the development of a systematic procedure to obtain the optimal relationship between the spool displacement and the corresponding metering orifice area. The material in the following sections has been published as a journal article [34] ().

2.1 System Description

2.1.1 System design

The actuation system consists of a low pressure reservoir with the hydraulic fluid. A pump driven by the engine supplies the pressurized fluid to the high pressure line. The reservoir and the high pressure line are common to all the actuators for each of the engine valves.

- Component {1} is a solenoid actuated 2-position valve *(supply valve)*, which connects the entire system to the high pressure line or the reservoir.

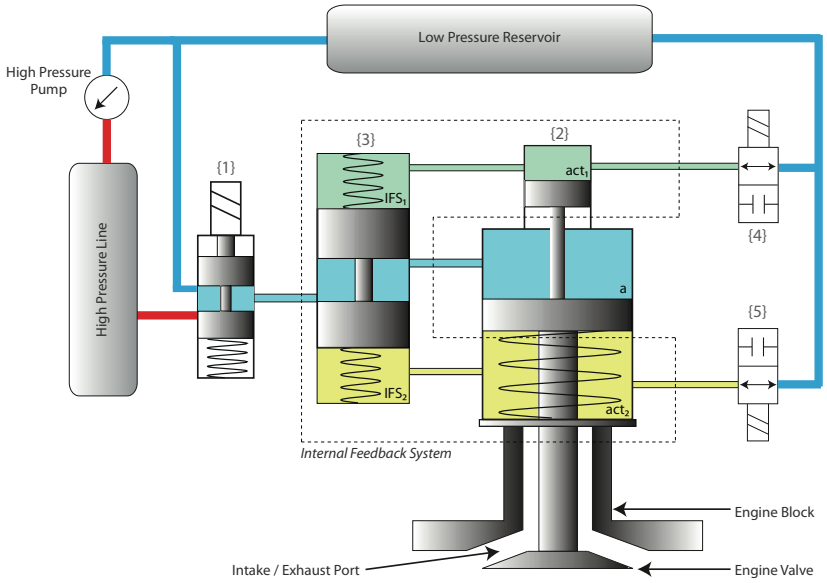

Figure 2.1: Schematic of the new variable valve actuation system

- Component {2} is a spring returned, single acting hydraulic actuator that is connected to or in contact with the engine valve's stem.

- Component {3} is a spool valve which acts as the feedback regulator. The spool's position depends on the difference in pressure between the top and bottom hydraulic chambers IFS_1 *and* IFS_2. These pressures are in turn dependent on the pressure of the top and bottom chambers of the actuator act_1 *and* act_2 as shown in the schematic. The feedback regulator is designed such that the orifice area affecting the fluid flow is maximum for the spool's undeflected position i.e., the resistance to the fluid flow is minimum and for both directions of movement of the spool, the orifice area decreases i.e., the resistance to fluid flow increases.

  The chambers act_1, act_2, IFS_1 *and* IFS_2 along with the spool valve form the internal feedback system *(IFS)* as highlighted in the schematic.

- Components {4} & {5} are on-off valves, which connect the two feedback chambers of the actuator to the reservoir. When both the on-off valves are open, there is a free flow of fluid between the actuator's feedback chambers and the low pressure reservoir. Closing either of the on-off valves restricts the flow out of the corresponding feedback chamber.

2.1.2 Working principle

At the beginning of a typical valve operation cycle, the supply valve {1} and both on-off valves {4 & 5} are in the de-energized state. Hence all the hydraulic chambers are connected to the low pressure reservoir. The engine valve is held in the closed position by its return spring. The spool in {3} is balanced in the center position due to the force exerted by its springs. To open the engine valve, the system is connected to the high pressure line by energizing the supply valve. The high pressure fluid accelerates the actuator downwards. When the engine valve reaches a desired lift, the bottom on-off valve {5} is shut off which restricts the fluid flow from the bottom feedback chamber to the reservoir and diverts it into the bottom chamber of the feedback regulator and thus deflects the spool upward. As the spool moves upward, the orifice area of the spool valve decreases and thus restricts the fluid flow through it. This reduces the pressure in the actuation chamber and causes the actuator to decelerate. The synchronized motion between the actuator and the spool valve will continue until flow to the actuator is completely shut off by the spool and the actuator comes to a stop smoothly. Hence by controlling the timing of the bottom on-off valve, we can control the maximum lift of the engine valve.

To close the engine valve, the supply valve is first de-energized. The bottom on-off valve is then opened which causes the spool of the regulator to return to the center position and thus connects the actuation chamber to the low pressure reservoir. The spring force becomes dominant and hence moves the actuator upwards which starts to close the engine valve. The top on-off valve {4} is closed when the engine valve is near the seat. By the same principle as explained previously, the spool is deflected in the downward direction which decreases the orifice area and thus restricts the flow out of the actuation chamber. The actuation chamber pressure thus increases which gradually decelerates the engine valve till it lands on the valve seat with a desired seating velocity.

2.1.3 Desirable performance characteristics

- *Component simplicity* : The actuation system comprises of simple two-state valves, hydraulic pistons and spools which are relatively inexpensive when compared to high precision servo valves. The mass production of such simple components can also reduce their price and thus keep the overall cost of the actuation system at a reasonable level manageable.

- *High bandwidth control subsystem* : Traditional feedback systems consist of a displacement sensor, a real-time (linear/nonlinear) controller and an electro-mechanically actuated proportional valve to vary the orifice area and regulate the flow to the actuator. Since the plant is nonlinear, a controller designed for a linearized system may not be able to provide

sufficient dynamic response. While a nonlinear controller may account for all the dynamics, the challenges associated with designing and implementing it in real-time make it unsuitable for mass production. The limited bandwidth of the electro-mechanically actuated proportional valve which directly affects the dynamic response of the control system is another constraint of the traditional approach. The unique advantage of this architecture is that, the extremely stiff hydro-mechanical internal feedback system acts as the high bandwidth nonlinear controller which modifies the control signal A_{spool} based on the output of the plant i.e., X_{act} and V_{act}.

- *Control simplicity* : The valve timing, lift, duration and seating velocity can all be controlled very precisely by just varying the timing of the 3 valves (the solenoid valve and the on-off valves). Since the the triggering times are calculated only once per cycle, the corresponding control algorithms tend to be much simpler and can thus be easily implemented on mass production systems.

- *Energy efficiency* : As mentioned earlier, the internal feedback mechanism has a very fast response when compared to electro-mechanical feedback loops. It can be engaged at the last moment possible and would thus lead to throttle-free operation during a major portion of the valve cycle. This leads to a minimization of throttling losses and hence results in a decrease in power consumption.

2.2 Prototype Experimental Setup

Fig. 2.2(a) shows the prototype multi-cylinder fully flexible valve actuation system. It consists of 4 engine valves which have been instrumented with internal feedback based actuator. All the actuators have sensors for measuring the valve displacement. In addition to this two actuators are also instrumented with sensors to measure the pressure in the main chamber i.e., "a" and, the feedback chamber pressures in the flow control valve i.e., IFS_1 and IFS_2 and the displacement of the flow control valve's spool. The system supply pressure can be monitored using the pressure sensor mounted on the High pressure line.

2.2.1 Demonstration of flexibilities

As mentioned earlier, all the engine valve event parameters can be varied by controlling the triggering timing of the various on-off valves. The duration control is demonstrated in Fig. 2.2(b) by controlling the time at which the 3-way valve {3} and on-off valve {5} are de-energized. Fig. 2.2(c) shows the lift control results obtained by varying the timing of the on-off valve {5}. The seating velocity is

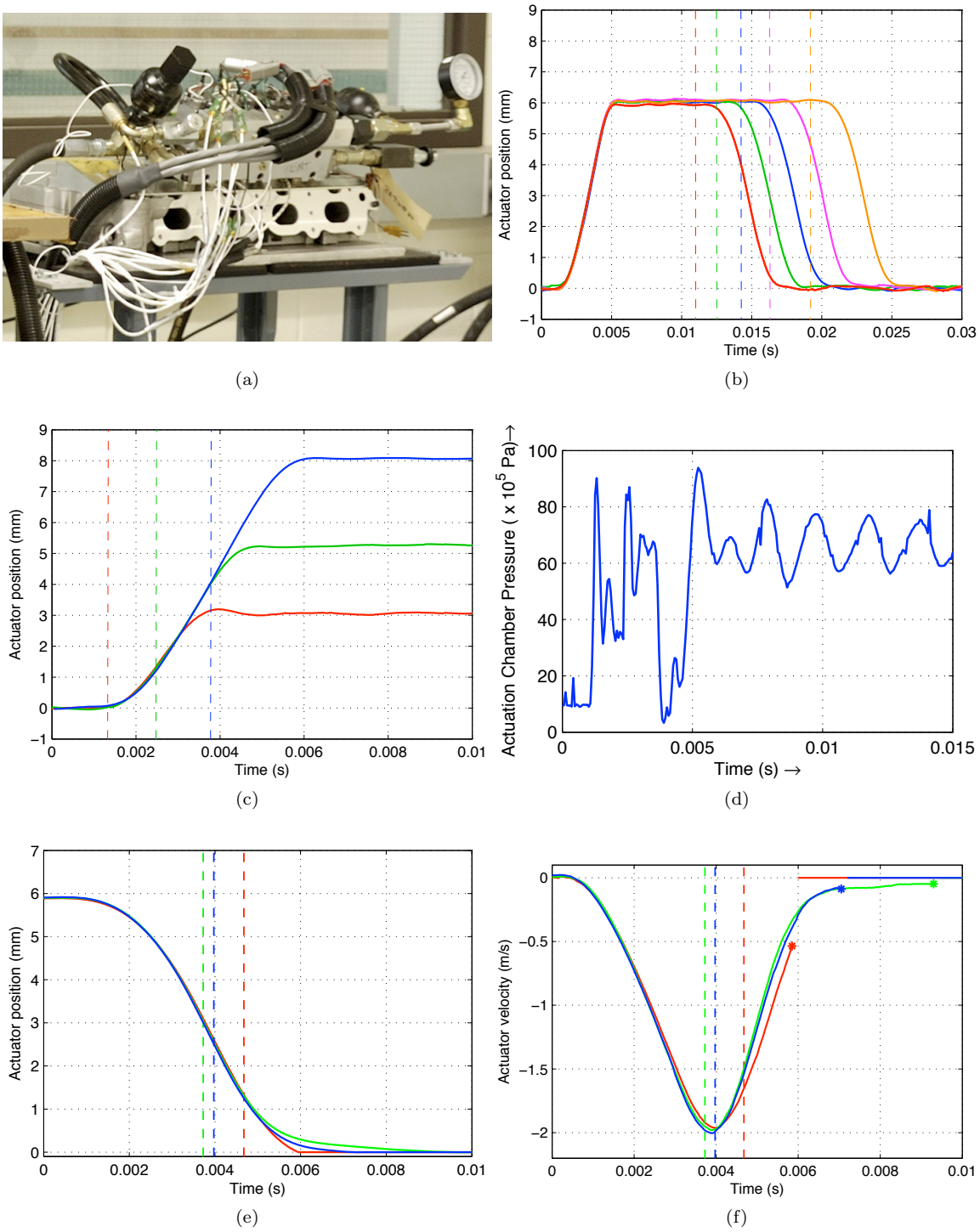

(a) (b) (c) (d) (e) (f)

Figure 2.2: (a) Prototype experimental setup (b) duration control (c) lift control (d) corresponding actuation chamber pressure during valve opening (e) & (f) position and velocity during seating control.

controlled by varying the time at which on-off valve {4} is triggered during valve closing. Fig. 2.2(f) shows that for the same initial conditions, i.e., returning from 6 mm, the velocity can be controlled between 0.5 m/s and 0.05 m/s which covers the entire range of the prescribed seating velocities for different operating conditions.

2.2.2 Identification of performance issues

Engine valve opening

The actuation chamber pressure traces corresponding to three valve lifts during valve opening are shown in Fig. 2.2(d). It can be seen that, for the low and medium lift cases, the pressure trace drops below the ambient for an extended period of time. The installed sensor is not capable of measuring pressures lower than ambient. It is possible that the actual pressure in the actuation chamber could be much lower and thus result in cavitation. Cavitation occurs when the flow rate to a particular chamber is not sufficient to maintain the chamber pressure $\geq P_{vap}$ (vapor pressure of the fluid). Hence, during valve opening, if the flow to the actuation chamber is shut off too quickly while the valve is still moving, it will result in a rapid pressure drop. Cavitation can severely damage the system and so it needs to be avoided by controlling the flow to the actuation chamber to maintain the actuation pressure above P_{vap}.

Engine valve closing

For valve closing, it can be seen from Fig. 2.2(e) & (f) that the system has a very conservative design. In order to ensure soft seating, the engine valve needs to be decelerated very early and hence it travels with a low velocity till it lands on the seat. Though this can ensure a low seating velocity, it keeps the valve near the seat for a long time before closing which leads to pumping losses in the engine. The peak pressure in the actuation chamber is also quite high and is not desirable from a structural design perspective since it can cause fatigue damage. An ideal trajectory for closing would be one in which both the closing time as well as the seating velocity are minimized and the peak pressure is also moderate.

2.3 Design Optimization Procedure

2.3.1 System dynamics modeling

The dynamics of the entire feedback system depend on a number of parameters like the physical dimension of each of the components, the stiffness of the various springs and the timing of the on-off

valves etc. It is therefore necessary that we have an accurate mathematical model of the system, which can be used to evaluate the effect of various parameters, validate design changes and thus assist in the control design process.

The equations describing the dynamics of the actuator, spool and pressures in the various chambers are presented in the following section. It should be noted that the intake/exhaust valves operate at 50Hz when the engine is running at 6000 RPM. Hence, to capture all the dynamics of the high-speed operation of the system, the effect of fluid compressibility needs to be considered since it becomes prominent at such high frequencies.

$$\dot{X}_{act} = V_{act} \tag{2.1}$$

$$\begin{aligned}\dot{V}_{act} = \frac{1}{M_{act}}[&P_a \cdot A_a + P_{act_1} \cdot A_{act_1} - P_{act_2} \cdot A_{act_2} - K_{act} \cdot X_{act} \\ &- b_{act} \cdot \dot{X}_{act} - F_{preload}]\end{aligned} \tag{2.2}$$

where, X_{act} and V_{act} are the position and velocity of the actuator, M_{act} is the moving mass of the actuator and valve assembly, P_a is the pressure in the actuation chamber, A_a is the area of the actuator's piston exposed to the high pressure fluid, P_{act_1}, P_{act_2} are the pressures in the actuator's top and bottom feedback chambers, A_{act_1} and A_{act_2} are the areas of the actuator's top and bottom feedback chambers, K_{act} is the stiffness of the actuator spring, $F_{preload}$ is the spring preload and b_{act} is the damping coefficient of the actuator.

$$\dot{X}_{spool} = V_{spool} \tag{2.3}$$

$$\begin{aligned}\dot{V}_{spool} = \frac{1}{M_{spool}}[&P_{IFS_1} \cdot A_{IFS_1} - P_{IFS_2} \cdot A_{IFS_2} - b_{IFS} \cdot \dot{X}_{spool} \\ &- (K_{IFS_1} + K_{IFS_2}) \cdot X_{spool}]\end{aligned} \tag{2.4}$$

where, X_{spool} and V_{spool} are the position and velocity of the spool, M_{spool} is the mass of the spool, P_{IFS_1} and P_{IFS_2} are the pressures in the spool valve's top and bottom feedback chambers, A_{IFS_1} and A_{IFS_2} are the areas of the feedback regulator's top and bottom feedback chambers, K_{IFS_1} and

K_{IFS_2} are the stiffness of the IFS springs and b_{IFS} is the damping coefficient of the IFS.

$$\begin{aligned}
\dot{P}_a &= \frac{\beta\left(Q_a - V_{act} \cdot A_a\right)}{\left(x^*_{act} + X_{act}\right) \cdot A_a} \\
\dot{P}_{act_1} &= \frac{\beta\left(-Q_{f1} - Q_{onoff_1} - V_{act} \cdot A_{act_1}\right)}{\left(x^*_{act_1} + X_{act}\right) \cdot A_{act_1}} \\
\dot{P}_{act_2} &= \frac{\beta\left(-Q_{f2} - Q_{onoff_2} + V_{act} \cdot A_{act_2}\right)}{\left(x^*_{act_2} - X_{act}\right) \cdot A_{act_2}} \\
\dot{P}_{IFS_1} &= \frac{\beta\left(Q_{f1} - V_{spool} \cdot A_{IFS_1}\right)}{\left(x^*_{spool_1} + X_{spool}\right) \cdot A_{IFS_1}} \\
\dot{P}_{IFS_2} &= \frac{\beta\left(Q_{f2} + V_{spool} \cdot A_{IFS_2}\right)}{\left(x^*_{spool_2} - X_{spool}\right) \cdot A_{IFS_2}}
\end{aligned} \tag{2.5}$$

where, β is the bulk modulus of the hydraulic fluid and x^*_{act}, $x^*_{act_1}$, $x^*_{act_2}$, $x^*_{spool_1}$ and $x^*_{spool_2}$ are the spaces in each of the corresponding chambers when the valve is in the closed position and the spool is in the center position. The flow rates between the chambers are calculated using the following equations.

$$\begin{aligned}
Q_a &= sgn(P_s - P_a) \cdot A_{spool} \cdot C_d \cdot \sqrt{\frac{2 \cdot |P_s - P_a|}{\rho}} \\
Q_{f1} &= sgn(P_{act_1} - P_{IFS_1}) \cdot A_{f1} \cdot C_d \cdot \sqrt{\frac{2 \cdot |P_{act_1} - P_{IFS_1}|}{\rho}} \\
Q_{f2} &= sgn(P_{act_2} - P_{IFS_2}) \cdot A_{f2} \cdot C_d \cdot \sqrt{\frac{2 \cdot |P_{act_2} - P_{IFS_2}|}{\rho}} \\
Q_{onoff_1} &= sgn(P_{act_1} - P_T) \cdot A_{onoff_1} \cdot C_d \cdot \sqrt{\frac{2 \cdot |P_{act_1} - P_T|}{\rho}} \\
Q_{onoff_2} &= sgn(P_{act_2} - P_T) \cdot A_{onoff_2} \cdot C_d \cdot \sqrt{\frac{2 \cdot |P_{act_2} - P_T|}{\rho}}
\end{aligned} \tag{2.6}$$

where, C_d is the discharge coefficient, ρ is the density of the fluid, The orifice area A_{spool} is a function of the displacement of the spool X_{spool} and the relation $A_{spool} = f(X_{spool})$ is called the area-schedule. A more detailed explanation of the area-schedule is presented in the control design section. In the case of Q_{onoff_1} and Q_{onoff_2}, the corresponding orifice areas A_{onoff_1} and A_{onoff_2} are set to either 0 or maximum depending on the state of the particular on-off valve. To account for the time delay in the actual on-off valves, the area is ramped from one state to the other with a transition time based on the manufacturer specified performance data.

The areas (A_{f1} and A_{f2}) correspond to the orifice in the channel between the feedback chambers. There is an initial surge followed by oscillations in the pressure of the feedback chambers

corresponding to the on-off valve that is closed. These pressure dynamics can result in undesirable oscillations of the spool. When sized correctly, these orifices can act as hydraulic dampers to filter out the high frequency pressure dynamics to avoid spool oscillations while still ensuring a fast response of the spool. The dimensions of the feedback chambers are designed such that, after the corresponding on-off valve is closed, the actuator can travel a maximum of $2mm$ while decelerating steadily. By the appropriate timing of the on-off valves, the maximum lift and the seating velocity of the engine valve can be controlled precisely.

2.3.2 Model validation

Fig. 2.3 presents three sets of valve lift and corresponding velocity data obtained from a prototype experimental system in which the maximum lift, duration and the valve seating velocity are independently controlled by the timing of the 3 valves (supply and on-off). While the variation in lift is easily observed, the variation in valve seating velocity can be identified by observing the slope of the valve lift's trajectory close to the seat. The choice of these specific sets of data can be attributed to the fact that they cover a wide range of operating conditions of the engine valve actuator.

To validate the developed mathematical model, it is simulated in matlab with the physical parameters corresponding to the prototype experimental setup. The results obtained from the simulations are then compared to those obtained from the experiments. Fig. 2.3 shows a good correlation between the experimental and simulation results for all 3 cases which correspond to a wide range of operating conditions. Hence it can be concluded that the model is representative of the physical system and can thus be used for control design purposes.

2.3.3 Identification of the control variable

Fig. 2.4 shows a control oriented block diagram of the system. The actuator is represented as the plant that needs to be controlled. The control signals to the plant are the supply pressure and the orifice area of the spool. To achieve precise control of the actuator, the flow to and from the actuation chamber needs to be controlled precisely during the entire operation of the feedback system. Since the supply pressure cannot be varied on an engine cycle basis i.e., during the operation of the IFS, the only way by which the flow can be varied in real-time is by controlling the orifice area of the spool valve.

A traditional feedback system would consist of a sensor to measure the displacement of the engine valve. A controller (linear/nonlinear) would then use the displacement information to control the spool of an electro-mechanically actuated proportional valve to vary the orifice area

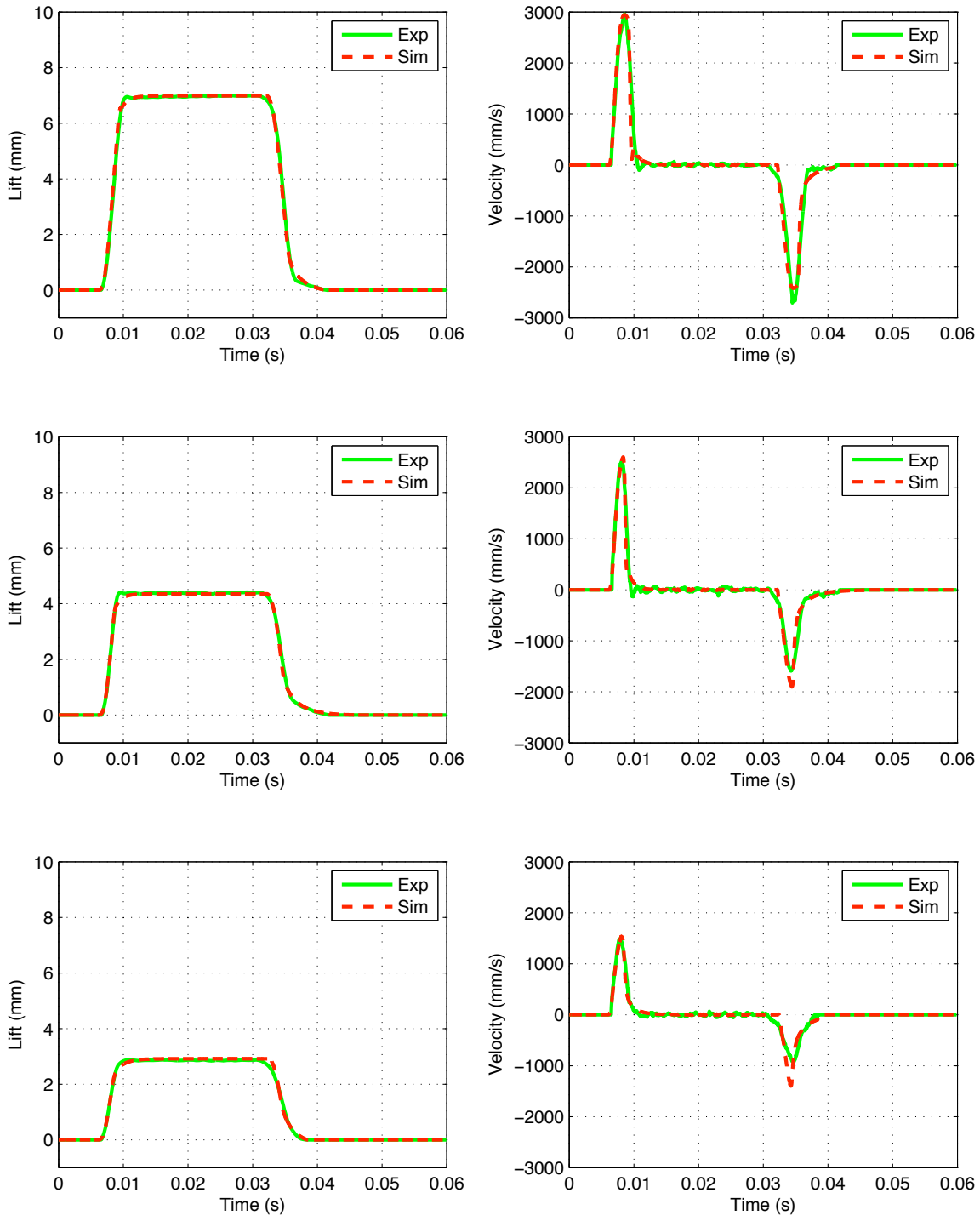

Figure 2.3: Comparison of data obtained from experiments and model simulations for different valve strategies.

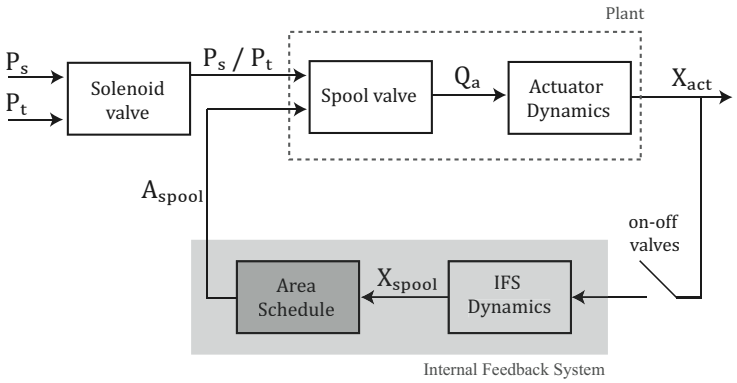

Figure 2.4: Control Block diagram of the system

in real-time and hence regulate the flow to the actuator. Since the plant is nonlinear, a controller designed for a linearized system may not be able to provide sufficient dynamic response. While a nonlinear controller may account for all the dynamics, the challenges associated with designing and implementing it in real-time make it unsuitable for this application. The limited bandwidth of the electro-mechanically actuated proportional valve which directly affects the dynamic response of the control system is another constraint of the traditional approach.

The unique advantage of this architecture is that, the internal feedback system acts as the nonlinear controller which when engaged, modifies the control signal A_{spool} based on the output of the plant i.e., X_{act} and V_{act}. Once the external control closes an on-off valve, the spool of the feedback regulator is hydro-mechanically linked to the actuator which makes the feedback loop extremely stiff and hence has a very quick response. However, since the spool is not directly controlled by external controls, to vary the orifice area as required, the relationship between the spool displacement and the corresponding orifice area i.e., the *Area-schedule* needs to be designed appropriately.

Once an appropriate area-schedule is calculated, it is built into the physical design of the valve during manufacturing by making modifications to the traditional spool valve assembly, the details of which are presented in the next chapter. The only fact that is relevant at this point is that it is possible to design the area-schedules for the valve opening and closing case independent of each other which further increases the flexibility in the control design.

2.3.4 Analysis of the internal feedback loop

In this section, we evaluate the stability of the system at its equilibrium point. The equilibrium point can be obtained by solving the dynamic equations (2.1)-(2.6) for a specific lift value. While evaluating the Jacobian matrix at the equilibrium point, some of entries become singular. For

example, during valve opening, the upper feedback chambers are connected to the reservoir and thus the pressure in both the chambers is almost equal to the reservoir pressure. The pressures in the bottom feedback chambers are almost identical when the system comes to a rest. The identical pressures imply that the flow rates between the corresponding chambers is very close to 0. Therefore, some of the partial derivatives of the equations describing the dynamics of these pressures become singular at the equilibrium point.

To avoid these numerical issues, the pressure in the upper feedback chambers is assumed to be equal to the reservoir pressure. The bottom feedback chambers are represented as a single volume whose pressure dynamics depend only on the motion of the actuator and the spool. These changes result in a 6^{th} order model which can represent the system's dynamics at the equilibrium point accurately.

The Jacobian matrix of the reduced order model for the valve opening case is constructed. The area-schedule is represented as $A_{spool} = f(X_{spool})$. The eigenvalues $\gamma_i(J(\chi_{eq}))$ of the Jacobian matrix at the equilibrium point are calculated in terms of $\frac{dA_{spool}}{dX_{spool}}$. The only condition required to place all the eigenvalues on the open left half plane i.e., $\gamma_i < 0$ was that $\frac{dA_{spool}}{dX_{spool}} > 0$. This constraint is automatically satisfied by the design of the system for all the physically realizable area-schedules. The equilibrium points corresponding to different lift values also showed the same characteristics and hence it can be stated that, for the engine valve opening case, the equilibrium points corresponding to each of the desired lift values are stable.

For the engine valve closing case, a similar analysis shows that the valve can be stopped at any desired position by activating the IFS appropriately and the corresponding equilibrium points are all stable. However, in actual practice, the engine valve is required to close with a finite seating velocity and hence the IFS is used only to decelerate the valve before it lands on the seat and is held against the seat by the preload force of the spring.

2.3.5 Effect of the area-schedule on system performance

From the above analysis, we find that the equilibrium point of the closed loop system is stable. However, we still need to control the $A_{spool}(t)$ such that the trajectory from the initial condition to the equilibrium point is desirable. Many of the system's trajectories from the initial condition to the equilibrium point are undesirable from a robust performance point of view. The internal feedback system should thus control the trajectory of the closed-loop system by varying the orifice area accordingly and this is done so by an appropriate design of the area-schedule.

A linear area-schedule i.e., $A_{spool} = k \cdot [1 - |X_{spool}|]$ similar to that of conventional proportional valves could cause cavitation inside the actuation chamber. Cavitation occurs when the flow rate to

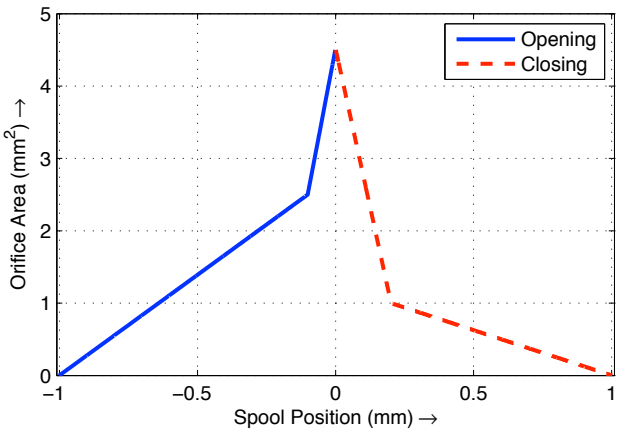

Figure 2.5: Hand tuned Area-schedules used in the simulations

a particular chamber is not sufficient to maintain the chamber pressure $\geq P_{vap}$ (vapor pressure of the fluid). Hence, during valve opening, if the flow to the actuation chamber is shut off too quickly while the valve is still moving, it will cause cavitation. Since cavitation can severely damage the system, it needs to be avoided by controlling the flow to the actuation chamber. A linear area-schedule also may not be able to decelerate the engine valve to acceptable seating velocities for conditions corresponding to an engine speed of 2500 RPM or above.

A more sophisticated area-schedule with two slopes as shown in Fig. 2.5. The point where the slope changes is a parameter that is tuned by trial and error to ensure satisfactory performance. It will be referred to as the "Hand-Tuned (HT)" area-schedule.

For valve opening, the best possible hand-tuned area-schedule can control the pressure profile to ensure that the minimum value is above $1\times10^5 Pa$ even for very demanding conditions. Although this is satisfactory when all parameters are exactly as modeled, in practice there will be variations due to dynamic operating conditions, manufacturing defects and wear. Simulations with perturbed parameters using the hand-tuned area-schedule indicate the possible occurrence of cavitation during valve opening. If an area-schedule is designed such that the minimum pressure in the actuation chamber is much higher than the hydraulic fluid's vapor pressures, the system would then become insensitive to parameter perturbations within a certain tolerance limit.

For valve closing, the hand-tuned area-schedule is a very conservative design because, it decelerates the engine valve very early and lets it travel with a low velocity till it lands on the seat. Though this can ensure a low seating velocity, it keeps the valve near the seat for a long time before closing which leads to pumping losses in the engine. The peak pressure in the actuation chamber is also quite high and is not desirable from a structural design perspective since it can

cause fatigue damage. An ideal trajectory for closing would be one in which the actuation chamber pressure is moderate and hence decelerates the engine valve steadily only when it is near the seat. This will minimize the closing time and hence avoid the throttling of cylinder gases.

If the area-schedules are designed by considering all the dynamics of the system, the pressure profile can be optimized to satisfy the requirements for both the valve opening and the closing case. The required area-schedules would then be more complicated than the 2-slope design. Due to the increased degrees of freedom and the complicated dynamics of the entire closed loop system, its design become non-intuitive and hence can no longer be designed by trial and error. A systematic design procedure which can account for all the dynamics of the system is thus required.

2.3.6 Optimization of the Area-Schedule

To optimize the area-schedule, assuming that A_{spool} is controllable independently, an $A_{spool}(t)$ that can ensure the desired trajectory for all the states of the system is determined. By matching the spool displacement $X_{spool}(t)$ corresponding to the obtained $A_{spool}(t)$, the optimal nonlinear mapping $A_{spool} = f(X_{spool})$ can then be determined. The plant and the controller are both nonlinear with discontinuities. This makes it difficult to obtain an analytical solution to the nonlinear optimization problem. However, since the area-schedule is a static physical design parameter which is built into the system during manufacturing, it can be evaluated offline. Therefore, it can be solved numerically and the computation time is not a limiting factor. Dynamic Programming [39] is used to solve the optimization problem since it can retain all the non-linearities in the dynamics and can also enforce complicated constraints and performance requirements.

The application of the conventional dynamic programming procedure for this problem turned out to be infeasible. This was mainly due to the extremely stiff nature of the system which required a very small time step for discretizing the dynamic model. The relationship between the grid size and the time step between each stage implied that, a smaller time step required a finer grid for each of the states. The fine gridding coupled with the large number of states (n = 9) gave rise to a problem commonly referred to as the "Curse of dimensionality" which makes the problem computationally infeasible due to insufficient memory and very high computation times.

To overcome these difficulties, the conventional dynamic programming procedure is modified using the techniques applied in [40, 41, 42] to make it suitable for solving this higher order problem. The following steps along with Fig. 2.6 gives a broad outline of the procedure used in the solution of the full order optimization problem.

The implementation details for each of the steps in the flow chart are given below

1. The interval of interest is chosen as the the time between the activation of the IFS and the

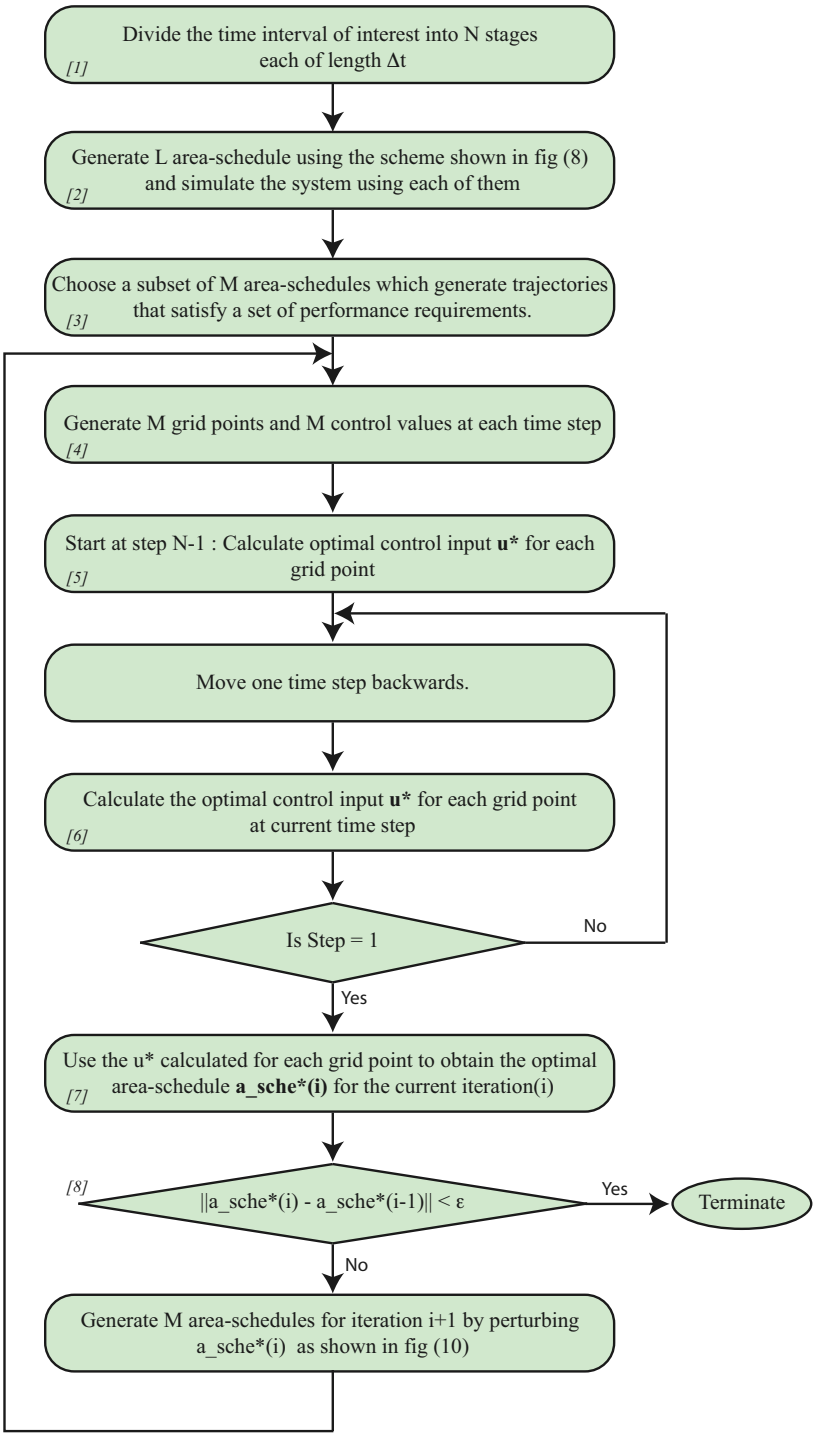

Figure 2.6: Flowchart for the area-schedule design procedure

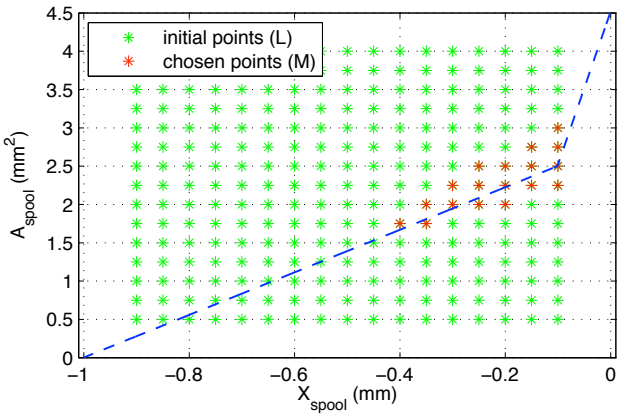

Figure 2.7: Area-schedule candidates for generating the grid points for the first iteration

approximate time at which the system reaches the equilibrium.

2. The L number of area-schedules are similar to that of the hand-tuned schedule i.e., contain 2-slopes . The X & Y coordinates of the green (light grey) points shown in Fig. 2.7 correspond to the point at which the slope changes in the area-schedule. A sample area-schedule corresponding to one of the points is also shown in the same figure. Perform simulations for all of the L area-schedules by using the system state at the instant when the IFS is activated as the initial condition.

3. Since, many of the L trajectories generated lie outside the acceptable range of values for the states, choose M trajectories based on a set of predetermined and slightly relaxed constraints. For example, for the opening case, $P_a(t) \geq -15 \times 10^5\ Pa$ is used as the constraint. The area-schedules that satisfy this condition are shown in red (dark grey) in Fig. 2.7. This step is used to reduce the computation effort i.e., number of grid points at each stage.

4. The M grid points are obtained by sampling the M trajectories at each time step. A grid point is defined as a combination of all the states $[x_1, x_2, ...x_9]$ at that time instant. M values of the control input $\mathbf{u}$ at each time step are obtained by sampling the $A_{spool}(t)$ corresponding to each of the M area-schedules.

5. For the stage N-1, integrate the system model using the first grid point as the initial state and each of the M values of the control input. Choose the control input that minimizes the cost defined by (2.7) and store it as the u^* corresponding to that grid point. The exact details of (2.7) are discussed later. Repeat this procedure for each of the M grid points and store the corresponding optimal control input for each grid point.

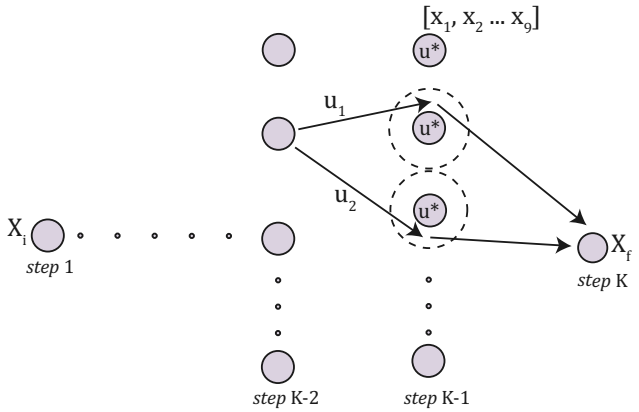

Figure 2.8: Illustration of the modified Dynamic Programming procedure

6. For stages $(N-2) \rightarrow 1$, start at each grid point and integrate the system's dynamic model using the first of the M control inputs over one stage length. Update the cost function based on the state generated by the integration. Choose the optimal control input assigned to the grid point that is closest to the state generated by the previous integration and continue integrating forward as shown in Fig. 2.8. Proceed till the last stage using the same procedure while updating the cost function at each stage. Repeat the same procedure for all the M control inputs and choose the control that gives the lowest value of the cost-function as the best control for that grid point. Carry out this procedure to calculate the corresponding best control for each grid point at each stage.

7. Starting at stage 1, integrate using the initial state and the stored value of the optimal control input over one stage length. Continue integrating till the last stage by following the procedure similar to the previous step. Store the optimal control input at each stage and the corresponding values for each of the states. By matching the optimal control sequence $u(k) = A_{spool}(k)$ and the corresponding $X_{spool}(k)$, the optimal area-schedule for the 1^{st} *iteration* is obtained.

8. Compare the obtained area-schedule with the optimal area-schedule from the previous iteration. For the 1^{st} iteration, the hand-tuned area-schedule can be used as the reference. If the difference is larger than a desired amount repeat the entire optimization procedure using perturbed area-schedules as shown in Fig. 2.9

Once the optimal area-schedule for the valve opening case is obtained, it is used to calculate the initial state for the closing case. Repeating steps 1 to 9 with the cost function modified as described

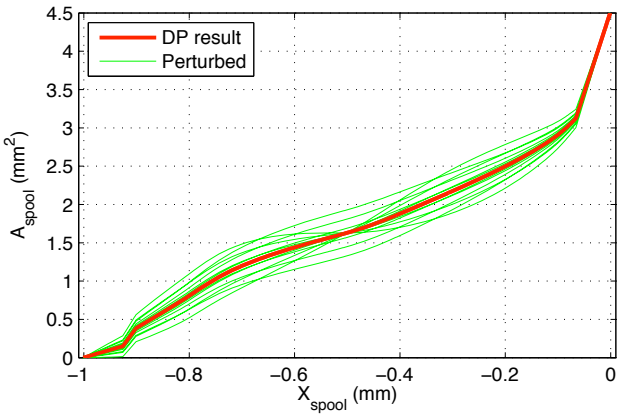

Figure 2.9: Area-schedule candidates for the next iteration obtained by perturbing the optimal area-schedule at the current iteration

in (2.8) results in the optimal area-schedule for the valve closing case. Since the grid points are chosen as a combination of the states rather than discretizing each of the states separately, the grid size becomes independent of the problem dimension. This makes the procedure computationally feasible. The cost functions used at each stage for valve opening and valve closing are presented in (2.7) and (2.8) respectively. $[X_{act}, V_{act}, X_{spool}, V_{spool}, P_a, P_{act1}, P_{act2}, P_{IFS1}, P_{IFS2}]$ are represented by $\chi = [X_1, X_2, ...X_9]$. A_{spool} is represented by u. "N" represents the total number of stages and "k" represents the current stage.

$$g = \lambda_1 \left(\chi(N) - \chi_f^*\right)^2 + \sum_{k=1}^{N-1} \begin{pmatrix} \lambda_2 \left(u(k) - u(k+1)\right)^2 + \lambda_3^* \left(X_2(k) - 0\right)^2 \\ +\lambda_4^* \left(X_4(k) - 0\right)^2 + \lambda_5^* \left(X_5(k) - P_{a(min)}^*\right)^2 \end{pmatrix} \tag{2.7}$$

$$\lambda_3^* = \begin{cases} \lambda_3 & \text{if } k > N/3; \\ 0 & \text{otherwise.} \end{cases} \quad \lambda_4^* = \begin{cases} \lambda_4 & \text{if } X_4(k) \geq 0; \\ 0 & \text{otherwise.} \end{cases} \quad \lambda_5^* = \begin{cases} \lambda_5 & \text{if } X_5(k) \leq P_{a(min)}^*; \\ 0 & \text{otherwise.} \end{cases}$$

$$g = \lambda_1 \left(\chi(N) - \chi_f^*\right)^2 + \sum_{k=1}^{N-1} \begin{pmatrix} \lambda_2 \left(u(k) - u(k+1)\right)^2 + \lambda_3^* \left(X_2(k) - X_2(k+1)\right)^2 \\ +\lambda_4^* \left(X_4(k) - 0\right)^2 + \lambda_5^* \left(X_5(k) - P_{a(max)}^*\right)^2 + \lambda_6^* \left(X_2(k)\right)^2 \end{pmatrix} \tag{2.8}$$

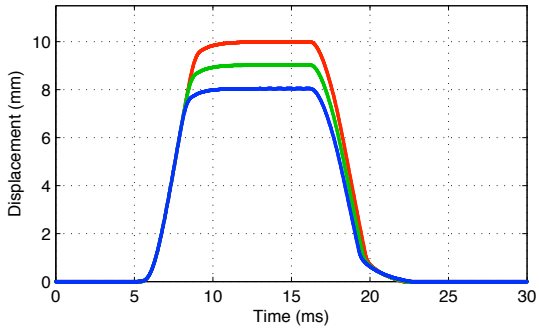

Figure 2.10: Displacement of the engine valve (Lift control)

$$\lambda_3^* = \begin{cases} \lambda_3 & \text{if } |X_2(k) - X_2(k+1)| \geq V_{seat}(des); \\ 0 & \text{otherwise.} \end{cases} \qquad \lambda_4^* = \begin{cases} \lambda_4 & \text{if } X_4(k) \leq 0; \\ 0 & \text{otherwise.} \end{cases}$$

$$\lambda_5^* = \begin{cases} \lambda_5 & \text{if } X_5(k) \geq P^*_{a(max)}; \\ 0 & \text{otherwise.} \end{cases} \qquad \lambda_6^* = \begin{cases} \lambda_6 & \text{if } 0 < |X_2(k)| < V_{min}(des); \\ 0 & \text{otherwise.} \end{cases}$$

The first term in the cost function ensures that the required final state χ_f^* is reached. The second term is designed to ensure a smoothly varying control input A_{spool} with respect to time. The third term minimizes fluctuations in the valve velocity at the end of the opening cycle and for the closing case, it ensures that the valve seating velocity is not higher than a specified value. The fourth term is designed to penalize any spool oscillations. The spool oscillations are undesirable as they get reflected as wave-like patterns in the designed area-schedules and make it very difficult to manufacture [43]. The fifth term is used to set the bounds on the actuation chamber pressure. The sixth term in the closing case penalizes all velocities less than a certain desired value which ensures that the engine valve slows down only at the last possible instant. A careful choice of the weighting parameters λ_1 to λ_6 can yield different designs for the area-schedule which can satisfy different performance requirements.

2.4 Case Studies

In this section, the technique developed previously is used for calculating the area-schedule for a system to satisfy a set of performance criteria. The physical design parameters of the system for which the designs are calculated are shown in Table. I. It is then followed by the analysis of the robustness of the calculated designs by simulating the system with perturbed parameters.

Fig. 2.10 and Fig. 2.11 show the displacement and velocity of the valve obtained by simulating

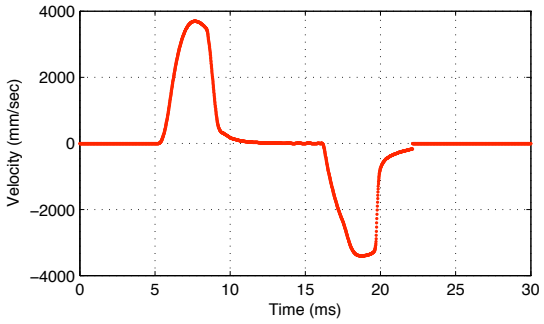

Figure 2.11: Velocity of the engine valve (10 mm lift case)

the mathematical model with the hand-tuned area schedule shown in Fig. 2.5. Valve lift is controlled to 8 mm, 9 mm and 10 mm by activating the IFS at different engine valve lift positions. For valve closing, activating the top on-off valve at different valve lift positions ensures that the valve seats with an appropriate velocity.

2.4.1 Area-schedules obtained from dynamic programming

This section presents the results of the optimization procedure for designing the area schedules for a set of performance requirements. The obtained designs are then verified by simulating the model with the obtained area-schedules and then compared to the trajectories obtained from simulations using the hand-tuned area schedules.

Engine Valve opening

For the valve opening case, the weights are tuned to ensure that the actuation chamber pressure does not drop below $10 \times 10^5 Pa$, which helps prevent cavitation even in the presence of parameter

Table 2.1: Parameter values for the Dynamic model

Parameter	Value *(units)*	Parameter	Value *(units)*
M_{act}	$80 \times 10^{-3}(Kg)$	A_a	$50 \times 10^{-6}(m^2)$
K_{act}	$20 \times 10^3(N/m)$	A_{act_1}, A_{act_2}	$4.9 \times 10^{-6}(m^2)$
$F_{preload}$	$150(N)$	A_{f1}, A_{f2}	$0.35 \times 10^{-6}(m^2)$
b_{act}	$20(N.s/m)$	$A_{spool}(max)$	$4.5 \times 10^{-6}(m^2)$
M_{spool}	$5 \times 10^{-3}(Kg)$	A_{IFS_1}, A_{IFS_2}	$9.8 \times 10^{-6}(m^2)$
K_{IFS_1}, K_{IFS_2}	$15 \times 10^3(N/m)$	C_d	0.6
b_{IFS}	$10(N.s/m)$	ρ	$890(Kg/m^3)$
P_T	$10 \times 10^5(Pa)$	$x^*_{act}, x^*_{act_1}$	$2 \times 10^{-3}(m)$
$P_s(opening)$	$40 \rightarrow 120 \times 10^5(Pa)$	$x^*_{act_2}$	$10 \times 10^{-3}(m)$
$P_s(closing)$	P_T	$x^*_{spool_2}, x^*_{spool_2}$	$5 \times 10^{-3}(m)$
β	$1724(MPa)$		

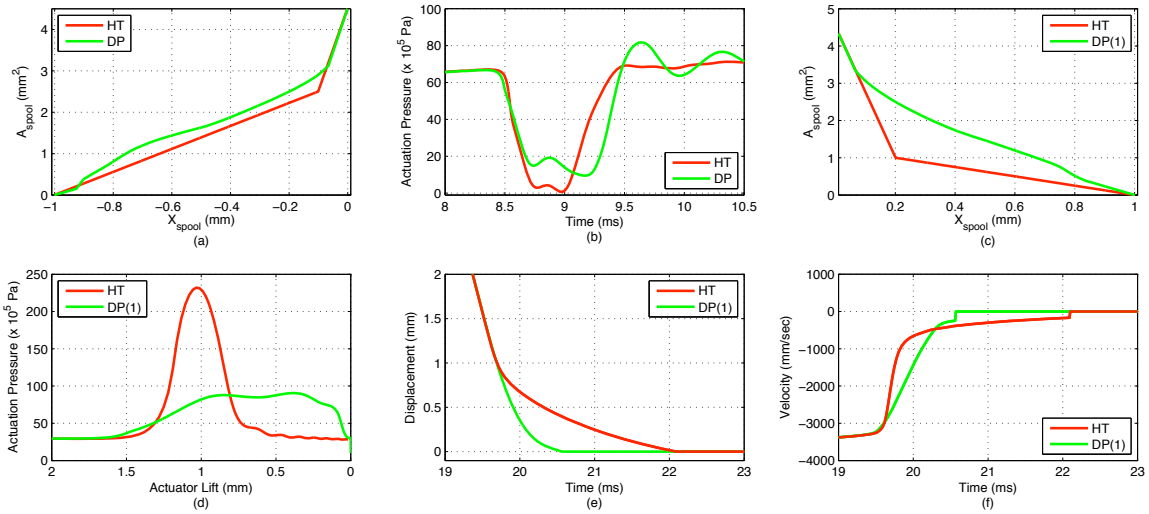

Figure 2.12: (a) Area-schedule for valve opening; (b) Actuation chamber pressure during opening; (c) Area-schedule for valve closing; (d) Actuation chamber pressure during closing; (e) Actuator displacement during closing; (f) Actuator velocity during closing.

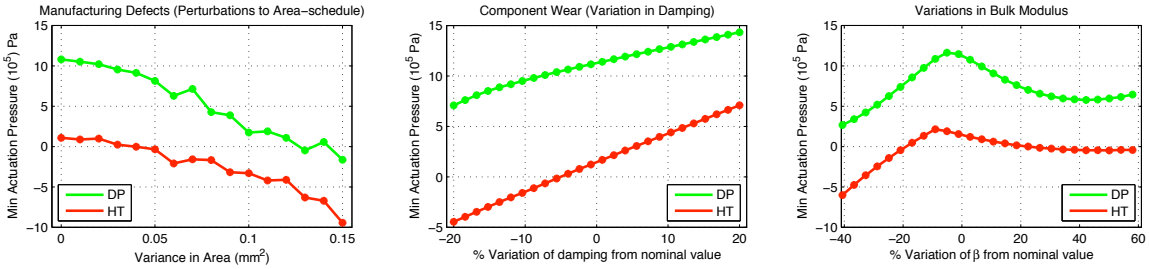

Figure 2.13: Effect of Parameter perturbations during valve opening (Manufacturing Defects, Component Wear and Variation in Bulk Modulus)

perturbations. By assigning penalties to positive velocities of the IFS spool, the oscillations are minimized and thus a smoothly varying area-schedule is obtained. The result obtained from the dynamic programming procedure is shown in Fig. 2.12(a). Fig. 2.12(b) shows that, the actuation chamber pressure does not drop below $10 \times 10^5 Pa$ when using the designed area-schedule.

Engine Valve closing

For the valve closing case, two designs are generated based on completely different performance criteria. For the first case, the weights are tuned to minimize the peak value of the actuation chamber pressure which results in a uniform deceleration of the engine valve and hence reduces the closing time compared to the hand-tuned case. For the second case, by assigning maximum penalty to low velocities ($|V_{act}| \leq 0.35 m/s$) and removing constraints on the peak value of the actuation chamber

pressure, a design which causes rapid deceleration at the very last moment is produced. This design would have the least valve closing time. Similar to the opening case, the IFS spool oscillations are penalized. The results obtained from the dynamic programming procedure are shown in Fig. 2.12(c). Fig. 2.12(d) shows the trace of actuation chamber pressure as a function of the engine valve position. It can be seen that, the hand tuned schedule raises the pressure to a high value very early and thus slows the engine valve down far away from the valve seat. The design obtained for the first set of constraints maintains a moderate value of pressure throughout the closing cycle and this is reflected in the displacement and velocity traces shown in Fig. 2.12(e) and (f). The second design raises the pressure to a high value very close to the seat causing the engine valve to decelerate at the last possible instant. This is also reflected in the reduction of the closing time.

2.4.2 Robustness to Parameter perturbations

The motivation behind designing the area-schedule systematically was to ensure that the resulting design would be able to satisfy the performance requirements in the presence of parameter variations. To analyze the effect of manufacturing defects in the area-schedule, perturbations are introduced to the area-schedule in the form of random amplitude variations. The nominal area-schedule is divided into 200 data points with a spacing of $0.01mm$. Each point in the array is then modified as follows,

$$A^*_{sche}(i) = A_{sche}(i) + \Psi(0, \nu) \tag{2.9}$$

for i = $[1 \rightarrow 200]$, and $\Psi(0, \nu)$ is a zero-mean normally distributed random number with variance of ν. The perturbed area-schedule that is used in the simulations is then generated by interpolating this array to obtain the A_{spool} for each of the X_{spool} values. Fifteen different realizations of the perturbed area-schedules are generated for each of the variance values by repeatedly using (2.9) to sufficiently capture all possibilities. The system is then simulated with each of the area-schedules and the parameter corresponding to the worst performance is recorded.

With the progress of time, various components in the system exhibit wear and this will be reflected in the damping between sliding surfaces. To the study the effect of the variation in damping, the system is simulated by varying the damping coefficients of both the actuator and the IFS spool. The system is simulated with bulk modulus values ranging from 60% to 160% of the nominal value to understand the effect of variations in the bulk modulus.

The following section presents the results of the simulations along with a detailed discussion of the various phenomena observed for each case.

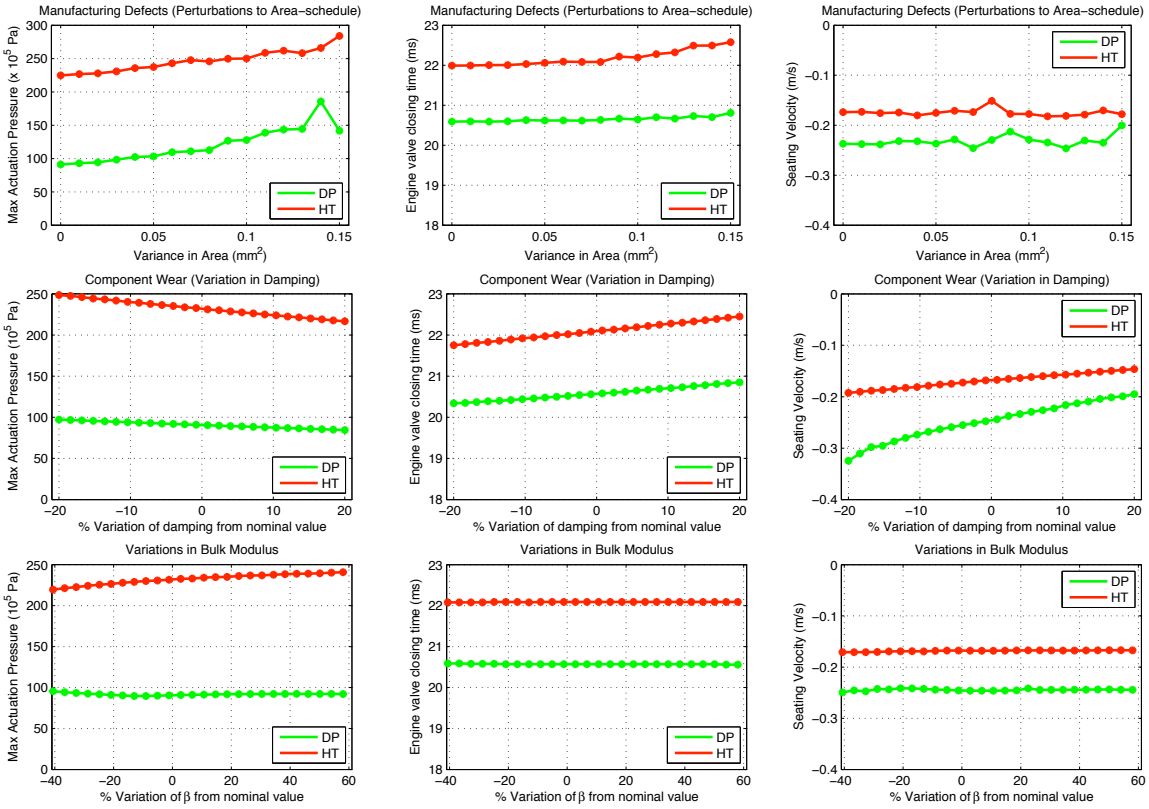

Figure 2.14: Effect of Parameter perturbations during valve closing (Manufacturing Defects, Component Wear and Variation in Bulk Modulus)

Engine Valve Opening

The parameter that is of interest during valve opening is the minimum value of the actuation chamber pressure. To avoid cavitation in the presence of parameter variations, the area-schedule has been designed such that, there is a safety margin i.e., $\min(P_a)$ is $10 \times 10^5 Pa$ for the nominal system. The comparison of the simulation results obtained using the DP designed area-schedule with those obtained by using the hand-tuned schedule are shown in Fig. 2.13.

An increase in the variations of the area-schedule from the nominal design alters the pressure profile significantly. For the same variance value, some realizations of the perturbed area-schedule increase the the minimum pressure, while others indicate a decrease. Since we only record parameters corresponding to the worst case performance, a steady trend indicating an almost linear relationship of the minimum pressure with the increasing variance is observed.

The damping coefficient affects the peak velocity of the actuator during engine valve opening and thus affects the minimum of the actuation chamber pressure. The pressure profile varies significantly when the bulk modulus is increased or decreased. The variation of the minimum pressure with respect

to the parameter perturbations is almost identical for both the hand-tuned and the DP designed area-schedules.

However, the reason the area-schedule designed from DP is able to perform better than the hand-tuned schedule in all the cases is because of the safety margin built into the system. Hence, a significant amount of perturbations can be tolerated before the pressure profile deteriorates to the extent that cavitation occurs.

Engine Valve Closing

For valve closing, apart from the requirement of a low valve seating velocity, it is desirable to minimize the valve closing time to avoid engine gas throttling and also have a reduced peak pressure in the actuation chamber. The second design using the dynamic programming has a very small valve closing time, which can be attributed to the rapid decelerating of the valve at the last moment. However, in the presence of parameter perturbations, it results in either valve bounce due to excessive actuation chamber pressure or high valve seating velocities due to a delayed pressure rise in the actuation pressure.

The first design ensures a moderate pressure throughout the operation of the IFS. This ensures that the deceleration is distributed evenly throughout the operation of the IFS and hence will not be adversely affected by the parameter variations. The first design is thus chosen and its performance is compared with the performance of the hand-tuned schedule.

The peak actuation chamber pressure, the valve closing time and the valve seating velocity together can serve as good indicators of the performance of the system during closing. A minimized value of the first two parameters while maintaining the third parameter below a certain desired value is a good indicator of satisfactory performance. The results of these tests are shown in Fig. 2.14.

For the case with perturbed area-schedules, the simulations for each variance value show that the peak actuation chamber pressure increases steadily with the increase in deviations. The deviations in the area-schedules affect the pressure profile locally, but there is an overall averaging effect of these fluctuations over the entire IFS operating cycle. Hence it does not affect the closing timing and the valve seating velocity to a great extent.

The effect of damping is almost identical to the opening case and thus affects the peak pressure and the closing times. The effect of the bulk modulus on the peak pressure is also quite intuitive. For the hand-tuned schedule, since the fluid is throttle heavily as soon as the IFS is activated, an increase in bulk modulus causes an increase in the peak actuation chamber pressure. For the DP designed area-schedule, the throttling is more steady and hence the effect of the bulk modulus is less pronounced. Since the pressure profile is automatically adjusted by the feedback system, the

closing time remains unaffected.

The results show that the seating velocities are within the acceptable limit. The variation of the seating velocity with respect to the change in parameters *(especially for the DP designs)* can be attributed to some oscillations of the actuator velocity between $0m/s$ and $-0.35m/s$ which can be easily suppressed by adding additional constraints if needed.

It can be observed that, even under significant parameter variations, the DP designed area-schedule is able to perform better than the hand-tuned schedule by closing 1 ms earlier with a valve seating velocity $< 0.35m/s$ and a lesser peak pressure in the actuation chamber.

2.5 Summary

This work focused on the development of a systematic design optimization procedure for a new production oriented EHVA system which is capable of full valve event flexibility. The system architecture is such that the performance of the system is largely dependent on the physical design parameters. Optimization of the design parameters based on trial and error or intuition to improve certain performance characteristics proved to be inadequate and thus motivated the development of a systematic model based design method. The design problem is converted into an optimal control problem and solved numerically using the dynamic programming procedure. The proposed method provides the flexibility of specifying the performance requirements and constraints for optimizing the designs for a wide range of performance requirements. The effectiveness of the obtained designs has been verified with case studies.

Chapter 3

Physical Design of the Spool Valve with the Optimal Area-Schedule

This chapter addresses the second aspect of the design optimization procedure for the valve actuation system with internal feedback i.e., physically realizing the optimal area-schedule obtained in the previous chapter. The modifications to a traditional spool that are required to realize a non-linear area-schedule are first presented. A systematic procedure for analyzing the modifications of the spool using a CFD based method is introduced. An accelerated analysis procedure based on the geometry of the spool is then introduced which enable the development of an iterative procedure for synthesizing the spool design with the required area-schedules.

3.1 Background on Traditional Design of Spool Valves

Spool based flow control valves are an integral part of a large class of fluid power systems and the basic operating principle for these devices is as follows. The valve body has grooves and channels machined into it which are connected to the various work ports of the valve. A cylindrical spool slides axially inside the valve body to allow or block fluid flow between various grooves which in turn controls the fluid flow between the corresponding ports. Depending on the number of ports, the design of the housing and the spool, and the mechanism for actuating the spool, a wide variety of flow control valves can be realized. These range from simple manually operated direction control valves to electro-mechanically actuated precision flow regulating servo valves. The various characteristics of a flow control valve, such as the metering orifice area, discharge coefficient, hydraulic flow forces and dynamic response are all dependent on the design of the valve body and the spool. Significant

progress in thoroughly understanding the relationship between the various design parameters and the performance characteristics has been made thanks to the research efforts of various investigators.

The flow induced force on the spool due to change in momentum of the fluid inside the valve has been extensively investigated since it can increase the actuation force requirement and thus decreases the dynamic response characteristics of the valve. [44, 45] presents the experimental and CFD (computational fluid dynamics) based analysis to evaluate the steady flow forces on open center hydraulic directional valves and also highlight the differences when compared to the conventional closed-center valves. [46] shows that the introduction of compensation profiles both on the spool and the valve body can lead to a significant reduction in the overall flow forces. [47, 48] present the idea of modifying the valve design to use the flow forces advantageously to make the spool dynamics unstable and thereby improve its agility. This is shown to improve the dynamic response of the valve while using the existing electromechanical actuator. Recent experimental investigations from [49] has shown that in addition to the steady flow forces, the forces due to the pressure transients induced by the spool motion also contribute significantly to the dynamic response of the valve. The spool valve under investigation in this study is part of a hydro-mechanical internal feedback loop (detailed explanation presented later) where the large magnitude of the hydraulic actuation force makes the flow induced forces less of a concern.

3.2 Spool Valves with Notches

In the current setting, since the spool position is not actively controlled by external means, to achieve the required flow characteristics, the design of the spool needs to be modified to alter the relationship between the spool stroke and the effective area. It is common practice to introduce notches on the spool and other modifications to the valve body to vary the performance characteristics of the valve. [50] presents the experimental investigation for determining the discharge coefficient of a spool valve with one specific notch design. [51] uses CFD to characterize the discharge coefficient of two types of notches i.e., "post notch" and "end-mill notch". [46] presents the CFD results for characterizing a spherical notch and the effect of using a cylindrical profile to control the metering at small openings.

In most cases, the notches are designed to influence the flow induced forces or the metering area at very small spool deflections. However for this application, the notch is used to influence the metering characteristics for the entire range of the spool motion and thus needs to be designed accordingly. Hence, the idea of choosing simplified geometries and only modifying their characteristic dimensions will severely limit the ability to arbitrarily control the shape of the spool position *vs.* metering area curve. At the same time, relying only on experiments and CFD to calculate the notch designs will be

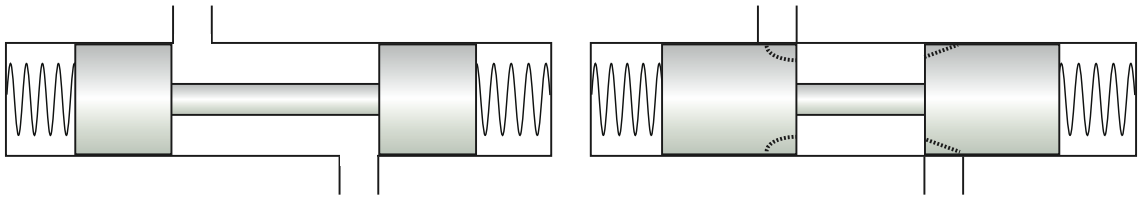

Figure 3.1: Schematic of a spool valve : (a) conventional design, (b) modified design with notches on the spool lands.

prohibitive due to the cost, computational effort and the lack of a "cause and effect" type knowledge about the geometry to guide the design process. The objective of this research work is to develop a systematic method to understand the effect of the 3-D geometric shape of the notches on the valve's effective area at each spool position. While, a CFD based method is first used for understanding the metering characteristics of some representative notch designs, a method based purely on the notch geometry is developed to reduce the time required for the analysis as well as gain a better understanding of the influence of the geometry on the metering characteristics. The geometry based method is then implemented into an iterative design procedure to calculate the notch geometry for any desired variation of metering area with respect to the spool-stroke. As mentioned previously, since the primary focus of this article is the investigation of the relationship of the metering orifice area with respect to the spool stroke, it will henceforth be referred to as the "area-schedule" for conciseness.

The design changes required to realize the desired area-schedule are as follows. The schematic of a conventional two-way spool valve is shown in Fig. 3.1(a). The valve body contains grooves which are connected to each of the ports. An axially sliding spool controls the flow rate by varying the area that is available for the fluid flow. For a given configuration i.e., spool position, the geometry corresponding to the section which predominantly restricts the fluid flow is called the metering geometry. For example, when the spool slides to the right, the groove on the left and the corresponding surfaces on the spool become the metering section. A significant portion of the pressure drop across the entire valve happens in this region and thus the flow rate is predominantly a function of the effective area of the metering geometry. The area-schedule for traditional flow control valves is typically linear. The arbitrary area-schedule is realized by modifying the conventional spool valve as shown in Fig. 3.1(b). The grooves in valve body are positioned such that, if a traditional spool is used, there would be no flow between the two ports for any position of the spool. Notches are then cut into the surface of the spool as shown in Fig. 3.1(b) to create the metering geometries. The center position of the spool corresponds to the maximum area and for any deflection of the

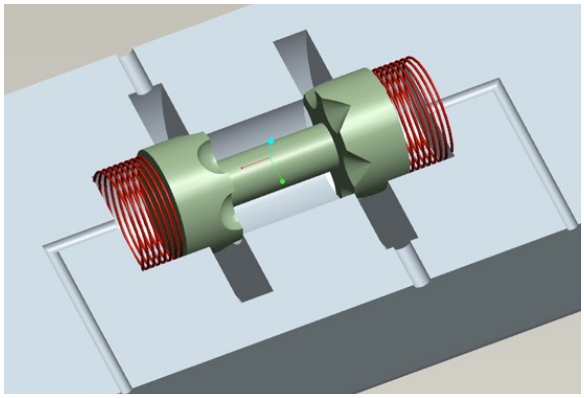

Figure 3.2: CAD model showing the valve body and the spool with the notches.

spool, the notch on the trailing edge starts to act as the metering geometry. For example, when the spool deflects to the right, the notches on the left surface start to throttle the flow while the effect of the notch on the right is diminished. Since the notches on both the faces are designed independent of each other, it is possible to design the notches to obtain completely different area-schedules for both directions of spool movement.

Fig. 3.2 shows a more detailed 3-D CAD model of the valve. The metering characteristics of spool valves with notches have been investigated previously. However, in some cases, the notches had simple geometries [52, 53] such that the orifice area can be described using analytical expressions. In other cases [51, 46], the notch designs were predetermined by other factors (flow forces) and the analysis was predominantly aimed at characterizing the discharge properties. In this section, a systematic method to calculate the effective metering characteristics for any given notch geometry is developed with the aim of guiding the notch design procedure. The well established CFD based procedure is first used for studying the effect of the notch geometries on the effective area. It is followed by the development of a method based purely on geometry to predict the metering orifice area for any given notch design. The geometry based procedure helps identify the fact that the mean area available for the flow through the notch predicts the effective area better than the conventional method of using the smallest restriction in the fluid path. Experimental results from a prototype spool with notches are then presented to validate the proposed analysis procedures.

3.3 CFD Analysis of the Notch Designs

Due to the complex three-dimensional nature of the fluid flow through the valve, the use of computational fluid dynamic simulations for the analysis of the valve design has become widely accepted. When compared to experimental methods, apart from the obvious advantages such as

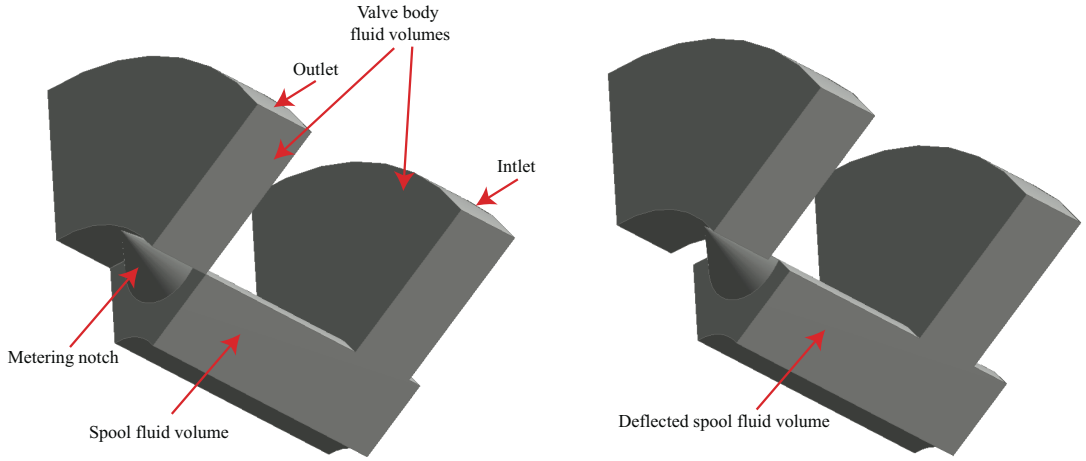

Figure 3.3: (a) Fluid volume corresponding to the spool and the valve body illustrating the metering geometry, (b) Fluid volume corresponding to a displaced spool.

reduced time and no manufacturing costs, CFD based methods also help in visualizing flow features inside a component which can offer various insights about the design. This section provides a brief description of the procedure for analyzing the effect of the notch geometry on the area-schedule. A commercially available package, "Fluent" is chosen for the simulations. The analysis procedure is first introduced using one specific notch design. It is followed by the results obtained from testing a set of representative notch geometries to obtain the corresponding area-schedules.

The first step in the analysis procedure is to model the fluid volume required for the CFD simulations by calculating the compliment of the valve's solid components as shown in Fig. 3.3(a). To avoid the effect of interaction between the notches on the two faces of the spool, the initial investigations consider the case where there are notches on only one face of the spool. The other face and housing are designed to offer minimal resistance to the fluid flow. Utilizing the symmetry of the fluid volume, it is sufficient to model just $1/6^{th}$ of the geometry with the appropriate boundary conditions. This helps to speed up the computations while maintaining the accuracy of the solutions. For the case where the spool is deflected from its center position, the fluid volume corresponding to the spool is displaced axially with respect to the fluid volume corresponding to the valve body as shown in Fig. 3.3(b). The corresponding metering geometry formed at the interface of the spool and the valve housing are highlighted in both the figures.

The fluid volume is then discretized using an unstructured scheme to achieve a balance between the accuracy of the solution and the computational effort as shown in Fig. 3.4. The appropriate pressure boundary conditions are applied to the two faces highlighted in Fig. 3.4. Hydraulic oil with

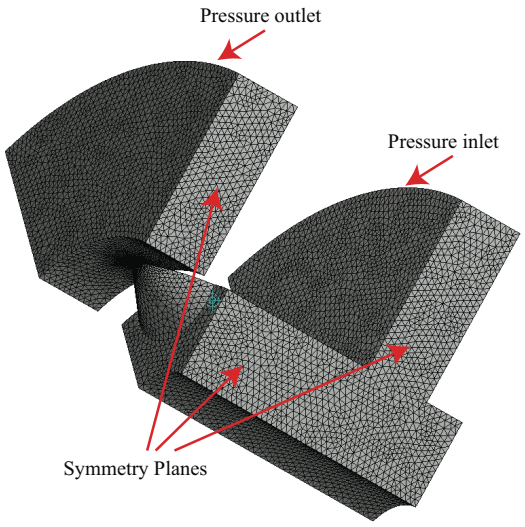

Figure 3.4: The discretized fluid volume (mesh) and the boundary conditions.

fluid density (ρ) = 865 Kg/m^3 and viscosity (μ) = 0.04 $Kgm^{-1}s^{-1}$ is used as the working fluid and a turbulence model based on the "$K-\epsilon$" scheme with the "RNG" option is chosen for the simulations. However, it was observed that except for cases where the spool is close to the center position with large pressure drops, the flow field tends to be laminar for most of the operating range. This is due to the fact that the flow area available for the fluid flow is extremely small when compared to the conventional spool valves of similar sizing. This phenomenon has the interesting effect that the flow is no longer directly proportional to the metering area for a given pressure drop. A more detailed discussion will be presented in the later sections.

Fig. 3.5 shows the path and velocity of the fluid in different parts of the valve. The fluid is accelerated in the metering section due to the reduction in the flow area. The mass flow rate is computed by integrating the mass-flux across each element at the inlet and outlet boundaries. As expected, the configuration with the deflected spool has a reduced flow rate when compared to the case with the centered spool. This process is repeated for incremental displacements of the spool to cover its entire range of motion and the flow rates corresponding to each case are computed. The tests are repeated for four different pressure drops ([P_1, P_2, P_3, P_4] =[3.5, 4.5, 5.5, 6.5] $\times 10^6$ Pa) across the valve and the results are shown in Fig. 3.6(a) . Following the standard technique of modeling the entire valve as an orifice, the effective area across the spool valve is calculated using,

$$C_d \cdot A = \frac{\dot{m}}{\sqrt{2\rho\Delta P}} \tag{3.1}$$

where $\dot{m}$ is the mass flow rate obtained from the CFD simulation, ΔP is the pressure drop across

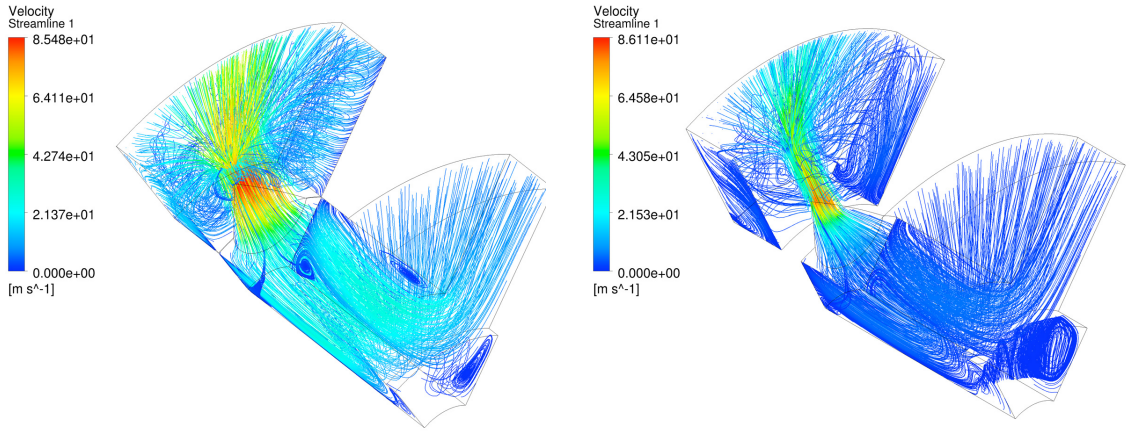

(a) (b)

Figure 3.5: Simulation results showing the path and speed of the fluid in various sections of the valve (a) when the spool is centered, (b) when the spool is deflected 50% of its stroke.

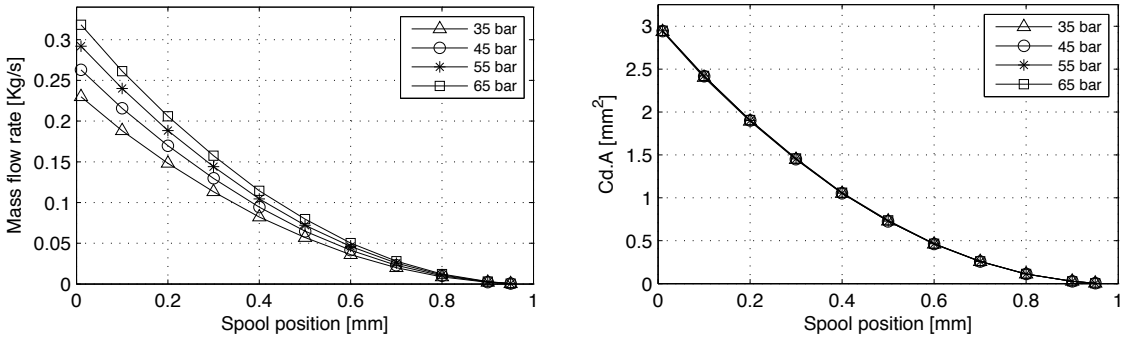

(a) (b)

Figure 3.6: (a) Variation of mass flow rate at different pressure drops, (b) Corresponding effective area calculated using the orifice equation.

the valve used in the simulation and ρ is the density of the working fluid. Fig. 3.6(b) shows the effective area corresponding to the four cases shown in Fig. 3.6(a). It can be seen that the four curves collapse into one, which suggests that the effective area is purely a function of the notch design.

Six different notch designs as shown in Fig. 3.7 are analyzed using the described CFD based method and the variation of the effective areas i.e., $C_d \cdot A$, for each case is shown in Fig. 3.8. The wide range of curves obtained from the six notch designs analyzed here suggest that by designing the notch appropriately, it would be possible to realize any required "area-schedule".

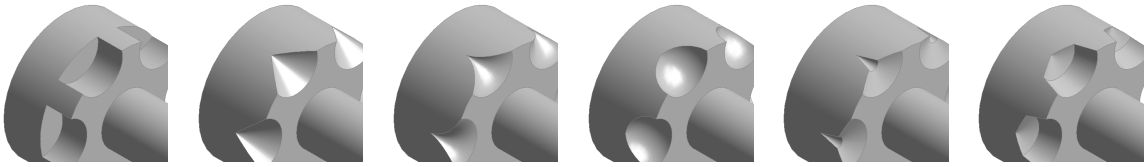

(a) (b) (c) (d) (e) (f)

Figure 3.7: Various notch geometries analyzed using the CFD based method.

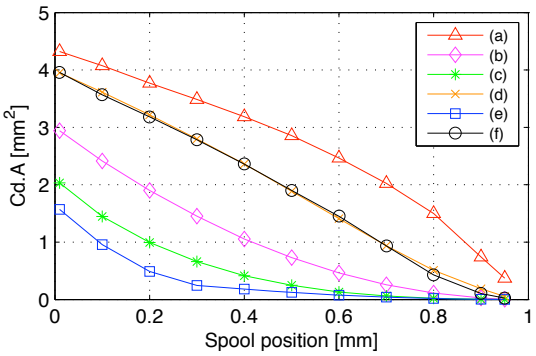

Figure 3.8: Effective orifice areas for notch designs shown in Fig. 3.7.

3.4 Geometric Analysis of the Metering Section

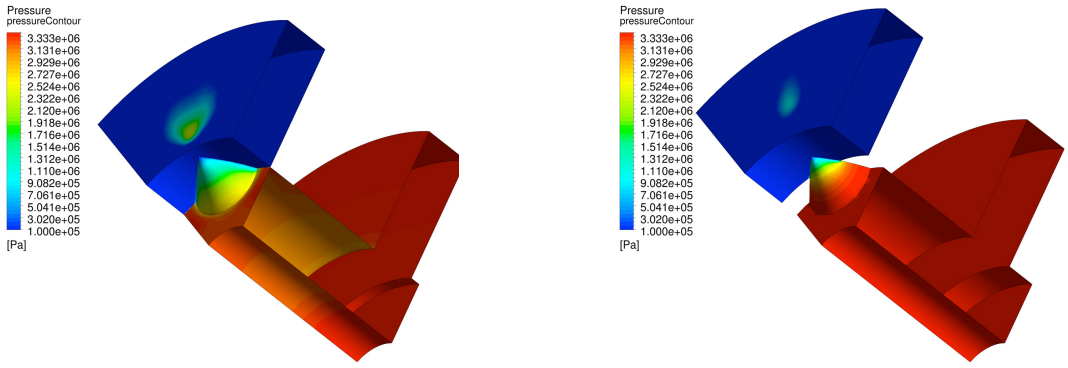

(a) (b)

Figure 3.9: Pressure distribution inside the valve for both configurations (a) centered spool, (b) deflected spool.

The technique presented in the previous section is useful for studying a given notch geometry. However, since the predicted effective area is a function of both the metering orifice area (depends on the geometry) and the discharge coefficient (depends on the geometry and the flow conditions), it cannot be directly used for the notch design purposes. For most of the conventional spool valves,

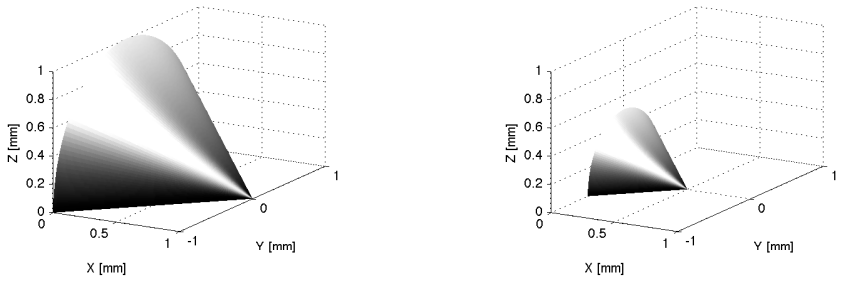

(a) (b)

Figure 3.10: Data required for the geometric analysis (a) region exposed to the groove in the valve body for the centre position, (b) region corresponding to 50% spool deflection.

the metering area is calculated analytically since the shape of the restriction is typically simple (intersection of regular geometries) and can be represented using analytical expressions. However, for the case with the 3-D notches, it is no longer possible to follow the same procedure since the metering section is now three-dimensional and can potentially have an arbitrary shape.

Hence, this section aims to develop a framework for rapidly estimating the metering area at each deflection for a given notch geometry of the spool. The proposed method is inspired by the data in Fig. 3.9 which shows the distribution of the pressure inside the entire valve for two configurations of the spool, i.e., the center position and a deflected position. It can be seen that, a significant portion of the pressure drop across the valve happens in the notch, especially in the region that is exposed to the groove in the valve body. Using this phenomenon, a method for calculating the metering area based purely on the geometry of the notch is proposed. Fig. 3.10(a) & (b) show the portions of the notch that are exposed to the groove in the valve body for two different positions of the spool (*un-deflected & 50% deflected*).

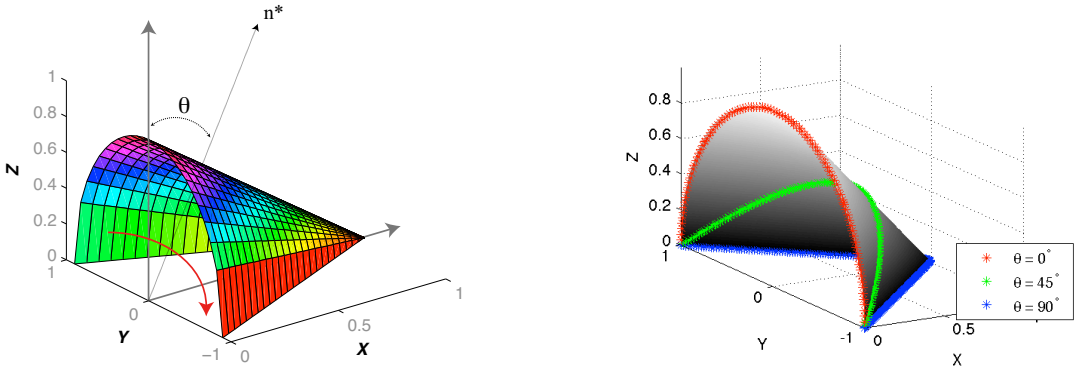

(a) (b)

Figure 3.11: (a) Nomenclature used in the analysis of the notch geometry, (b) Sample cross-sections corresponding to various values of θ overlaid on the notch geometry.

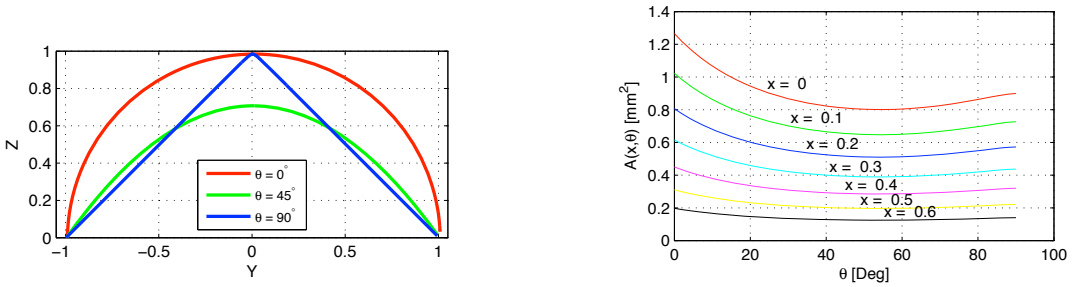

(a) (b)

Figure 3.12: (a) Comparison of the cross-sections, (b) Cross sectional area-variation as a function of θ for each value of spool deflection x.

The nomenclature used for the geometric analysis of the notch design is presented in Fig. 3.11(a). The fluid enters the notch through the Y-Z plane and exits the notch through the X-Y plane as indicated by the red arrow. Let n^* be a vector in the X-Z plane and θ be the angle between n^* and the Z-axis. Let $A_{inst}(\theta)$ be the area obtained by intersecting the notch with a plane that passes through the Y-axis and contains the vector n^*. The physical interpretation for $A_{inst}(\theta)$ is that, it is the area perpendicular to the fluid flow at a given position within the notch. Hence, $A_{inst}(0°)$ is the area at the entrance of the notch and $A_{inst}(90°)$ corresponds to the exit.

The area $A_{inst}(\theta)$ corresponding to $\theta : 0° \rightarrow 90°$ can be calculated numerically by integrating the curve obtained by the intersection of the notch geometry and the plane described earlier. As an example, three such curves corresponding to $\theta : 0°, 45°, 90°$ are shown in Fig. 3.11(b) and Fig. 3.12(a). The $P_{inst}(\theta)$ i.e., the perimeter of each of these curves is also computed and stored to help calculate the Reynolds numbers. This process is repeated for the notch data corresponding to various spool deflections, i.e., $x : 0 \rightarrow x_{max}\ mm$. The obtained data can be compactly represented as $A_{inst}(x, \theta)$, where x represents the spool deflection and θ is the angle used to describe the plane perpendicular to the fluid flow as described in the previous paragraph. Fig. 3.12(b) shows the sample curves for $A_{inst}(x, \theta)$ at certain deflections corresponding to the notch geometry shown in Fig. 3.11(a). This data needs to be interpreted to calculate the area-schedule i.e., $A(x)$. Note that, the calculated $A(x)$ corresponds to just one notch. Since the CFD based analysis was performed using a spool which had six identical notches, the $A(x)$ obtained from the geometry based procedure needs to be scaled by a factor of six.

If the notch is modeled using the traditional approach of treating it as an orifice, the minimum area for fluid flow is the parameter of interest. Hence the metering area at each spool deflection would be obtained using $A(x) = min\left[A_{inst}(x, \theta)\right]$. The results obtained using this method are shown in Fig. 3.13(a). This can be combined with the data in Fig. 3.6(b) which corresponds to the effective

orifice area i.e., $C_d \cdot A$ to calculate the valve's discharge coefficient C_d.

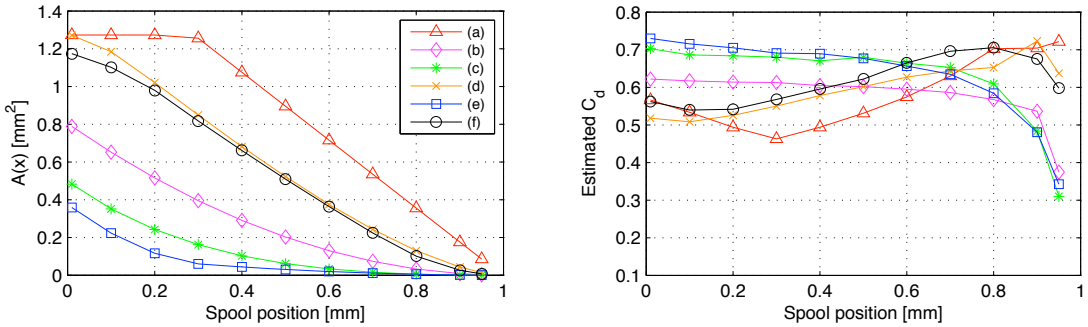

(a) (b)

Figure 3.13: (a) The metering areas, (b) the discharge coefficients predicted by the "min" approximation.

The estimate of the discharge coefficient for various notch designs and spool deflections is presented in Fig. 3.13(b). Since the valve design for each case is exactly the same except for the notches, it is reasonable to expect that, a good estimate of the notch metering area should help in the characterization of the variation of C_d based on the flow conditions. [53] has shown that for a spool valve with rectangular slots as the metering section, once the metering orifice area is calculated analytically, the variation of C_d can be predicted for both laminar and turbulent conditions using the following equation.

$$C_d(x) = C_{dt}\sqrt{\frac{R_e(x)}{R_e(x) + K_c}} \qquad R_e(x) = \frac{V(x)D_H(x)}{\nu} \tag{3.2}$$

where, $C_{dt} = 0.66$ is the discharge coefficient corresponding to turbulent flow, $R_e(x)$ is the reynolds number of the flow at the critical cross-section (corresponding to the smallest area) and $K_c = 100$ is the coefficient associated with the critical reynolds number. $V(x)$ is the average fluid velocity in the critical cross-section and is computed as $V(x) = \dot{m}(x)/(\rho \cdot A(x))$, D_H is the hydraulic diameter computed as $4A(x)/P(x)$, where $P(x)$ is again the perimeter of the critical cross-section and $\nu = \mu/\rho$ is the kinematic viscosity. However the data in Fig. 3.15(a) shows significant deviations from the trend predicted by Eq. 3.2 as shown in Fig. 3.15(c). The data shown here is limited to one pressure drop to retain the clarity of the plot. However a similar trend was observed for cases with different pressure drops as well. One explanation for the deviations could be an inaccurate estimate of the metering area which is failing to capture the flow characteristics of the notch.

An alternate approach is to calculate the mean area available for fluid flow as it makes the 90° turn as shown in (3.3),

$$A(x) = \frac{\Delta\theta}{90}\sum A_{inst}(x, \theta) \tag{3.3}$$

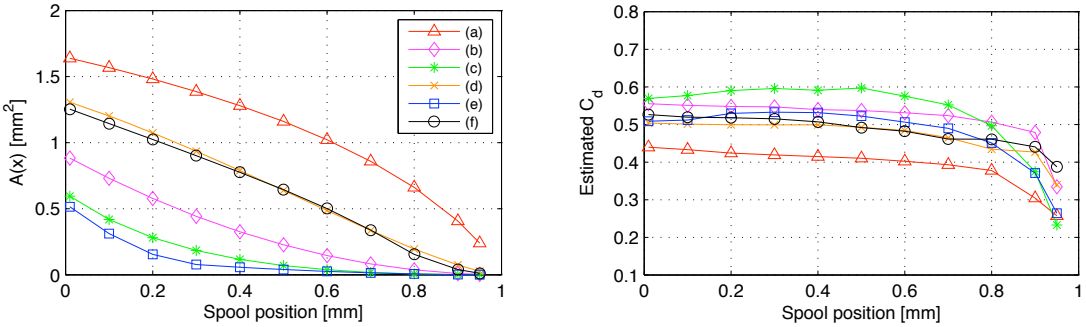

(a) (b)

Figure 3.14: (a) The metering areas, (b) the discharge coefficients predicted by the "mean" approximation.

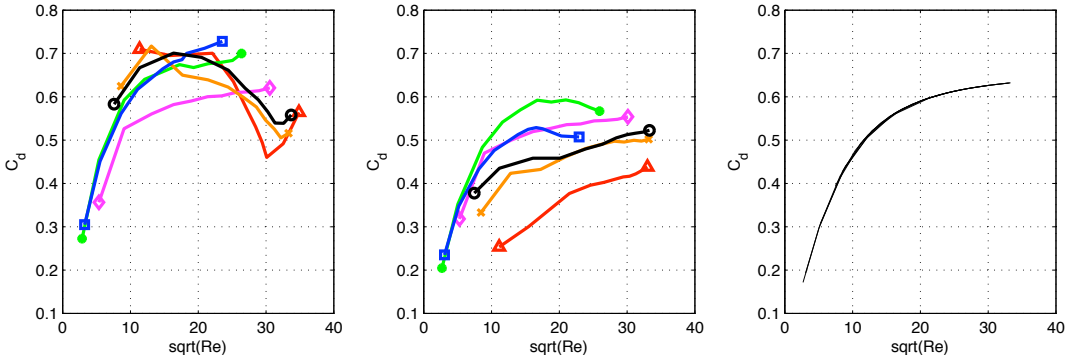

(a) (b) (c)

Figure 3.15: The variation of discharge coefficient with respect to the Reynolds number for (a) the "min" approximation, (b) the "mean" approximation and (c) a typical theoretical case.

where $\Delta\theta$ is the sampling interval between $\theta = 0° \rightarrow 90°$. Fig. 3.14(a) & (b) shows the estimated metering areas and the corresponding discharge coefficients for various geometries and the spool deflections. For the calculation of the Reynold's number, the approximation of the perimeter $P(x)$ is based on the same formula used for calculating the mean area i.e., the mean of the perimeters corresponding to various values of θ. From Fig. 3.15(b), it can be seen that for a given notch geometry, the trend of the variation of the discharge coefficients with respect to the reynolds number is similar to that predicted by the theory Fig. 3.15(c). This suggests that, the mean area serves as a better estimate of the metering area corresponding to the notch. A significant benefit of the proposed geometry based analysis procedure is that, the time required for computing the area-schedule for a given notch *(under 2 minutes)* is many orders of magnitude less when compared to the CFD analysis procedure *(7 hours)*. It can thus be used to develop automated design procedures for rapidly synthesizing the notch geometry for a desired area-schedule.

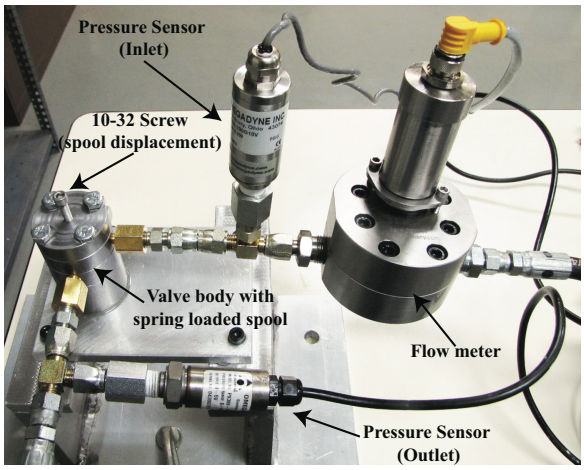

Figure 3.16: The experimental test setup for characterizing the spool with notches.

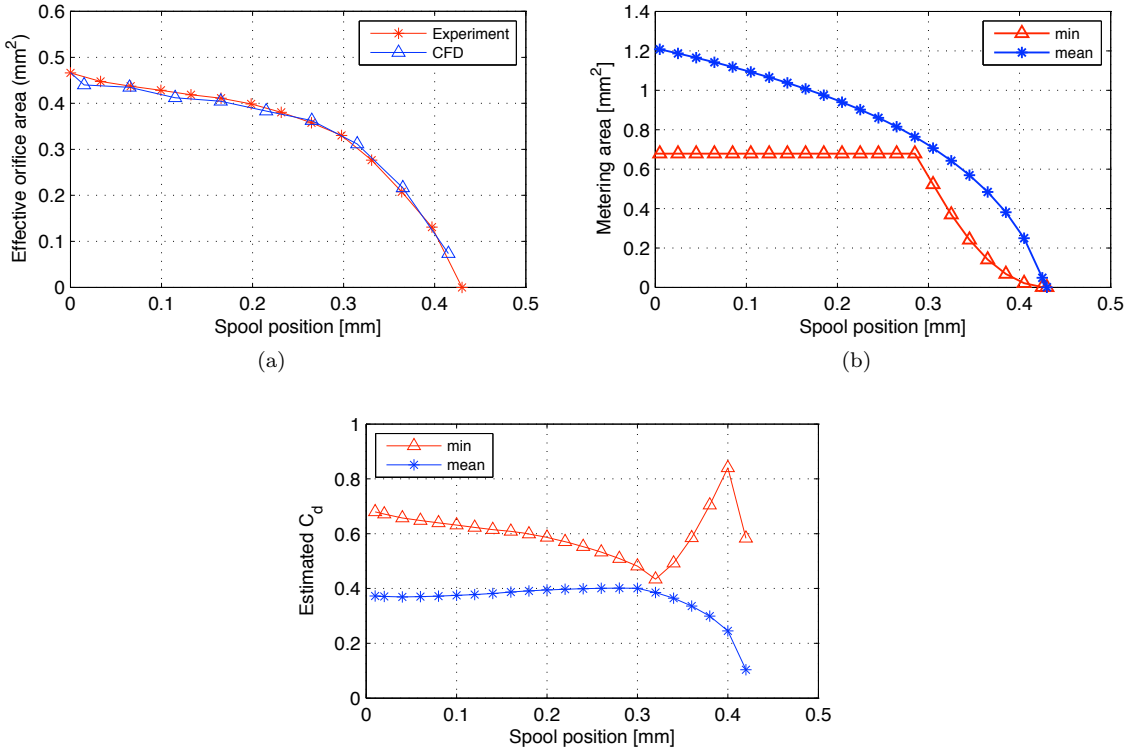

Figure 3.17: (a) The effective orifice area from experimental testing and the CFD analysis, (b) The metering area calculated using the geometric analysis procedure, (c) The estimated discharge coefficient.

3.4.1 Experimental investigations

To validate the proposed analysis procedures, a prototype spool with notches similar to that shown in Fig. 3.7(a) was tested using an experimental test setup as shown in Fig. 3.16. It was instrumented

to measure the volumetric flow rate (MAX-G015) and the pressure (Omegadyne PX-309 series) at the inlet and outlet of the valve. The displacement of the spool is controlled by using a spring on one end and a 10-32 screw on the other end which has a pitch of $0.79375mm$. Displacing the screw by 15° between each measurement (manually using a graduated disc) ensured a position resolution of $33\mu m$. CFD simulations using the CAD model of the spool were carried out under operating conditions similar to the experimental setup. Fig. 3.17(a) shows the effective areas ($C_d.A$) computed using data obtained from the experiments and the simulations which highlights the effectiveness of the CFD based analysis procedure.

The metering area, $A(x)$ using both the interpretations i.e., the "min" and "mean" of the area-variation inside the notch as computed by the geometry-based analysis technique is shown in Fig. 3.17(b). The discharge coefficient (C_d) calculated from the $C_d.A$ corresponding to the experimental data and $A(x)$ values obtained from the "min" and "mean" approximations shown in Fig. 3.17(c) highlights that the "mean" approximation serves as a better estimate of the metering area.

3.5 Synthesis of Notch Designs for Arbitrary Area-Schedules

This section presents a method for calculating the notch design for a specified area-schedule by utilizing the geometric analysis procedure described earlier. The technique is limited to generating axisymmetric notch designs i.e., the cases where the entire notch geometry can be characterized with the notch radius at each location on the spool. To better illustrate this condition, Fig. 3.18 shows a plot of the notch radius as a function of the spool position and the corresponding 3-D notch geometry. It can be seen that the relationship $z(x)$ can completely describe the geometry of the notch.

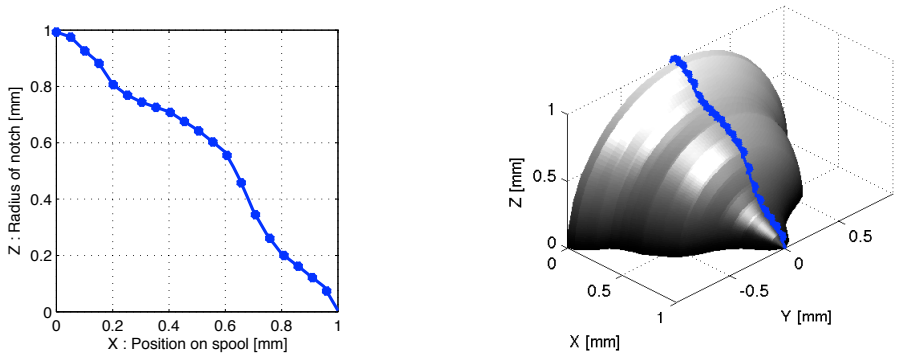

(a) (b)

Figure 3.18: Illustration of the axisymmetric notch design (a) 2D representation, (b) 3-D feature.

The objective of this procedure is to automatically calculate the notch radius at each location on the spool i.e., $z(x)$ such that the corresponding 3-D notch has the desired area-schedule $A(x)$. It is worth reiterating the observation made in the previous section i.e., the metering orifice area A^* for a given spool deflection x^* is purely dependent on the notch geometry corresponding to $x \geq x^*$. This characteristic can be used to uniquely determine the value of $z(x = x^*)$ based on the knowledge of $z(x > x^*)$ and the required A^*. Since the metering orifice area at the maximum spool displacement is always zero i.e., $A(x_{max}) = 0$, it automatically implies that $z(x_{max}) = 0$. These properties can be leveraged to develop a recursive procedure to calculate $z(x)$ by starting at $x = x_{max}$ and working backwards. To solve the problem numerically, it is first discretized by dividing the entire stroke of the spool into "K" steps where, $k \in [1, 2, ..., K]$ such that $x(1) = 0$ and $x(K) = x_{max}$ ($1mm$ for this specific example). $z(k)$ is the radius of the notch at $x(k)$. $A(k)$ is the desired metering orifice area corresponding to a spool deflection of $x(k)$.

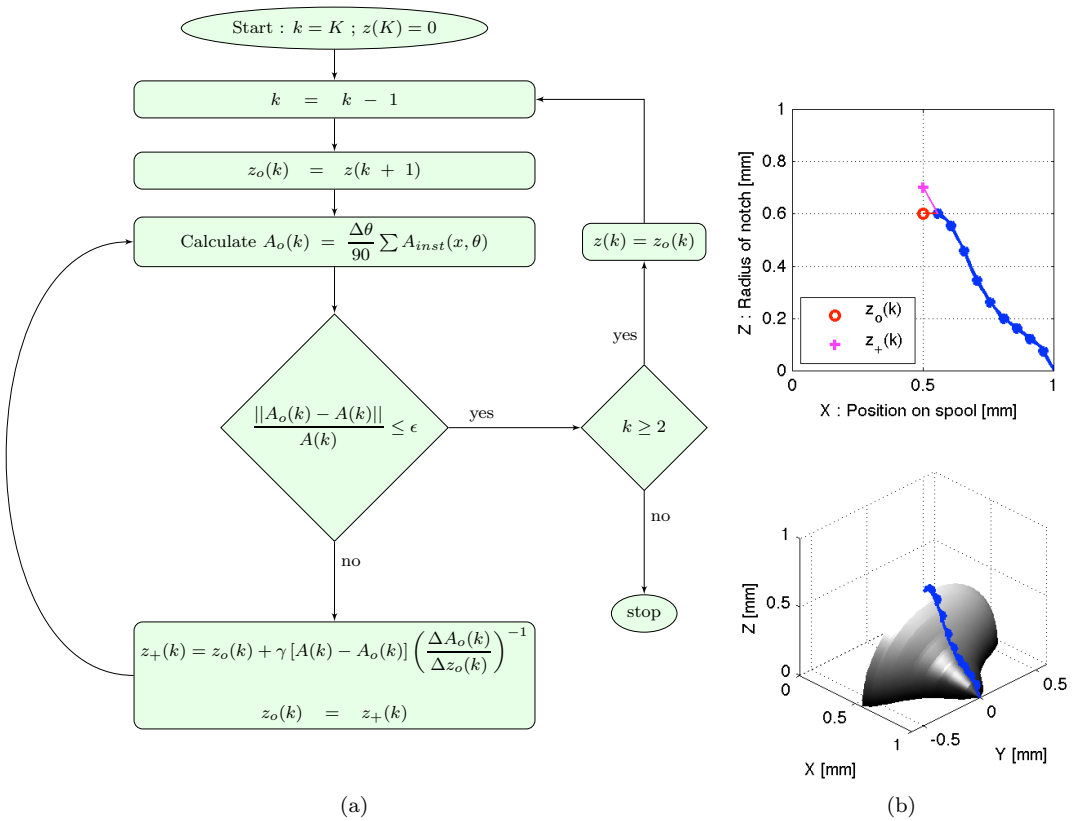

Figure 3.19: Method for calculating the notch design for a given area-schedule : (a) Flow chart for the overall procedure, (b) Illustration of the process for updating the estimate of the notch radius.

Fig. 3.19 shows the various steps involved in calculation of the notch radius $z(k)$ at each step. Starting with $z(K) = z(x_{max}) = 0$, the notch radius at each $k < K$ is calculated progressively. The

terminology adopted is as follows. $z_o(k)$ is the current estimate of the notch radius at step "k". $A_o(k)$ is the metering area calculated by applying the geometry based analysis to the portion of the notch corresponding to $[z_o(k), z(x > x(k))]$. If the $A_o(k)$ obtained is different from the desired $A(k)$, the estimate of the notch radius is updated to a new value $z_+(k)$. In this work, it is updated based on the gradient of $A_o(k)$ with respect to $z_o(k)$, a technique commonly used in optimization problems. The gradient can be calculated by perturbing the current value of $z_o(k)$ and calculating the corresponding change in $A_o(k)$ and can then be used to update $z_+(k)$ as shown in (3.4).

$$z_+(k) = z_o(k) + \gamma \left[A(k) - A_o(k)\right] \left(\frac{\Delta A_o(k)}{\Delta z_o(k)}\right)^{-1} \tag{3.4}$$

This is repeated until the difference between $A_o(k)$ corresponding to $z_o(k)$ and the desired $A(k)$ becomes smaller than a predetermined threshold. γ is a damping factor which can be tuned to improve the convergence of the iterative process and is typically chosen $\in [0.5, 0.85]$. The process is then repeated at each value of "k" using the notch radius corresponding to $x(k+1)$ i.e., $z(k+1)$ as the initial estimate of $z_o(k)$ and performing the iterations discussed earlier. The result at end of the procedure is the notch design $z(x)$ corresponding to the desired area-schedule $A(x)$.

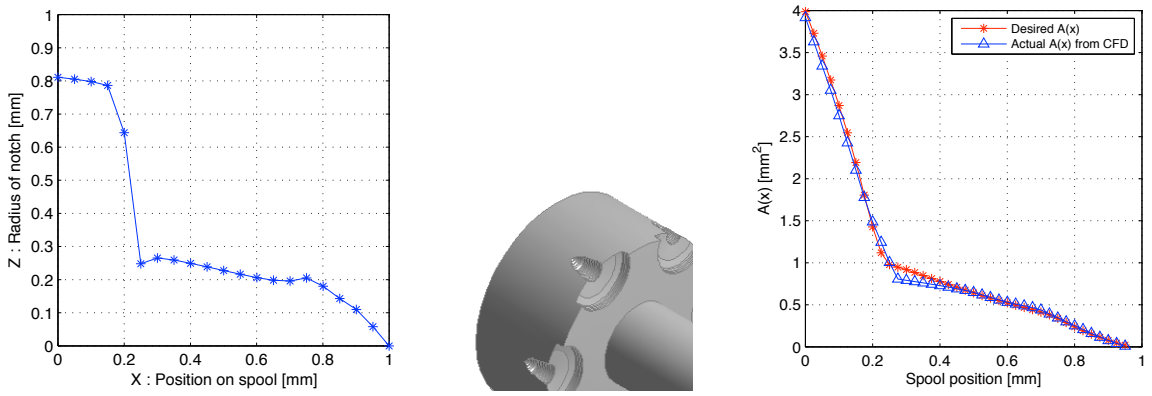

(a) (b) (c)

Figure 3.20: Case 1 : (a) Notch radii from the design procedure, (b) Corresponding 3D geometry on the spool, (c) Area-schedule comparison (Desired and actual).

This technique is applied to two arbitrarily chosen area-schedules for generating the corresponding notch radii i.e., $z(x)$ as shown in Fig. 3.20(a) & Fig. 3.21(a). The 3-D notch designs shown in Fig. 3.20(b) & Fig. 3.21(b) are tested using the CFD analysis method presented earlier. The metering area $A(x)$ at each spool displacement is calculated using (3.1) and a discharge coefficient $C_d = 0.5$. The comparisons of the area-schedules $A(x)$ as shown in Fig. 3.20(c) & Fig. 3.21(c) indicate a good agreement between the desired and the actual area-schedule obtained by testing the notch geometries using the CFD based analysis. It should be noted that, the variation of C_d as a function

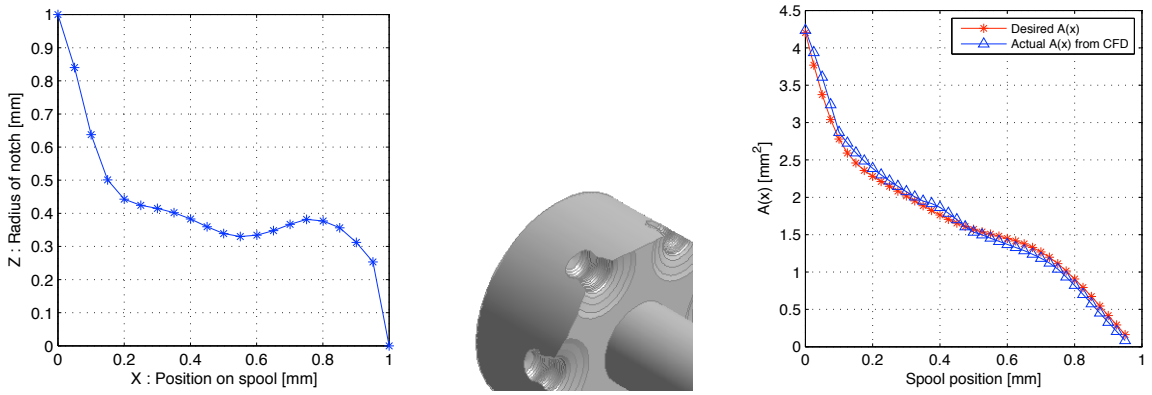

(a) (b) (c)

Figure 3.21: Case 2 : (a) Notch radii from the design procedure, (b) Corresponding 3D geometry on the spool, (c) Area-schedule comparison (Desired and actual).

of the Reynold's number (which depends on the orifice area at different spool locations) was not factored into the synthesis to simplify the procedure and since the obtained results were satisfactory for this particular setting. To further improve the accuracy of the geometry design, the $A(x)$ used for the synthesis can be obtained by modifying the desired $A(x)$ by factoring a variable C_d estimated based on the expected valve operating conditions.

3.6 Summary

This work focused on developing techniques to complement the existing experimental and CFD based methods for analyzing and designing spool based flow control valves with notches. The objective was the development of a systematic method for designing the notch geometries to realize any arbitrary relationship between the spool position and the metering orifice area across the flow control valve. The CFD based analysis was used to validate the idea that any "area-schedule" can be realized by designing the notches appropriately. The shortcomings of the CFD based analysis i.e., computational time and the lack of insight about the design procedure are rectified by developing an analysis procedure based purely on the geometry of the notch. The geometry based analysis also highlights the fact that factoring the entire notch volume as opposed to the traditional approach of considering only the smallest restriction significantly improves the prediction of the metering area across the valve. Experiments are then conducted to validate the proposed method. Finally, the fast turn around time of the geometry based method is used to develop an iteration based procedure to calculate the notch design for any given area-schedule.

Chapter 4

Tracking Control Design for Engine Speed Transients

A typical engine valve profile corresponding to one full cycle of a 4-stroke IC engine using a cam-based actuation system and the terminology used for describing the valve event is shown in Fig. 4.1. Removing the camshaft makes it necessary for the actuation system to control the valve motion in real-time to follow this trajectory during each cycle of the engine. As mentioned earlier, the high speed operation of the engine coupled with the limitations of the actuation hardware make the motion control problem challenging.

One commonly adopted approach is to sacrifice the ability to fully influence the shape of the valve

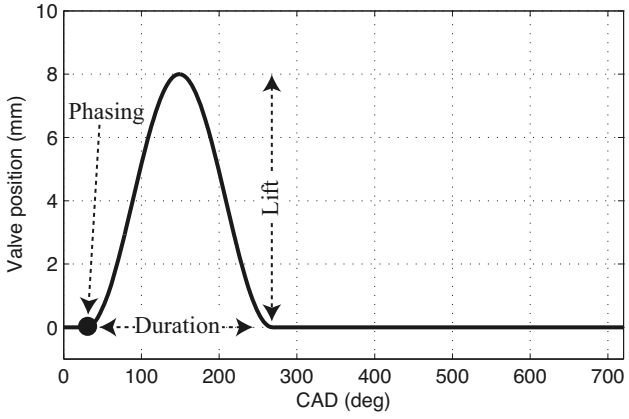

Figure 4.1: A typical engine valve profile and the associated terminology

motion profile to simplify the control requirements to a certain degree. Examples include electro-hydraulic actuation systems such as the design presented in the previous chapters and other concepts based on digital valves [54] and electro-mechanical systems based on solenoids [1, 21]. Controllers designed in [35, 55, 56] were able to ensure the desired valve event characteristics such as the timing, duration, lift and the seating velocities in the presence of external disturbances.

It is still desirable to have systems which can completely control the shape of the valve motion profile. Such systems with the ability to simulate various cam-profiles [37] can significantly accelerate the research and development of cam-based variable valve actuation systems which are currently being deployed in large quantities. Once an actuation system with sufficient bandwidth is realized, the immediate challenge is the development of control algorithms to enable the required tracking performance. The tracking problem for steady state operation, i.e., constant engine speed and fixed valve event has been solved using the LTI repetitive controller by utilizing the time periodicity of the reference signal [28]. However, during engine speed transients, the signal is no longer periodic and thus requires more advanced controllers.

Several modifications to the repetitive controller have been proposed by researchers to handle the variation in the signal's period during rotational speed transients. One approach was to adaptively identify the period and modify the repetitive controller in real-time [57]. The dynamics of the adaptation make it difficult to achieve precise tracking control during the transients. [58] presents a specialized implementation of a repetitive controller to improve the performance obtained using a linear quadratic regulator. The error signal is partitioned into repetitive states and the average error of each partition is used as the sample error for the repetitive controller. Engine speed variations are handled by that fact that, changes in the signal's period are reflected in the variation of the number of samples in each partition. [59] presents an LPV controller for stabilizing the parameter varying plant obtained by sampling the system in an alternate spatial domain and applying repetitive control in the spatial domain. [37] presents an approach where the reference signal is decomposed into periodic and aperiodic sections and the algorithm switches between LTI repetitive and PI controllers.

This research is motivated by the asymptotic tracking performance enabled by the controllers based on the internal model principle and thus focuses on obtaining explicit models for the aperiodic reference signal and using them in the design of internal model based controllers. The internal model principle, first introduced in [60, 61] for linear time invariant systems states that, for a feedback system to track/reject signals with known generating dynamics, a suitable copy of the generating dynamics should be embedded within the feedback loop. This principle was later extended to non-linear [62] and linear periodic systems [63]. A systematic design method for constructing the time-varying internal model units in the Input/Output setting which was presented in [38] will be

used for this study.

4.1 Problem Formulation

The key features that enabled the precise tracking performance of the LTI repetitive controller are as follows,

1. The frequency domain representation of the reference signal shows that the magnitudes are concentrated at discrete locations which are integer multiples of the fundamental frequency. The closed-loop system using the repetitive controller is designed to have small sensitivities at these exact frequencies.

2. The repetitive controller is a specialized implementation of the more general internal model principle where the known discrete time domain dynamics $1 - z^{-N}[r] = 0$ for the periodic reference signal $r(t) = r(t - N\Delta t)$ are used for the control design.

Based on these ideas, this section aims to obtain the generating dynamics i.e., modeling the reference signal as an output of another autonomous dynamical system, which is later used in the design of an internal model based controller.

4.1.1 Approach 1 : Time domain control of frequency varying sinusoids

This approach is based on adapting the standard Fourier series approximation for periodic signals to model the aperiodic reference signal as a combination of frequency varying sinusoids as shown in Eqn. 4.1. The valve event parameters i.e., the lift, phasing and duration are captured by the amplitudes γ_0, γ_1, ... γ_ρ and the phases ϕ_1, ϕ_2, ... ϕ_ρ. The frequency of the various harmonics are given by $[\omega_1(t), \omega_2(t), ..\omega_\rho(t)] = [1, 2, \cdots, \rho] \times \omega(t)$, where $\omega(t)$, the fundamental harmonic is related to the engine speed W [RPM] by $\omega(t) = W(t) \times \pi/60$. It is also obvious that the valve profile can be represented with increasing accuracy by increasing the value of ρ.

$$r(t) = \gamma_0 + \sum_{i=1}^{\rho} \gamma_i \sin\left[\int \omega_i(t)dt + \phi_i\right] \tag{4.1}$$

The above signal can be written as the output of a dynamical system (generating dynamics) whose state-space representation is shown below in Eq. 4.2,

$$\dot{x}_r(t) = \underbrace{\begin{bmatrix} A_{r_1}(t) & 0 & 0 & \cdots & 0 \\ 0 & A_{r_2}(t) & 0 & \cdots & 0 \\ 0 & 0 & A_{r_3}(t) & \cdots & 0 \\ \vdots & \vdots & \vdots & \ddots & \vdots \\ 0 & 0 & 0 & \cdots & A_{r\rho}(t) \end{bmatrix}}_{A_r(t)} x_r(t) \tag{4.2}$$

$$r(t) = \underbrace{\begin{bmatrix} C_{r_1}(t) & C_{r_2}(t) & C_{r_3}(t) & \cdots & C_{r\rho}(t) \end{bmatrix}}_{C_r(t)} x_r(t)$$

where $x_r \in \mathbb{R}^{2\rho \times 1}$, for each $j \in [1, 2, \cdots, \rho]$, we have

$$A_{rj}(t) = \begin{bmatrix} 0 & \omega_j(t) \\ -\omega_j(t) & 0 \end{bmatrix} \qquad C_{rj}(t) = \begin{bmatrix} 1 & 0 \end{bmatrix}$$

The amplitudes $\gamma_0, \gamma_1, \cdots, \gamma_\rho$ and the phases $\phi_1, \phi_2, \cdots, \phi_\rho$ are determined by the initial state $x_r(0)$. It can be seen that, as engine speed $W(t)$ varies with respect to time, the generating dynamics of the reference signal becomes time-varying.

4.1.2 Approach 2 : Rotational angle domain control

This approach is based on the design and implementation of the controller in the rotational angle domain to leverage the dependance of the valve profile on the crankshaft position. The valve reference trajectory (for a fixed valve event) is thus periodic in the rotational domain and can be represented using $r(\theta) = r(\theta - N\Delta\theta)$, where N is the number of samples in one cycle and $\Delta\theta$ is the angular sampling resolution. Hence, the reference signal in the rotational angle domain can be written as $r(k) = r(k - N)$ i.e., the generating dynamics is time-invariant. However, the time interval between successive sampling instants i.e., $\Delta t(k) = \Delta\theta(k)/\left(6W(k)\right)$ changes as the rotational speed changes in real time. Hence the model of the plant (valve actuator) with time-invariant dynamics becomes time(parameter)-varying in the rotational angle domain [64].

For both these approaches, the generating dynamics of the reference signal is known and thus makes it ideally suited for designing controllers based on the internal model principle. Based on the above observations, it is clear that either the plant (valve actuator) or the reference generating dynamics becomes time-varying and thus the LTI Internal model principle are no longer applicable.

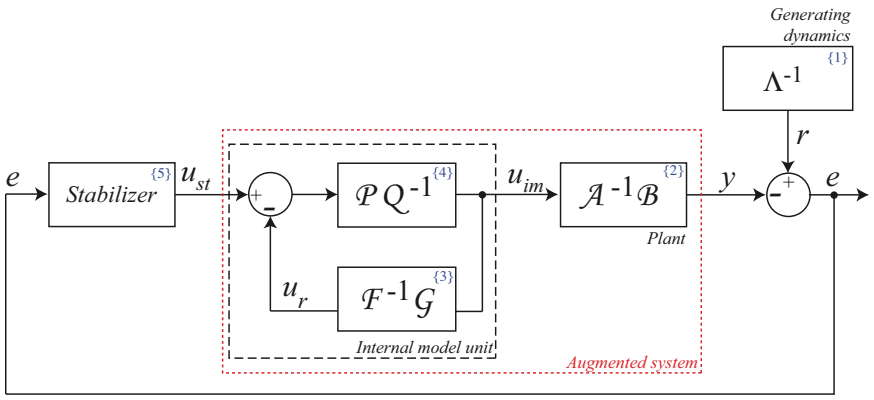

Figure 4.2: Block diagram of the time-varying internal model based control system

This motivates the use of the recently developed time-varying internal model based controller.

4.2 Time-varying Internal Model based Controller

A block diagram of the closed loop system with the time-varying internal model based controller is shown in Fig. 4.2 The justification for the choice of the specific structure of the controller as well as the derivations and proofs required to design each block in the controller have been discussed in sufficient detail in [38]. For the sake of conciseness, only the material relevant to the design and implementation of the controller for this application will be discussed in this section. To help clarify various aspects in the control design procedure, sample calculations for each step are shown. Due to space constraints, a 2^{nd} order plant and 2^{nd} order generating dynamics are used for the examples.

4.3 I/O Representation of Linear Time-Varying Systems

A significant portion of the controller design is carried out using the Input/Output (I/O) representation of the relevant systems. Hence a brief summary of the mathematical preliminaries from [65] and [66] for representing time-varying systems in the I/O form is first presented. Consider two general linear time-varying differential equations as shown below,

$$\frac{d^n y(t)}{dt^n} + c_{n-1}(t)\frac{d^{n-1}y(t)}{dt^{n-1}} + \cdots c_1(t)\frac{dy(t)}{dt} + c_0(t)y(t) = u(t)$$

$$\frac{d^n [y(t)c_n(t)]}{dt^n} + \cdots \frac{d[y(t)c_1(t)]}{dt} + c_0(t)y(t) = u(t)$$

Using the differential operator $s = \frac{d}{dt}(.)$, these equations can be represented using algebraic

expressions as shown below,

$$\underbrace{s^n + c_{n-1}(t)s^{n-1} + \cdots c_1(t)s + c_0(t)}_{\mathcal{C}_l(s,t)}[y(t)] = u(t)$$

$$\underbrace{s^n c_n(t) + s^{n-1} c_{n-1}(t) + \cdots s c_1(t) + c_0(t)}_{\mathcal{C}_r(s,t)}[y(t)] = u(t)$$

where, $\mathcal{C}_l(s,t)$ and $\mathcal{C}_r(s,t)$ are called the left and right polynomial differential operators (PDOs) respectively and in addition, $\mathcal{C}_l(s,t)$ is a monic PDO since the coefficient of the highest power of "s" is 1. The inverse operator ${\mathcal{C}_l}^{-1}(s,t)$ is called a polynomial integral operator (PIO) and it maps the input to the zero state response of the differential equation described by the PDO $\mathcal{C}_l(s,t)$ i.e., $y(t) = {\mathcal{C}_l}^{-1}(s,t)[u(t)]$. Similarly the linear time-varying difference equations shown below,

$$c_n(k)y(k-n) + \cdots c_1(k)y(k-1) + y(k) = u(k)$$

$$c_n(k-n)y(k-n) + \cdots c_1(k-1)y(k-1) + c_0(k)y(k) = u(k)$$

By defining z^{-1} as the one step delay operator i.e., $y(k-1) = z^{-1}y(k)$, the above equations can be converted to algebraic form as shown below,

$$\underbrace{c_n z^{-n}(k) + c_1(k) \cdots z^{-1} + 1}_{\mathcal{C}_l(z,k)}[y(k)] = u(k)$$

$$\underbrace{z^{-n} c_n(k) + \cdots z^{-1} c_1(k) + c_0}_{\mathcal{C}_r(z,k)}[y(k)] = u(k)$$

where, $\mathcal{C}_l(z,k)$ and $\mathcal{C}_r(z,k)$ are called the left and right polynomial difference operators (PDOs) respectively and in addition, $\mathcal{C}_l(z,k)$ is a monic PDO since the coefficient of "z^{-0}" is 1. The inverse operator ${\mathcal{C}_l}^{-1}(z,k)$ is called a polynomial summation operator (PSO) and it maps the input to the zero state response of the difference equation described by the PDO $\mathcal{C}_l(z,k)$ i.e., $y(k) = {\mathcal{C}_l}^{-1}(z,k)[u(k)]$.

For both the approaches, the control requires the plant model and the generating dynamics to be represented using *right PDOs*.

4.4 Generating Dynamics $^{\{1\}}$

For the first approach, the time-varying state-space representation of the reference signal generating dynamics from Eq. 4.2 needs to transformed to the observer canonical form as shown in Eq. 4.3, to obtain the required I/O representation.

$$\begin{aligned}\dot{\tilde{x}}_r(t) &= \underbrace{\begin{bmatrix} -\lambda_{N-1}(t) & 1 & 0 & \cdots & 0 \\ -\lambda_{N-2}(t) & 0 & 1 & \cdots & 0 \\ \vdots & \vdots & \vdots & \ddots & \vdots \\ -\lambda_1(t) & 0 & 0 & \cdots & 1 \\ -\lambda_0(t) & 0 & 0 & \cdots & 0 \end{bmatrix}}_{A_{ro}(t)} \tilde{x}_r(t) \\ r(t) &= \underbrace{\begin{bmatrix} 1 & 0 & \cdots & 0 \end{bmatrix}}_{C_{ro}(t)} \tilde{x}_r(t)\end{aligned} \tag{4.3}$$

The complete details of the various steps involved in deriving these relations are presented in the Appendix at the end of this thesis. Only the steps relevant to the control design process are shown here. The system needs to be transformed to a coordinate system $\tilde{x}_r(t) = P_c(t)x_r(t)$ such that the transformation matrix satisfies the following relationship.

$$\begin{aligned}\dot{\tilde{x}}_r(t) &= \underbrace{\left[P_c(t)A_r(t) + \dot{P}_c(t)\right] P_c^{-1}(t)}_{A_{ro}(t)} \tilde{x}_r(t) \\ r(t) &= \underbrace{C_r(t)P_c^{-1}(t)}_{C_{ro}(t)} \tilde{x}_r(t)\end{aligned} \tag{4.4}$$

To find the time-varying transformation matrix $P_c(t)$, let $Q_c(t) = P_c^{-1}(t)$. Utilizing the special structure of the matrices $A_{ro}(t)$ & $C_{ro}(t)$, the relations described in Eq. 4.4 and some algebraic manipulations, the columns of $Q_c(t)$ i.e., $q_1(t),\ q_2(t),\ \cdots,\ q_N(t)$ can be calculated using the recursive

expressions shown below,

$$q_m(t) = \begin{cases} \begin{bmatrix} \eta_1(t) \\ \eta_2(t) \\ \vdots \\ \eta_N(t) \end{bmatrix}^{-1} \begin{bmatrix} 1 \\ 0 \\ \vdots \\ 0 \end{bmatrix} & m = N \\ \\ A_r(t)q_{m+1}(t) - \dot{q}_{m+1}(t) & m \in [1, N-1] \end{cases} \tag{4.5}$$

where,

$$\eta_j(t) = \begin{cases} C_r(t) & j = N \\ \\ \eta_{j+1}(t)A_r(t) + \dot{\eta}_{j+1}(t) & j \in [1, N-1] \end{cases} \tag{4.6}$$

The observer canonical form directly gives the coefficients of the required PDO as shown in Eq. 4.7.

$$\underbrace{s^N + s^{N-1}\lambda_{N-1}(t) + \cdots + s\lambda_1(t) + \lambda_0(t)}_{\Lambda(s,t)}[r(t)] = 0 \tag{4.7}$$

Example : For a 1 harmonic sinusoid i.e., $\rho = 1$, based on Eq. 4.2, the state representation of the generating dynamics is obtained as,

$$A_r(t) = \begin{bmatrix} 0 & \omega(t) \\ -\omega(t) & 0 \end{bmatrix} \qquad C_r(t) = \begin{bmatrix} 1 & 0 \end{bmatrix}$$

Substituting this into Eq. 4.6, Eq. 4.5 and Eq. 4.4, the transformation matrix $P_c(t)$ and the coefficients of the corresponding state space representation in the observer canonical form are

obtained as,

$$P_c(t) = \begin{bmatrix} 1 & 0 \\ -\dfrac{\dot{\omega}(t)}{\omega(t)} & \omega \end{bmatrix}$$
$$\lambda_1(t) = -\frac{\dot{\omega}(t)}{\omega(t)}$$
$$\lambda_0(t) = \frac{\omega^4(t)\dot{\omega}^2(t) + \ddot{\omega}(t)\omega(t)}{\omega^2(t)}$$

For the second approach, the difference equation corresponding to the generating dynamics i.e., $r(k) - r(k-N) = 0$ is readily converted to the time-invariant (parameter-independent) I/O representation as shown below.

$$\underbrace{1 - z^{-N}}_{\Lambda(z)}[r(k)] = 0 \tag{4.8}$$

The general form for both the approaches (by neglecting the indices) can thus be written as $r = \Lambda^{-1}[0]$.

4.5 Plant $^{\{2\}}$

For the first approach, the I/O representation of the plant model is the traditional n^{th} LTI transfer function and is derived based on first principles or obtained experimentally from the frequency response of the actuator. The value of n is chosen to capture the dynamics of the plant sufficiently well in the frequency range of interest.

$$\mathcal{A}(s) = s^n + s^{(n-1)}\alpha_{n-1} + \cdots s^1\alpha_1 + \alpha_0$$
$$\mathcal{B}(s) = s^{(n-1)}\beta_{n-1} + \cdots s^1\beta_1 + \beta_0$$

The LTI PDO $\mathcal{A}(s)$ needs to be monic (easily satisfied by dividing both the PDOs by the appropriate scalar) and the transfer function is assumed to be strictly proper i.e., $order(\mathcal{B}(s)) < order(\mathcal{A}(s))$

For the second approach, using the LTI model described earlier, the discrete model of the

plant in the rotational angle domain is obtained based on the method discussed in [67],

$$\begin{aligned} x(k+1) &= A_p(k)x(k) + B_p(k)u(k) \\ y(k) &= C_p(k)x(k) \end{aligned} \tag{4.9}$$

$$\begin{aligned} A_p(k) = e^{A_{pc}\Delta t(k)}, \quad B_p(k) &= \left[e^{A_{pc}\Delta t(k)} - I\right] A_{pc}^{-1} B_{pc} \\ C_p(k) = C_{pc}, \quad \Delta t(k) &= \frac{\theta(k+1) - \theta(k)}{6W(k)} \end{aligned}$$

where, $A_{pc},\ B_{pc}$ & C_{pc} correspond to the state space representation of the continuous LTI model of the plant. It is evident that, when the rotational speed $W(k)$ changes, the plant model in the rotational angle domain becomes time(parameter)-varying and its state space representation can be written in the general form as,

$$\begin{aligned} A_p(k) &= \begin{bmatrix} a_{11}(k) & a_{12}(k) & \cdots & a_{1n}(k) \\ a_{21}(k) & a_{22}(k) & \cdots & a_{2n}(k) \\ \vdots & \vdots & \ddots & \vdots \\ a_{n1}(k) & a_{n2}(k) & \cdots & a_{nn}(k) \end{bmatrix}, \ B_p(k) = \begin{bmatrix} b_1(k) \\ b_2(k) \\ \vdots \\ b_n(k) \end{bmatrix} \\ C_p(k) &= \begin{bmatrix} c_1(k) & c_2(k) & \cdots & c_n(k) \end{bmatrix} \end{aligned} \tag{4.10}$$

Similar to the continuous time case discussed earlier, we need to find a transformation $\tilde{x}_p(k) = P_d(k)x_p(k)$ to represent the system in the observable canonical form,

$$\begin{aligned} \tilde{x}(k+1) &= A_{po}(k)\tilde{x}(k) + B_{po}(k)u(k) \\ y(k) &= C_{po}(k)\tilde{x}(k) \end{aligned} \tag{4.11}$$

$$A_{po}(k) = \begin{bmatrix} -\alpha_1(k) & 1 & 0 & \cdots & 0 \\ -\alpha_2(k) & 0 & 1 & \cdots & 0 \\ \vdots & \vdots & \vdots & \ddots & \vdots \\ -\alpha_{n-1}(k) & 0 & 0 & \cdots & 1 \\ -\alpha_n(k) & 0 & 0 & \cdots & 0 \end{bmatrix}, \; B_{po}(k) = \begin{bmatrix} \beta_1(k) \\ \beta_2(k) \\ \vdots \\ \beta_n(k) \end{bmatrix}$$

$$C_{po}(k) = \begin{bmatrix} 1 & 0 & 0 & \cdots & 0 \end{bmatrix}$$

The relationship between the two systems and the transformation matrix is obtained as,

$$\begin{aligned} \tilde{x}_p(k+1) &= \underbrace{P_d(k+1)A_p(k)P_d^{-1}(k)}_{A_{po}(k)}\tilde{x}_p(k) + \underbrace{P_d(k+1)B_p(k)}_{B_{po}(k)}u(k) \\ y_p(k) &= \underbrace{C_p(k)P_d^{-1}(k)}_{C_{po}(k)}\tilde{x}_p(k) \end{aligned} \tag{4.12}$$

Again, defining $Q_d(k) = P_d^{-1}(k)$, using the special structure of the matrices $A_{po}(k)$ & $C_{po}(k)$ and the expressions in Eq. 4.12, the columns of $Q_d(k)$ at the current step i.e., $q_1(k),\ q_2(k),\ \cdots,\ q_n(k)$ are calculated based on the recursive relations shown below,

$$q_m(k) = \begin{cases} \begin{bmatrix} C_p(k)\eta_1(k) \\ C_p(k-1)\eta_2(k) \\ C_p(k-2)\eta_3(k) \\ \vdots \\ C_p(k-n+1)\eta_n(k) \end{bmatrix}^{-1} \begin{bmatrix} 1 \\ 0 \\ 0 \\ \vdots \\ 0 \end{bmatrix} & m = 1 \\ \left[\prod_{i=0}^{m-2} A_p^{-1}(k+i)\right] q_1(k+m-1) & m \in [2,n] \end{cases} \tag{4.13}$$

$$\eta_j(k) = \begin{cases} I_{n\times n} & j = 1 \\ \eta_{m-1}(k)A_p^{-1}(k-m-1) & j \in [2,n] \end{cases} \tag{4.14}$$

which can be used to obtain the transformation matrix corresponding to the current step i.e., $P_d(k) = Q_d^{-1}(k)$. $P_d(k+1)$ is then calculated in a similar way by shifting the indices accordingly, which when

substituted into Eq. 4.12 gives the system matrices in the observer canonical form. The coefficients of the time-varying I/O representation of the plant are then directly obtained from these matrices i.e.,

$$\mathcal{A}(z,k) = 1 + z^{-1}\alpha_1(k) + z^{-2}\alpha_2(k) + \cdots z^{-n}\alpha_n(k)$$
$$\mathcal{B}(z,k) = z^{-1}\beta_1(k) + z^{-2}\beta_2(k) + \cdots z^{-n}\beta_n(k).$$

The fact that $\beta_0(k) = 0$ is a consequence of the assumption that the plant model is strictly proper.

Example : For a second order plant model i.e., $n = 2$, based on Eq. 4.9, the state representation of the generating dynamics is obtained as,

$$A_p(k) = \begin{bmatrix} a_{11}(k) & a_{12}(k) \\ a_{11}(k) & a_{12}(k) \end{bmatrix} \qquad B_p(t) = \begin{bmatrix} b_1(k) \\ b_2(k) \end{bmatrix} \qquad C_p(t) = \begin{bmatrix} c_1(k) & c_2(k) \end{bmatrix}$$

Substituting this into Eq. 4.14, Eq. 4.13 and Eq. 4.12, the transformation matrix $P_d(k)$ and the coefficients corresponding to the state space representation in the observer canonical form are obtained as,

$$P_d(k) = \begin{bmatrix} 1 & 0 \\ -\dfrac{a_{12}(k)a_{22}(k-1)}{a_{12}(k-1)} & a_{12}(k) \end{bmatrix}$$

$$\alpha_1(k) = -a_{11}(k) - \frac{a_{12}(k)a_{22}(k-1)}{a_{12}(k-1)}$$
$$\alpha_2(k) = -a_{12}(k+1)a_{21}(k) + \frac{a_{11}(k)a_{12}(k)a_{22}(k)}{a_{12}(k)}$$
$$\beta_1(k) = b_1(k)$$
$$\beta_2(k) = a_{12}(k+1)b_2(k) - \frac{a_{12}(k+1)a_{22}(k)b_1(k)}{a_{12}(k)}$$

4.6 Internal Model Unit {3,4}

This section focuses on the design of the internal model unit as shown in Fig. 4.2 which can be thought of as the feedforward portion of the controller i.e., when i.e., $e \to 0$ & $u_{st} \to 0$, it can persistently generate the required control signal u_{im} to maintain the tracking error at $e = 0$. Due to the similarity in the design method for the continuous-time and the discrete case, the indices "(s,t)"

and "(z,k)" are dropped for the sake of conciseness. The basic idea behind the design of the internal model unit is that, if the I/O characteristics of the block {3} are the same as that of the plant i.e., $u_r = \mathcal{A}^{-1}\mathcal{B}[u]$ and if the interconnection of the two blocks i.e., $\{3, 4\}$ is designed to produce the reference signal r at u_r, then u_{im} is the required control signal to make the plant track the reference signal r. This can be achieved by designing the subsystems as follows,

$$\begin{aligned} \mathcal{F} &= \mathcal{L}\mathcal{A} \\ \mathcal{G} &= \mathcal{L}\mathcal{B} \end{aligned} \tag{4.15}$$

Typically, $order(\mathcal{A}) \leq order(\Lambda)$ and hence the monic LTI polynomial differential/difference operator $\mathcal{L}$ is chosen to make $order(\mathcal{F}) = order(\Lambda)$. If $order(\mathcal{A}) > order(\Lambda)$, then we choose $\mathcal{L} = 1$ and augment Λ with a similar LTI PDO.

The coefficients of the PDOs $\mathcal{P}$ and $\mathcal{Q}$ are obtained by solving Eq. 4.16. $\mathcal{Q}$ needs to be a monic PDO. Choosing $order(\mathcal{P}) = order(\mathcal{Q}) = N - 1$ ensures that the overall order of the controller is as small as possible while still ensuring the solvability of Eq. 4.16.

$$\mathcal{F}\mathcal{Q} + \mathcal{G}\mathcal{P} = \Lambda\mathcal{Q} \tag{4.16}$$

Care needs to be taken when carrying out the multiplication of the PDOs since the operators "s" and "z^{-1}" do not commute with the time-varying coefficients, i.e., $s\alpha(t) = \alpha(t)s + \dot{\alpha}(t)$ and similarly, $\alpha(k)z^{-1} = z^{-1}\alpha(k+1)$. The $2N-1$ unknown coefficients i.e., $p_0,\ p_1,\ \cdots p_{N-1},\ q_1,\ q_2,\ \cdots q_{N-1}$ are obtained by multiplying the polynomials in Eq. 4.16 and collecting the terms corresponding to the like powers of either "s" or "z^{-1}" and solving the resulting system of linear equations.

Examples :

For approach 1, the plant model is time-invariant and hence the trailing "(t)" for all its coefficients can be dropped and $s\alpha = s\alpha$. Also, since the orders of the plant model and the reference signal generating dynamics are equal, $\mathcal{L}(s) = 1$.

$$\left[s^2 + s\alpha_1 + \alpha_0\right]\left[s + q_0(t)\right] + \left[s\beta_1 + \beta_0\right]\left[sp_1(t) + p_0(t)\right] = \left[s^2 + s\lambda_1(t) + \lambda_0(t)\right]\left[s + q_0(t)\right]$$

$$\begin{aligned} s^3 + s^2 q_0(t) + s\alpha_1 s + s\alpha_1 q_0(t) + \alpha_0 s + \alpha_0 q_0(t) = \quad & s^3 + s^2 q_0(t) + s\lambda_1(t)s + s\lambda_1(t)q_0(t) \\ +s\beta_1 s p_1(t) + s\beta_1 p_0(t) + \beta_0 s p_1(t) + \beta_0 p_0(t) \quad & +\lambda_0(t)s + \lambda_0(t)q_0(t) \end{aligned}$$

$$s^3 + s^2 q_0(t) + s^2\alpha_1 + s\alpha_1 q_0(t) + s\alpha_0 + \alpha_0 q_0(t) = s^3 + s^2 q_0(t) + s^2\lambda_1(t) - s\dot{\lambda_1}(t)$$
$$+s^2\beta_1 p_1(t) + s\beta_1 p_0(t) + s\beta_0 p_1(t) + \beta_0 p_0(t) \qquad +s\lambda_1(t)q_0(t) + s\lambda_0(t) - \dot{\lambda_0}(t) + \lambda_0(t)q_0(t)$$

Collecting the coefficients of the like powers, we get

$$q_0(t) + \alpha_1 + \beta_1 p_1(t) = q_0(t) + \lambda_1(t)$$
$$\alpha_1 q_0(t) + \alpha_0 + \beta_1 p_0(t) + \beta_0 p_1(t) = -\dot{\lambda_1}(t) + \lambda_1(t)q_0(t) + \lambda_0(t)$$
$$\alpha_0 q_0(t) + \beta_0 p_0(t) = -\dot{\lambda_0}(t) + \lambda_0(t)q_0(t)$$

Solving the above equation, we get the expressions for coefficients as,

$$q_0(t) = \frac{\beta_0^2\left[\lambda_1(t) - \alpha_1\right] - \beta_1\beta_0\left[\lambda_0(t) - a_0 - \dot{\lambda_1}(t)\right] - \beta_1^2\dot{\lambda_0}(t)}{\beta_1^2\left[\alpha_0 - \lambda_0(t)\right] - \beta_1\beta_0\left[\alpha_1 - \lambda_1(t)\right]} \tag{4.17}$$

$$p_0(t) = \frac{\beta_0\left[\alpha_0 - \lambda_0(t)\right]\left[\lambda_1(t) - \alpha_1\right] + \beta_1\left[\alpha_0 - \lambda_0(t)\right]\left[\lambda_0(t) - \alpha_0 - \dot{\lambda_1}(t)\right] - \beta_1\left[\alpha_1 - \lambda_1(t)\right]\dot{\lambda_0}(t)}{\beta_1^2\left[\alpha_0 - \lambda_0(t)\right] - \beta_1\beta_0\left[\alpha_1 - \lambda_1(t)\right]}$$

$$p_1(t) = \frac{\lambda_1(t) - \alpha_1}{\beta_1}$$

For approach 2, the generating dynamics is time-invariant i.e., $\Lambda(z) = 1 - z^{-2}$ and the plant model is time-varying i.e., $\mathcal{A} = 1 + z^{-1}\alpha_1(k) + z^{-2}\alpha_2(k)$ and $\mathcal{B} = z^{-1}\beta_1(k) + z^{-2}\beta_2(k)$. Again, since the order of the plant model and the reference signal generating dynamics are equal, $\mathcal{L}(z) = 1$.

$$\left[1 + z^{-1}\alpha_1(k) + z^{-2}\alpha_2(k)\right]\left[1 + z^{-1}q_1(k)\right] = \left[1 - z^{-2}\right]\left[1 + z^{-1}q_1(k)\right]$$
$$+\left[z^{-1}\beta_1(k) + z^{-2}\beta_2(k)\right]\left[p_0(k) + z^{-1}p_1(k)\right]$$

$$1 + z^{-1}q_1(k) + z^{-1}\alpha_1(k) + z^{-2}\alpha_1(k+1)q_1(k) + z^{-2}\alpha_2(k) = 1 - z^{-2} + z^{-1}q_1(k) - z^{-3}q_1(k)$$
$$+z^{-3}\alpha_2(k+1)q_1(k) + z^{-1}\beta_1(k)p_0(k) + z^{-2}\beta_2(k)p_0(k)$$
$$+z^{-2}\beta_1(k+1)p_1(k) + z^{-3}\beta_2(k+1)p_1(k)$$

Collecting the coefficients of the like powers, we get

$$\begin{aligned} q_1(k) + \alpha_1(k) + \beta_1(k)p_0(k) &= q_1(k) \\ \alpha_1(k+1)q_1(k) + \alpha_2(k) + \beta_2(k)p_0(k) + \beta_1(k+1)p_1(k) &= -1 \\ \alpha_2(k+1)q_1(k) + \beta_2(k+1)p_1(k) &= -q_1(k) \end{aligned}$$

To solve the above set of equations, they are first written in the matrix form as shown below and solved online numerically.

$$\begin{bmatrix} 0 & \beta_1(k) & 0 \\ \alpha_1(k+1) & \beta_2(k) & \beta_1(k+1) \\ \alpha_2(k+1)+1 & 0 & \beta_2(k+1) \end{bmatrix} \begin{bmatrix} q_1(k) \\ p_0(k) \\ p_1(k) \end{bmatrix} = \begin{bmatrix} -\alpha_1(k) \\ -\alpha_2(k) - 1 \\ 0 \end{bmatrix} \tag{4.18}$$

The reason for not solving the above equation symbolically to obtain explicit expressions for each parameter as done for the previous case is discussed shortly.

Comments about Continuous-time vs Discrete domain design

The discussions up to this point show that this control framework can be designed and implemented in either the continuous-time or the discrete domain. However, the time-varying nature of the entire system creates some unique challenges which were previously not of concern in the time-invariant setting.

This is mainly due to the operators "s" and "z^{-1}" not commuting with the time-varying coefficients. This property poses some serious implementation challenges with the continuous-time implementation as shown below. Consider the multiplication of just two terms from different PDOs given by,

$$s^2\alpha(t) \cdot s^2\beta(t) = \underbrace{s^4\alpha(t)\beta(t)}_{\star} - 2s^3\dot{\alpha}(t)\beta(t) + s^2\ddot{\alpha}(t)\beta(t) \tag{4.19}$$

An expression which would have contained one term i.e., ($\star$) in the time-invariant case now contains 3 terms. The number and complexity of the terms increases quickly with the increase in order of the corresponding PDOs. Every stage of the control design process i.e., obtaining the time-varying I/O representation of the plant/reference generating dynamics, the design of the internal model unit and the stabilizer (discussed later) involves similar manipulation of the PDOs and thus makes the implementation process extremely challenging for higher order PDOs which are essential to model the plant/reference signal dynamics accurately. The discrete systems exhibit a key difference from

the continuous case as shown below.

$$z^{-2}\alpha(k) \cdot z^{-2}\beta(k) = z^{-4}\alpha(k+2)\beta(k) \tag{4.20}$$

The multiplication of each pair of terms from the PDOs results in just one term. Hence, the implementation procedure remains tractable even for very high order PDOs.

Upon closer inspection of the examples shown earlier, another issue can be identified. Even though the process of designing the internal model unit is the same for both the approaches, the last step of solving the resulting system of equations was treated differently for each of them. This is because, for the stabilizer design, in addition to the internal model parameters, their derivatives (previews in the case of discrete domain design) are also needed. The key difference is that the preview of the coefficients can be obtained simply by changing the time-step index of the all the relevant parameters in Eq. 4.18. However to obtain the derivatives, the full symbolic expressions as shown in Eq. 4.17 are required and the expressions for the derivatives again become extremely complicated for high order systems. Also, for implementation purposes, it is easier to work with previews and memories as opposed to derivatives since the latter would require increasing degrees of smoothness of the relevant parameter trajectories.

The continuous time implementation in addition to Approach 1 can also be applied to Approach 2 by transforming all the dynamics using an appropriate scaling variable i.e., the rotational speed to make the rotational angle as the independent variable in place of time. Similarly, the discrete implementation in addition to being applicable to approach 2 as described earlier can also be used for approach 1. The plant model is obtained by discretizing the continuous LTI dynamics with a desired sample time to obtain a time-invariant difference equation. The generating dynamics i.e., Eq. 4.2, when discretized with the same sample time results in the general time-varying state space representation similar to Eq. 4.9 which can then be transformed to the I/O representation using the steps based on Eqs. 4.11→4.13. The design procedure for the internal model unit remains the same for all cases.

Since there are no obvious benefits associated with working in the continuous-time domain either for design or implementation, the discrete version of the controller is used for all further investigations. If the reader wishes to pursue the application of the continuous-time approach for higher order systems, the information provided up to this point can be used in conjunction with [68], which presents a tutorial overview of applying the controller to a hydraulic hydrostatic dynamometer for tracking a low order signal i.e., a 1-harmonic frequency varying sinusoid.

4.7 Stabilizer Unit {5}

As mentioned previously, the internal-model unit by itself can only produce the feedforward component of the control signal which can guarantee the tracking performance under idealized conditions. However, practical issues such as model uncertainty, external disturbances and unknown initial conditions of the various dynamic systems in the controller require that the entire augmented system (i.e., the plant and the internal model unit) needs to be stabilized before the controller can be implemented.

4.7.1 Dynamic SISO unit

A dynamic single-input single-output (SISO) stabilizer based on pole placement was introduced in [38]. The system is designed in the I/O representation such that $u_{st} = \mathcal{N}\mathcal{M}^{-1}[e]$, where the PDOs $\mathcal{N}$ and $\mathcal{M}$ are obtained by solving Eq. 4.21.

$$\begin{aligned} \Lambda Q\bar{\mathcal{M}} + \mathcal{G}\mathcal{P}\bar{\mathcal{N}} &= \mathcal{A}_s \\ \mathcal{N} &= Q\bar{\mathcal{N}} \\ \mathcal{M} &= Q\bar{\mathcal{M}} \end{aligned} \tag{4.21}$$

where, $\bar{\mathcal{M}}$ is a monic PDO and $\mathcal{A}_s$ is chosen such that the PSO ${\mathcal{A}_s}^{-1}$ is exponentially stable since it directly influences the transient behavior of the entire closed loop system. Similar to the internal model unit, choosing $order(\bar{\mathcal{N}}) = order(\bar{\mathcal{M}}) = 2N - 2$ ensures the solvability of Eq. 4.21 while minimizing the overall order of the controller. The same examples shown for the internal model unit can be used for solving Eq. 4.21. The simplicity of the design procedure of this stabilizer allows it to be implemented relatively easily as long as the complexity of the plant/reference generating dynamics i.e., the values of N, n and the resulting controller are within the capability of the computing hardware/software. This is especially useful for simulating the controller to validate the design of the internal model unit. However, this stabilization approach is currently not capable of addressing the following requirements to enable its implementation on experimental hardware.

- **Robustness :** Systematic way to ensure robustness to handle uncertainties in the actuator dynamics.
- **Control Saturation :** Ability to constrain the magnitude of the control signal during transients to avoid potential actuator saturation.

- **High order dynamic nature :** of the stabilizer poses challenges in achieving sufficient bandwidth (sample times) for online implementation on real-time hardware.

4.7.2 Parameter-dependent output gain injection

To overcome these challenges, a new approach for designing a low order and robust stabilizer was first proposed in [68] for the continuous-time implementation and later extended to the discrete setting in [69] and [70]. For the reasons explained earlier, only the information pertaining to the discrete domain are summarized below.

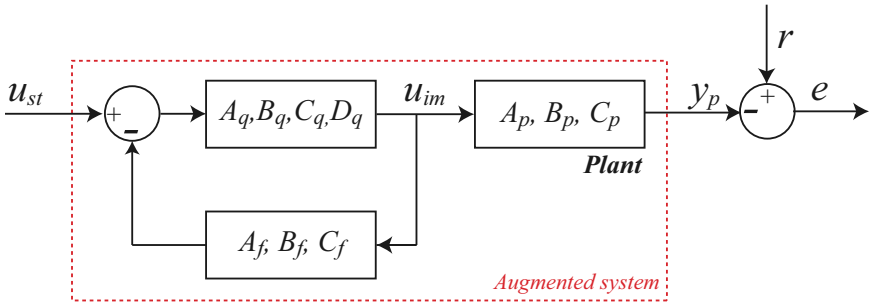

Figure 4.3: Schematic of the augmented system in the state space representation

The design and implementation of the stabilizer in the new approach is carried out using the state space representation of the relevant systems. A schematic of the augmented system to be stabilized is shown in Fig. 4.3. Here, $A_p(k)$, $B_p(k)$ & $C_p(k)$ correspond to the model of the plant dynamics. Since block {3} is designed such that, the I/O characteristics are the same as the dynamics of the plant, matrices $A_f(k)$, $B_f(k)$ & $C_f(k)$ can be chosen to be the same as $A_p(k)$, $B_p(k)$ & $C_p(k)$. $A_q(k)$, $B_q(k)$, $C_q(k)$ & $D_q(k)$ are the state space matrices corresponding to the minimal realization of the dynamics for the {4} block in Fig. 4.2 and are given by,

$$A_q(k) = \begin{bmatrix} 0 & 1 & 0 & \cdots & 0 \\ 0 & 0 & 1 & \cdots & 0 \\ \vdots & \vdots & \vdots & \ddots & \vdots \\ 0 & 0 & 0 & \cdots & 1 \\ A_{q1}(k) & A_{q2}(k) & A_{q3}(k) & \cdots & A_{qN-1}(k) \end{bmatrix}, \; B_q(k) = \begin{bmatrix} 0 \\ 0 \\ \vdots \\ 0 \\ 1 \end{bmatrix} \tag{4.22}$$

$$C_q(k) = \begin{bmatrix} C_{q1}(k) & C_{q2}(k) & C_{q3}(k) & \cdots & C_{qN-1}(k) \end{bmatrix}$$

$$D_q(k) = p_0(k)$$

$$A_{qi}(k) = q_{N-i}(k-N+i)$$
$$C_{qi}(k) = p_{N-i}(k-N+i) - p_0(k)q_{N-i}(k-N+i)$$

Using the above information, the state space representation of the augmented system to be stabilized i.e., the interconnection of the plant and the internal-model unit can be written as follows,

$$\begin{aligned} x_a(k+1) &= A_a(k)x_a(k) + B_a(k)u_{st}(k) \\ y_p(k) &= C_a(k)x_a(k) \\ e(k) &= r(k) - y_p(k) \end{aligned} \tag{4.23}$$

$$x_a(k) = \begin{bmatrix} x_p(k) \\ x_q(k) \\ x_f(k) \end{bmatrix},\ A_a(k) = \begin{bmatrix} A_p(k) & B_p(k)C_q(k) & -B_p(k)D_q(k)C_p(k) \\ 0 & A_q(k) & -B_q(k)C_p(k) \\ 0 & B_p(k)C_q(k) & A_p(k) - B_p(k)D_q(k)C_p(k) \end{bmatrix}$$
$$B_a(k) = \begin{bmatrix} 0 \\ B_q(k) \\ 0 \end{bmatrix},\ C_a(k) = \begin{bmatrix} C_p(k) & 0 & 0 \end{bmatrix}$$

The objective is to generate the signal u_{st} based on e such that the entire closed loop system dynamics becomes exponentially stable. It is worth noting that, the structure of the input matrix i.e., B_a is a consequence of injecting the stabilizer control signal at the specific location as shown in Fig. 4.3. However, since the entire internal model unit is a virtual subsystem, the portion of the input matrix corresponding to states of the internal model unit can be arbitrarily chosen. For this application, it will be chosen as an identity matrix I i.e., $N+n-1$ control signals are injected directly into the state of the internal model. The additional degrees of freedom provided by the multiple control signals are expected to improve the performance of the stabilizer.

To further aid the control design, a dynamic compensator is added in parallel to the internal model unit as shown in Fig. 4.4. By following the techniques described in [70], the state space matrices of the compensator i.e., $A_c,\ B_c,\ C_c$& D_c are chosen as follows,

$$\begin{aligned} x_c(k+1) &= A_c(k)x_c(k) + B_c(k)U_c(k) \\ y_c(k) &= C_c(k)x_c(k) + D_c(k)U_c(k) \end{aligned} \tag{4.24}$$

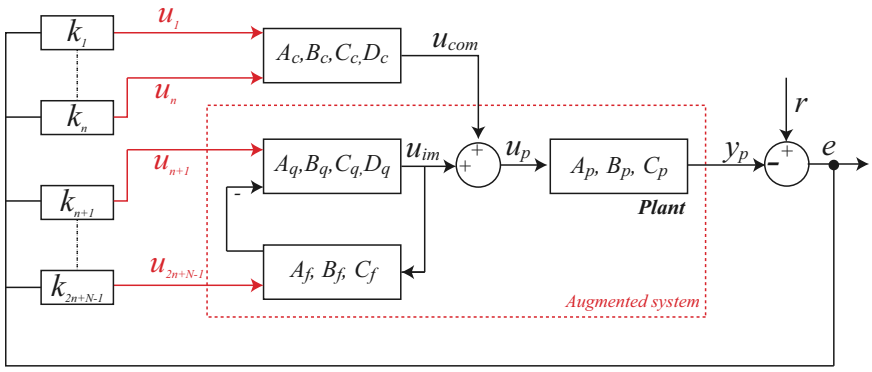

Figure 4.4: Schematic of the augmented system with the dynamic compensator in parallel with the internal model unit and the output gain injection feedback

$$A_c(k) = \begin{bmatrix} \frac{-\beta_2(k)}{\beta_1(k+1)} & 1 & 0 & \cdots & 0 \\ \frac{-\beta_3(k)}{\beta_1(k+2)} & 0 & 1 & \cdots & 0 \\ \vdots & \vdots & \vdots & \ddots & \vdots \\ \frac{-\beta_{n-1}(k)}{\beta_1(k+n-2)} & 0 & 0 & \cdots & 1 \\ \frac{-\beta_n(k)}{\beta_1(k+n-1)} & 0 & 0 & \cdots & 0 \end{bmatrix}_{n-1\times n-1}$$

$$B_c(k) = \begin{bmatrix} \frac{-\beta_2(k)}{\beta_1(k+1)\beta_1(k)} & \frac{1}{\beta_1(k+1)} & 0 & 0 & \cdots & 0 \\ \frac{-\beta_3(k)}{\beta_1(k+2)\beta_1(k)} & 0 & \frac{1}{\beta_1(k+2)} & 0 & \cdots & 0 \\ \vdots & \vdots & \vdots & \ddots & \cdots & \vdots \\ \frac{-\beta_{n-1}(k)}{\beta_1(k+n-2)\beta_1(k)} & 0 & 0 & 0 & \frac{1}{\beta_1(k+n-2)} & 0 \\ \frac{-\beta_n(k)}{\beta_1(k+n-1)\beta_1(k)} & 0 & 0 & 0 & \cdots & \frac{1}{\beta_1(k+n-1)} \end{bmatrix}_{n-1\times n}$$

$$C_c(k) = \begin{bmatrix} 1 & 0 & 0 & \cdots & 0 \end{bmatrix}_{1\times n-1},\ D_c(k) = \begin{bmatrix} \frac{1}{\beta_1(k)} & 0 & 0 & \cdots & 0 \end{bmatrix}_{1\times n}$$

This alters the dynamics of the augmented system such that, the input matrix from the signals $U_c(k) = [u_1(k),\ u_2(k),\ \cdots,\ u_n(k)]$ to the states corresponding to the actual plant now becomes $I_{(n\times n)}$. Hence the overall input matrix of the augmented system i.e., $B_a(k) = I$, which essentially means that the stabilizer can be designed to directly influence all the states of the system. The utility of this unique feature becomes obvious later on during the synthesis of the controller. Consider a

stabilizer based on parameter-dependent output gain injection as shown below,

$$
\begin{aligned}
u_{st}(k) &= -K(k) \cdot e(k) \\
u_{st}(k) &= \begin{bmatrix} u_1(k) & u_2(k) & \cdots & u_{2n+N-1}(k) \end{bmatrix}^T \\
K(k) &= \begin{bmatrix} k_1(k) & k_2(k) & \cdots & k_{2n+N-1}(k) \end{bmatrix}^T
\end{aligned} \tag{4.25}
$$

The unforced closed loop system i.e., when $r = 0$ can be written as,

$$
\begin{aligned}
x_{cl}(k+1) &= A_{cl}(k)x_{cl}(k) + \bar{B}(k)r(k) \\
\bar{y}(k) &= \bar{C}(k)x_{cl}(k) + \bar{D}(k)r(k) \\
A_{cl}(k) &= A_a(k) + B_a(k)K(k)C_a(k) \\
C_{cl}(k) &= C_a(k) \\
\bar{B}(k) &= -B_a(k)K(k)
\end{aligned} \tag{4.26}
$$

$\bar{C}$ and $\bar{D}$ are matrices chosen depending on the signal of interest "$\bar{y}$" (discussed later). Since the stabilizer has no dynamics, the states of the closed loop system are the same as the states of the augmented system i.e., $x_{cl}(k) = x_a(k)$. The problem of synthesizing the time-varying gain vector $K(k)$ is converted into finding a time-varying positive definite matrix sequence $\mathcal{P}(k) > 0$ such that $\mathcal{V}(k) = x_{cl}(k)^T\mathcal{P}(k)x_{cl}(k) > 0$ everywhere except when $x_{cl}(k) = 0$. Based on the well documented lyapunov stability criteria, the forced system is exponentially stable and the L_2-norm in the $r - \bar{y}$ channel is less than $\gamma > 0$ i.e., $sup_{r \in L_2} \dfrac{||\bar{y}||_2}{||r||_2} < \gamma$ if

$$
\mathcal{V}(k+1) - \mathcal{V}(k) + \bar{y}^T\bar{y} - \gamma^2 r^T r < 0 \tag{4.27}
$$

$$
x_{cl}(k+1)^T\mathcal{P}(k+1)x_{cl}(k+1) - x_{cl}(k)^T\mathcal{P}(k)x_{cl}(k) + \bar{y}(k)^T\bar{y}(k) - \gamma^2 r(k)^T r(k) < 0
$$

Substituting the system matrices, the above equation can be written as follows. For notational convenience, the indices for the current time step i.e., "(k)" are dropped and the subscript "k+1" is used for terms corresponding to the time step "(k+1)"

$$
\left[A_{cl}x_{cl} + \bar{B}r\right]^T \mathcal{P}_{k+1} \left[A_{cl}x_{cl} + \bar{B}r\right] - x_{cl}^T\mathcal{P}x_{cl} + \left[\bar{C}x_{cl} + \bar{D}r\right]^T \left[\bar{C}x_{cl} + \bar{D}r\right] - \gamma^2 r^T r < 0
$$

Expanding and collecting the coefficients,

$$x_{cl}^T \left[A_{cl}^T \mathcal{P}_{k+1} A_{cl} - \mathcal{P} + \bar{C}^T \bar{C}\right] x_{cl} + x_{cl}^T \left[A_{cl}^T \mathcal{P}_{k+1} \bar{B} + \bar{C}^T \bar{D}\right] r$$
$$+ r^T \left[\bar{B}^T \mathcal{P}_{k+1} A_{cl} + \bar{D}^T \bar{C}\right] x_{cl} + r^T \left[\bar{B}^T \mathcal{P}_{k+1} \bar{B} + \bar{D}^T \bar{D} - \gamma^2\right] r < 0$$

Rewriting the above expression in the matrix form,

$$\begin{bmatrix} x_{cl}^T & r^T \end{bmatrix} \underbrace{\begin{bmatrix} A_{cl}^T \mathcal{P}_{k+1} A_{cl} - \mathcal{P} + \bar{C}^T \bar{C} & A_{cl}^T \mathcal{P}_{k+1} \bar{B} + \bar{C}^T \bar{D} \\ \bar{B}^T \mathcal{P}_{k+1} A_{cl} + \bar{D}^T \bar{C} & \bar{B}^T \mathcal{P}_{k+1} \bar{B} + \bar{D}^T \bar{D} - \gamma^2 \end{bmatrix}}_{\dagger} \begin{bmatrix} x_{cl} \\ r \end{bmatrix} < 0$$

The original problem has now been transformed into solving for the unknown variables i.e., the Lyapunov matrix $\mathcal{P}$ and the gain vector K such that the matrix † is negative definite. Well established mathematical techniques are available for the solution of matrix inequalities in the linear setting. However, they cannot be directly applied to the problem at hand since the above inequality is both infinite dimensional and non-linear. The following steps are aimed at transforming this inequality into a form that is solvable using the available tools.

Definition : Schur Complement

The Schur's complement formula is one of the standard techniques used to convert inequalities resulting from control problems into LMIs. It states that the following statements are equivalent.

$$\begin{bmatrix} \Phi_{11} & \Phi_{12} \\ \Phi_{12}^T & \Phi_{22} \end{bmatrix} < 0 \qquad \Longleftrightarrow \qquad \begin{cases} \Phi_{22} < 0 \\ \Phi_{11} - \Phi_{12} \Phi_{22}^{-1} \Phi_{12}^T < 0 \end{cases}$$

Hence, a quadratic matrix inequality such as † can be transformed as follows,

$$\left[\begin{array}{cc|c} A_{cl}^T \mathcal{P}_{k+1} A_{cl} - \mathcal{P} & A_{cl}^T \mathcal{P}_{k+1} \bar{B} & \bar{C}^T \\ \bar{B}^T \mathcal{P}_{k+1} A_{cl} & \bar{B}^T \mathcal{P}_{k+1} \bar{B} - \gamma^2 & \bar{D}^T \\ \hline \bar{C} & \bar{D} & -I \end{array}\right] < 0$$

Once again, applying the schur's complement, we get

$$\left[\begin{array}{c|cc|c} -\mathcal{P}_{k+1} & \mathcal{P}_{k+1} A_{cl} & \mathcal{P}_{k+1} \bar{B} & 0 \\ \hline A_{cl}^T \mathcal{P}_{k+1} & -\mathcal{P} & 0 & \bar{C}^T \\ \bar{B}^T \mathcal{P}_{k+1} & 0 & -\gamma^2 & \bar{D}^T \\ 0 & \bar{C} & \bar{D} & -I \end{array}\right] < 0 \tag{4.28}$$

The above transformations have enabled the reduction in the number of quadratic terms in the inequality. The next step is to convert it into a finite-dimensional problem by utilizing the fact that the augmented system matrices are dependent on the parameter $\omega(k)$. The entire space of ω is gridded and the lyapunov matrix at each grid point "ψ" is denoted by $\mathcal{P}_\psi$ and $\mathcal{P}_{k+1}$ is approximated using Ω_ψ as defined below

$$\Omega_\psi = \mathcal{P}_{k+1} \approx= \mathcal{P}_{\psi+1} + \Delta t \frac{\mathcal{P}_{\psi+1} - \mathcal{P}_\psi}{\omega_{\psi+1} - \omega_\psi} \overline{\dot{\omega}_\psi}$$

where $\overline{\dot{\omega}_\psi}$ is the estimate of the worst case variation of ω_ψ i.e., $max(\dot{\omega}_\psi)$. Eq. 4.28 at each grid point then becomes,

$$\begin{bmatrix} -\Omega_\psi & \Omega_\psi A_{cl} & \Omega_\psi \bar{B} & 0 \\ A_{cl}^T \Omega_\psi & -\mathcal{P}_\psi & 0 & \bar{C}^T \\ \bar{B}^T \Omega_\psi & 0 & -\gamma^2 & \bar{D}^T \\ 0 & \bar{C} & \bar{D} & -I \end{bmatrix} < 0$$

Substituting the matrices corresponding to the closed loop system, we get

$$\underbrace{\begin{bmatrix} -\Omega_\psi & \Omega_\psi \left[A_a + B_a K_\psi C_a\right] & -\Omega_\psi B_a K_\psi & 0 \\ \left[A_a + B_a K_\psi C_a\right]^T \Omega_\psi & -\mathcal{P}_\psi & 0 & \bar{C}^T \\ -\left[B_a K_\psi\right]^T \Omega_\psi & 0 & -\gamma^2 & \bar{D}^T \\ 0 & \bar{C} & \bar{D} & -I \end{bmatrix}}_{\star} < 0$$

All the closed loop system matrices i.e., A_a, B_a and C_a are also evaluated at each grid point by assuming the worst case variation in ω for the preview/memory information of various time-varying parameters. The above inequality is non-convex (more specifically, bilinear due to the multiplication of "K_ψ" with both "$\mathcal{P}_{\psi+1}$" and "$\mathcal{P}_\psi$"). To remove this, the following transformation using a general positive definite matrix variable "$\mathcal{H}_\psi$" is introduced

$$\begin{bmatrix} \mathcal{H}_\psi \Omega_\psi^{-1} & 0 & 0 & 0 \\ 0 & I & 0 & 0 \\ 0 & 0 & I & 0 \\ 0 & 0 & 0 & I \end{bmatrix} \begin{bmatrix} & & & \\ & \star & & \\ & & & \end{bmatrix} \begin{bmatrix} \Omega_\psi^{-1} \mathcal{H}_\psi^T & 0 & 0 & 0 \\ 0 & I & 0 & 0 \\ 0 & 0 & I & 0 \\ 0 & 0 & 0 & I \end{bmatrix} < 0$$

Simplifying this, we get

$$\begin{bmatrix} -\mathcal{H}_\psi \Omega_\psi^{-1} \mathcal{H}_\psi^T & \Omega_\psi \left[A_a + B_a K_\psi C_a\right] & -\Omega_\psi B_a K_\psi & 0 \\ \left[A_a + B_a K_\psi C_a\right]^T \Omega_\psi & -\mathcal{P}_\psi & 0 & \bar{C}^T \\ -\left[B_a K_\psi\right]^T \Omega_\psi & 0 & -\gamma^2 & \bar{D}^T \\ 0 & \bar{C} & \bar{D} & -I \end{bmatrix} < 0 \tag{4.29}$$

Based on the result from [71], we use the fact that,

$$-\mathcal{H}_\psi \Omega_\psi^{-1} \mathcal{H}_\psi^T < -\mathcal{H}_\psi^T - \mathcal{H}_\psi + \Omega_\psi$$

To show that, the matrix variables satisfying the following inequality automatically satisfy (4.29),

$$\begin{bmatrix} -\mathcal{H}_\psi^T - \mathcal{H}_\psi + \Omega_\psi & \mathcal{H}_\psi \left[A_a + B_a K_\psi C_a\right] & -\mathcal{H}_\psi B_a K_\psi & 0 \\ \left[A_a + B_a K_\psi C_a\right]^T \mathcal{H}_\psi^T & -\mathcal{P}_\psi & 0 & \bar{C}^T \\ -\left[B_a K_\psi\right]^T \mathcal{H}_\psi^T & 0 & -\gamma^2 & \bar{D}^T \\ 0 & \bar{C} & \bar{D} & -I \end{bmatrix} < 0$$

The non-convexity due to the bilinear entries is removed by using the fact that $B_a = I$ and introducing a new matrix variable $\mathcal{L}_\psi = \mathcal{H}_\psi K_\psi$. The above inequality then becomes an LMI,

$$\begin{bmatrix} -\mathcal{H}_\psi^T - \mathcal{H}_\psi + \Omega_\psi & \mathcal{H}_\psi A_a + \mathcal{L}_\psi C_a & -\mathcal{L}_\psi & 0 \\ A_a^T \mathcal{H}_\psi^T + C_a^T \mathcal{L}_\psi^T & -\mathcal{P}_\psi & 0 & \bar{C}^T \\ -\mathcal{L}_\psi^T & 0 & -\gamma^2 & \bar{D}^T \\ 0 & \bar{C} & \bar{D} & -I \end{bmatrix} < 0$$

These LMIs can be solved offline using commercially available software to calculate the gain vector $K_\psi = \mathcal{H}_\psi^{-1} \mathcal{L}_\psi$ at each grid point. During online implementation, the gains at each time step i.e., $K(k)$ can be interpolated from the stored values of $K_\psi(\omega_\psi)$. The specific details associated with ensuring the three desirable properties of the stabilizer are presented next.

- **Robustness :** The ideas discussed in [68], can be used to ensure stability of the closed loop if the effect of the uncertainties in the plant model can be written in the form of parameter perturbations of the closed loop matrices. This is achieved by formulating multiple LMIs based on Eq. 4.30 by replacing A_a with $A_a + \Delta_i^*$, where Δ_i^*, are matrices of same dimension as A_a and are chosen to capture the extreme values of the parameters of the closed loop matrices. Each Δ_i^*, requires an additional LMI at each grid point and hence care needs to be exercised

during the design procedure to keep the overall number of LMIs to a manageable number. The gains obtained based on this synthesis can ensure stability of the closed loop system as long as the parameter perturbations are within the boundaries specified in the design. Other ideas for dealing with unstructured uncertainties by the appropriate choice of γ, $\bar{C}^T$ and $\bar{D}^T$ have also been discussed in the same paper, but have not been implemented for this study.

- **Control Saturation :** By modifying Eq. 4.30 using $\bar{C} = \begin{bmatrix} 0_{1\times n} & 1 & 0 & \cdots & 0 \end{bmatrix}$, $\bar{D} = 0$ and γ based on the plant's I/O characteristics, it is possible to restrict the magnitude of the signal from the internal model unit to avoid potential control saturation during transients

$$sup_{r\in L_2} \frac{||u_{im}||_2}{||r||_2} < \gamma$$

Similarly, to restrict the magnitude of the control signal from the dynamic compensator, the methods described in [68] can be used to include additional LMI constraints at each grid point to constrain the magnitude of the gains $K_1 \rightarrow K_n$ as shown below,

$$\begin{bmatrix} -\lambda_\alpha \alpha & \mathcal{L}_\psi^T \\ \mathcal{L}_\psi & -\lambda_\alpha \alpha \mathcal{H}_\psi \end{bmatrix} < 0 \qquad \begin{bmatrix} \lambda_\beta \beta & g \\ g^T & \lambda_\beta \beta \mathcal{H}_\psi \end{bmatrix} > 0 \tag{4.30}$$

$$\Rightarrow ||g\mathcal{H}_\psi^{-1}\mathcal{L}_\psi||_2 < \lambda_\alpha \lambda_\beta \alpha \beta$$

For minimizing gain K_1, choose $g = \begin{bmatrix} 1 & 0 & 0 & \cdots \end{bmatrix}$ and $\lambda_\alpha = ||\mathcal{H}_\psi^{-\frac{1}{2}}\mathcal{L}_\psi||_2$ and $\lambda_\beta = ||g\mathcal{H}_\psi^{-\frac{1}{2}}||_2$ from the baseline synthesis i.e., the solution obtained by solving only Eq. 4.30 at each grid point. The choice of α and β needs to be performed iteratively to ensure they are as small as possible while ensuring the feasibility of the entire synthesis procedure. Similarly for minimizing gain K_2, choose $g = \begin{bmatrix} 0 & 1 & 0 & \cdots \end{bmatrix}$ and repeat the process described previously to add two additional LMIs at each grid point. The same procedure can be applied to constrain all the gains corresponding to the compensator. It should also be noted that, the control signal u_{com} was not part of the original design of the internal model based controller i.e., it is only a consequence of the theoretical requirement that $B_p = I$ for the LMI based gain synthesis purpose. Hence it is expected that, minimizing the signal u_{com} based on the discussions above will not affect the performance of the overall system.

- **Computational complexity :** Since the dynamic compensator is of low order i.e., $n-1$ and the rest of the stabilizer is based on interpolation of the parameter-dependent gains, the

computational complexity of this approach at each time-step during online implementation is very low. Hence this approach for stabilizer design includes all the desirable characteristics required for implementation on experimental systems.

Remark : One potential challenge with this approach is that, as the order of the plant/reference generating dynamics increases, the dimensions of the matrix variables and subsequently the dimensions of the LMIs at each grid point also increase quickly. To avoid issues associated with the offline synthesis, care needs to be exercised in choosing the gridding interval to keep the overall quantity of the unknown variables within a reasonable limit.

Chapter 5

Implementation of the LTV - Internal Model based Controller

The discussions about the various steps involved in the design of various units in the time-varying internal model based controller presented earlier indicate that, as the order of the PDOs describing the plant/generating dynamics increases, the challenges associated with the design and real-time implementation of the control framework also increase accordingly. However, it is also desirable to use higher order PDOs to increase the accuracy of modeling the dynamics and thus improve the tracking performance. To help address these conflicting requirements, this chapter aims to guide the practical implementation of the control framework to realize the best tracking performance while remaining tractable. Experimental results are used to both validate the proposed ideas as well as motivate further research into addressing the issues associated with extending the framework to very high order systems.

5.1 Fixed vs Variable Sampling in Angle Domain Control

For the second approach, i.e., angle domain control, the reference signal generating dynamics are given by $\Lambda^{-1}(z,k) = 1 - z^{-N}$, where N is the number of discrete sampling instants in one period of the signal. Figs. 5.1(a) shows the angular sampling achieved by representing the reference signal using a model of order $N = 24$. The angular sampling interval is directly obtained from $\Delta\theta = 720/N = 30^\circ$. Since the control is updated only at these points, to achieve precise reference tracking, it is desirable to have an increased number of samples especially in the portion corresponding to valve motion i.e., $0^\circ \rightarrow 240^\circ$. However, as the number of samples in this interval increases, the

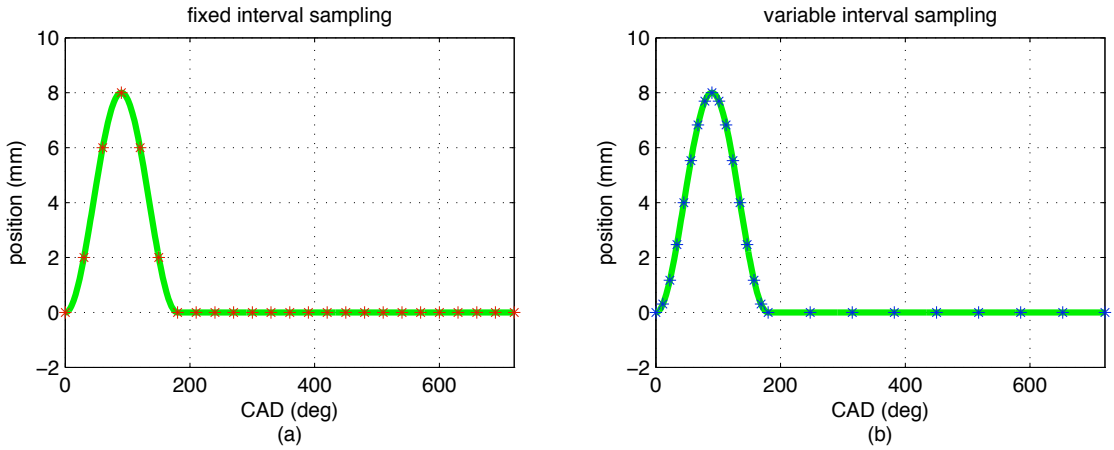

Figure 5.1: Comparison between fixed and variable angle-interval sampling.

overall order of the signal i.e., N also increases drastically.

One approach to improving the resolution of the reference signal is to utilize a unique property of this control framework. Since this controller is designed to handle the varying time periods between each sample i.e., $\Delta t(k) = \Delta\theta(k)/6W(k)$ to account for variations in $W(k)$, we can use this property to vary $\Delta\theta(k)$ within each cycle without altering the underlying principle of the controller. It would then be possible to sample more in certain portions of the trajectory and less in other portions. Such a modification is not possible with LTI controllers even for the constant speed case.

The advantage of doing so becomes evident from Fig. 5.1(b). By increasing the sampling between $0^\circ \rightarrow 240^\circ$ and decreasing the sampling between $240^\circ \rightarrow 720^\circ$, better representation of the reference signal can be achieved for the same order of the generating dynamics. For the example shown, the resolution during the lift portion can be increased to 11.25° while reducing the resolution to 67.5° during the portion when the valve is at rest. However, the scheme for distributing these sample points should not be too aggressive since it could lead to undesirable inter-sample behavior during the rest portion.

5.2 Time vs Angle Domain Control

The motivation for comparing these two approaches comes from Fig. 5.2. Using the same order of the reference generating dynamics i.e., $N = 8$, it can be seen that the approximation characteristics are quite different for both the approaches. As the duration changes from $150^\circ \rightarrow 300^\circ$, the approximation error varies significantly when using the first approach. However, for the second approach, the approximation error remains unaffected by the change in valve profile and thus appears

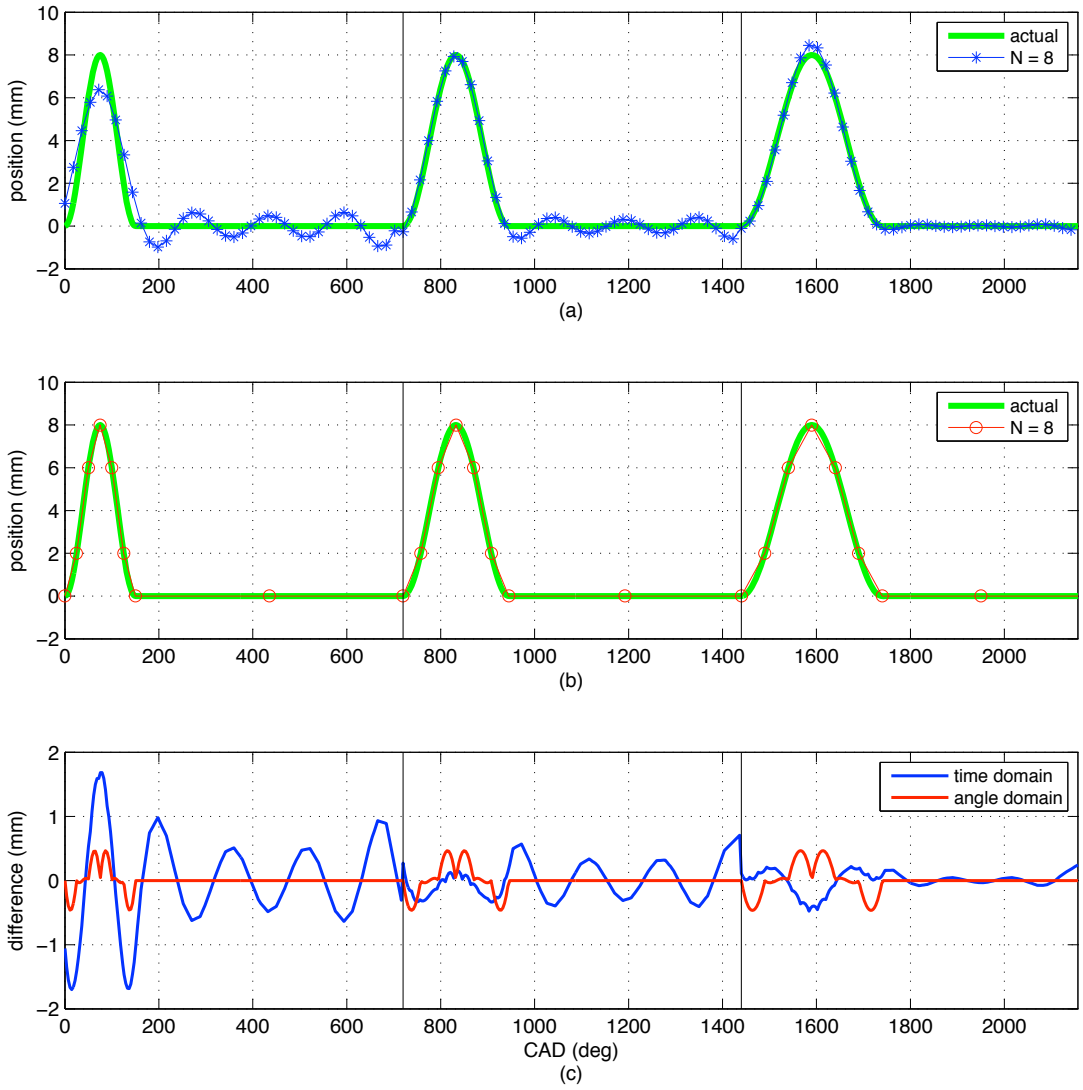

Figure 5.2: Approximation of the valve reference signal using the two approaches for various valve profiles (variable duration) and the corresponding error

to be more effective from this perspective.

On the other hand, it is reasonable to expect the feedback controller to sample the system as often as possible to ensure good tracking performance. For approach 1, the markers "*" on Fig. 5.2(a) are the result of using a sample time of 1 ms for an engine speed of 3000 RPM. The corresponding angular sampling resolution is 18°. Both these metrics indicate that it is possible to track the approximated signal with good accuracy. For approach 2, with an aggressive application of variable sampling, the angular resolutions are obtained as 25°, 37.5°& 50° for the lift portion and 285°, 247.5°& 210° for the rest portion. The time intervals corresponding to 3000 RPM range between 1.4& 15.8 ms and will further increase at lower engine speeds thus causing degradation in the tracking performance. Hence the order of N needs to be increased to much higher values to enable practical implementation of the second approach.

In summary, although approach 1 leads to larger approximation errors for lower order generating dynamics and shorter duration valve profiles, it will be able to track the approximated profile well. The second approach cannot be implemented till N is increased beyond a certain value. However, once the threshold is crossed, the signal representation and thus the tracking accuracy become independent of the valve profile.

5.3 Online Computation vs Storage of Controller Coefficients

During the implementation of traditional time-invariant controllers, the main computational burden comes from the arithmetic operations involving the update of the states of the relevant dynamic systems and calculating the control signals. However, since the dynamics of the systems in this controller are time-varying, the relevant parameters i.e., the coefficients of the various PDOs or the entries of the state space matrices need to be computed at each sample instant of the controller as well.

The number and complexity of these operations increases quickly with the order of the plant/generating dynamics. As a motivating example, we consider one particular implementation using the first approach for a plant model with $n = 2$ and the reference generating dynamics with $N = 8$. The following is a summary of arithmetic operations required at each sampling instant

1. Interpolations to obtain the gain vector $K(k)$.
2. Calculation of the stabilizer control signals $u_{st}(k)$.
3. Update the states and outputs of the dynamic compensator and the internal model unit.

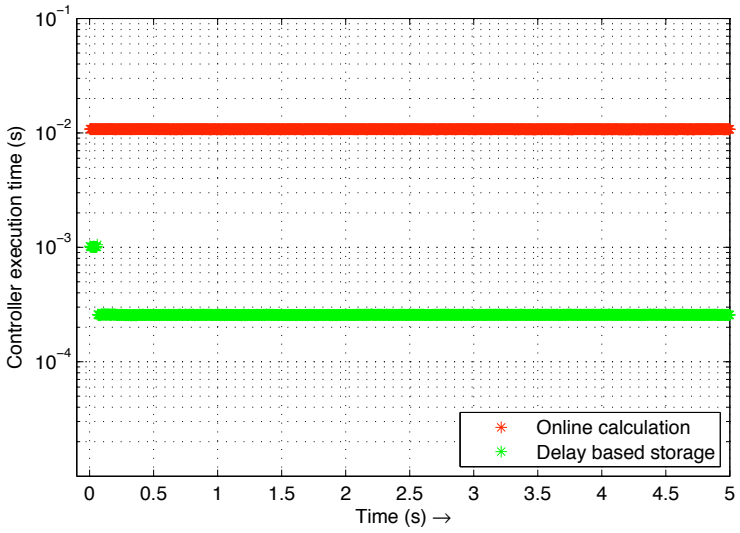

Figure 5.3: Comparison of execution times during each step for the controllers based on full online computation and partial storage.

4. Coefficients of the internal model unit PDOs i.e., $\mathcal{P}(k+x)$, $\mathcal{Q}(k+x)$, $x \in [-7, 0]$

5. Coefficients of the generating dynamics PDO i.e., $\Lambda(k+x)$, $x \in [-7, 7]$

As explained earlier, operations $1 \rightarrow 3$ are inherent to all control frameworks and typically cause minimal computational burden. However the operation 4 involves the inversion of a high dimensional matrix for solving the systems of linear equations and operation 5 also involves a number of matrix manipulations as described in Eqs. 4.12 & 4.13. A closer inspection reveals a number of redundant arithmetic operations in both these steps. For example, in operation 4, by storing the internal model unit coefficients, only the parameters for the current step i.e., $k = 0$ needs to be computed at each control execution. Similarly for operation 5, it is sufficient to computer the coefficients corresponding to $k = 7$ and use the stored values for other parameters. Further reduction in the computational burden can be achieved by observing that in Eqs. 4.12 & 4.13 a number of parameters are available from the previous step as well. A queue is implemented using delay operators to store the redundant parameters. Hence only the new entries at each step need to be calculated and added to the queue while the remaining entries are directly read from the queue.

Fig. 5.3 shows the execution times for both these controllers on real-time hardware *(specifications given in a later section)*. The controller based on full online computation took approximately 10 ms to execute for each sampling instant. Utilizing the storage based control, it was possible to reduce the execution time on the real-time hardware to 0.3 ms. Notice that, for the storage based controller, the execution time for the 1^{st} few samples is large some additional calculations need to be performed

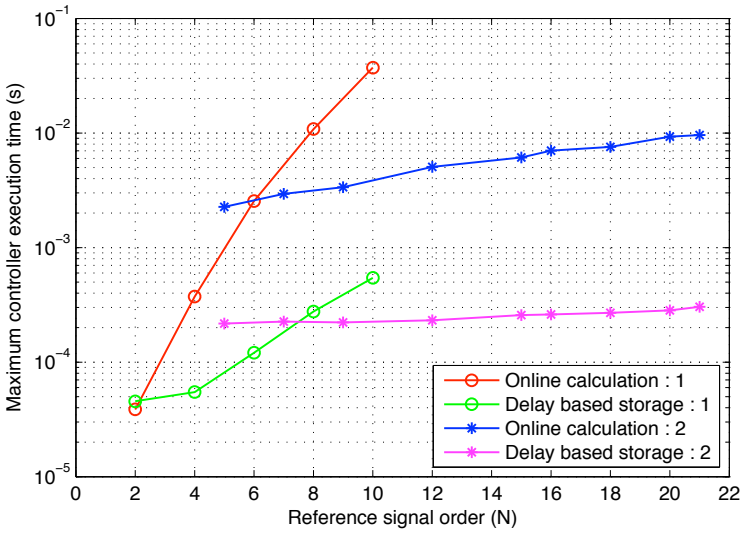

Figure 5.4: Comparison of maximum execution times for the both approaches and both types of implementation.

online till all the delay blocks have been initialized to the appropriate values. If even this issue causes concerns while implementation, it can be avoided by calculating the parameters offline and initializing the delay blocks accordingly. These ideas can help in optimizing the controller implementation to account for the resources available (memory/processor speed) and the sampling times desired.

Fig. 5.4 shows a comparison of the maximum execution times for the controllers designed to track 1, $2, \cdots 5$ harmonics for both these implementations. It is clear from the figure that with approach 1, the execution time increases drastically with the increase in the valve of N because the order of the computationally intensive canonical transformation procedure is directly related to the value of N.

For approach 2 i.e., angle domain implementation the order of the plant and thus the complexity of the canonical transformation remains the same. To emphasize this fact, the execution times for controllers based on approach 2 is also shown using both these implementations. A plant model with "$n = 4$" is used and the controllers are designed for reference signal dynamics corresponding to "$N : 5 \rightarrow 21$". Due to the difficulties explained earlier, the stabilizer based on pole placement is used. Note that, the pole placement based stabilizer is more computationally intensive because it involves the inversion of a high order matrix at each sample instant. However, it is seen that even with the added computational burden of the dynamic stabilizer (involves the inversion of a high order matrix at each sample instant), the rate at which the controller execution time increases is much slower when compared to the first approach.

5.4 Numerical issues with the Canonical Transformation

The operations involved in obtaining the canonical representation for the time-varying systems involve a number of matrix manipulations and hence are sensitive to the order of the matrices and the numerical values of the coefficients. It was observed that, as the order increases, the condition number of Q_d in Eq. 4.13 also increased. This directly corresponds to the accuracy of the coefficients of the I/O representation and when the condition number became too large, it led to problems with the gain synthesis based on the LMI optimization. Although the exact reason is unknown, there was a strong correlation between the condition number and the feasibility of the synthesis.

To get a better understanding of this phenomenon, the condition number of the transformation matrix Q_d was calculated for various system orders under different scenarios. For the first method, by holding the system sampling time constant, the engine speed (signal frequency) was varied and the observations are plotted in Fig. 5.5. For the second method, using plant models with similar frequency responses and by holding the angular sampling resolution constant, the engine speed is varied and the corresponding condition numbers are documented in Fig.5.6

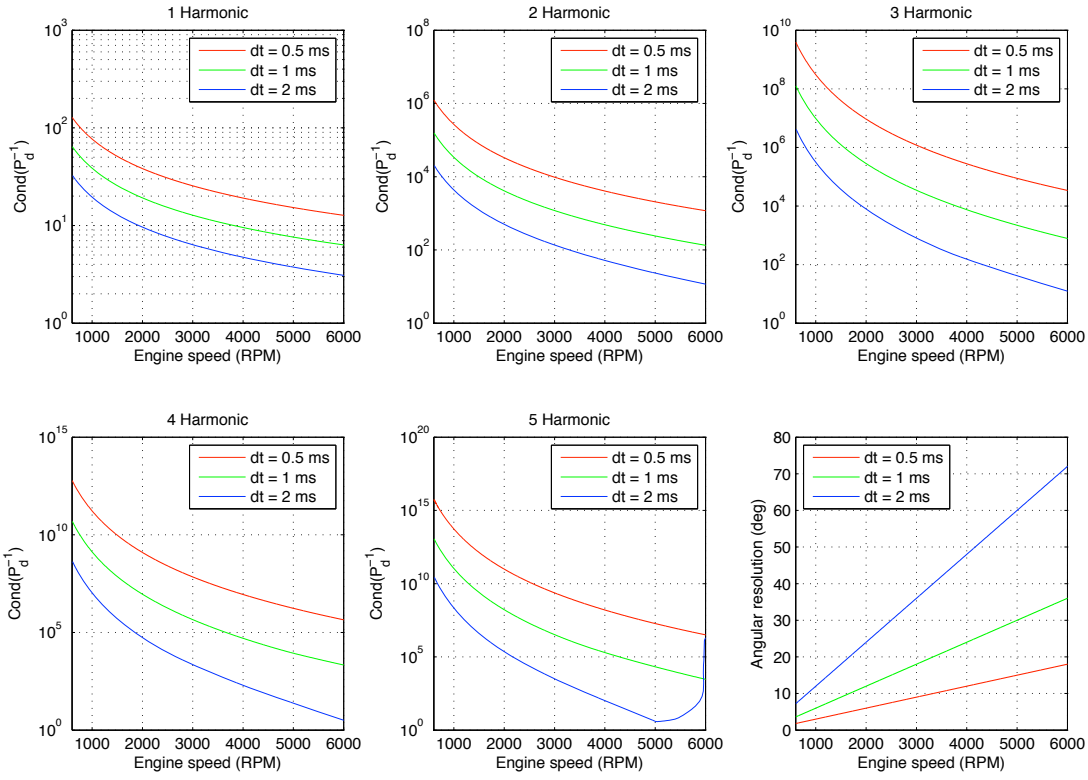

Figure 5.5: Effect of sampling time on the canonical transformation procedure in approach 1

The gain synthesis procedure failed for cases when the condition number of $Q_d(k) \approx 10^{10}$. Based on this observation, it suggests that, for high order harmonics, the it is not possible to use small sampling times for signals with lower frequencies and common intuition highlights that using large sampling times will lead to performance degradation at higher frequencies as shown in the last plot in Fig. 5.5. For the second method, for the specific plant model, using a 4^{th} order model will be able to largely avoid all these issues for all engine speeds and for most reasonable angular sampling resolutions. Higher order models are still susceptible to this phenomenon and hence these factors need to be carefully considered during the control design procedure and chosen based on the plant dynamics and signal characteristics.

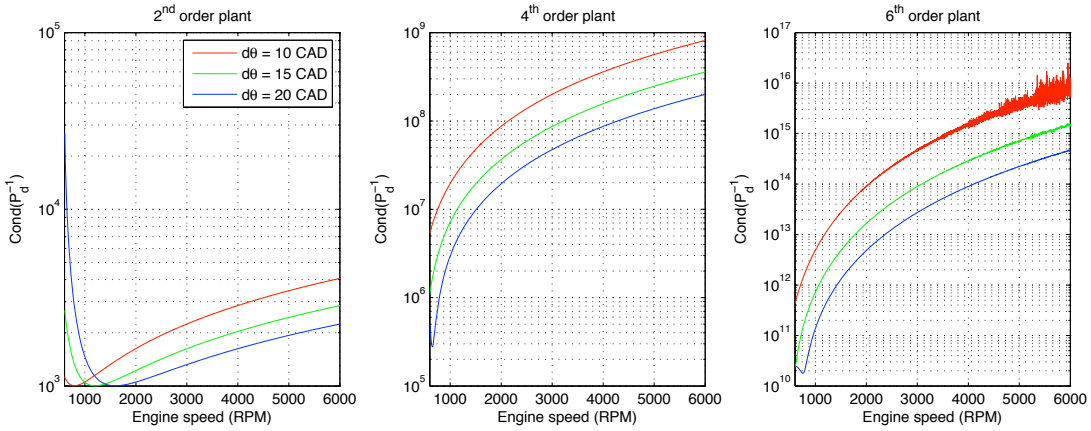

Figure 5.6: Effect of sampling time on the canonical transformation procedure in approach 2

5.5 Experimental Investigations

This section presents the results from the implementation of the proposed control framework on an experimental system.

5.5.1 Hardware setup

The setup shown in Figs. 5.7(a) and (b) is an electro-hydraulic valve actuator, which consists of a hydraulic piston that is in contact with the spring-loaded engine valve. A voice-coil actuated 3-way spool valve is used to control the flow of high pressure fluid into and out of the actuator. The displacement of the engine valve is measured using a non-contact DVRT sensor. The control hardware consists of a xPC-Target based Real-Time Operating system running on desktop computer

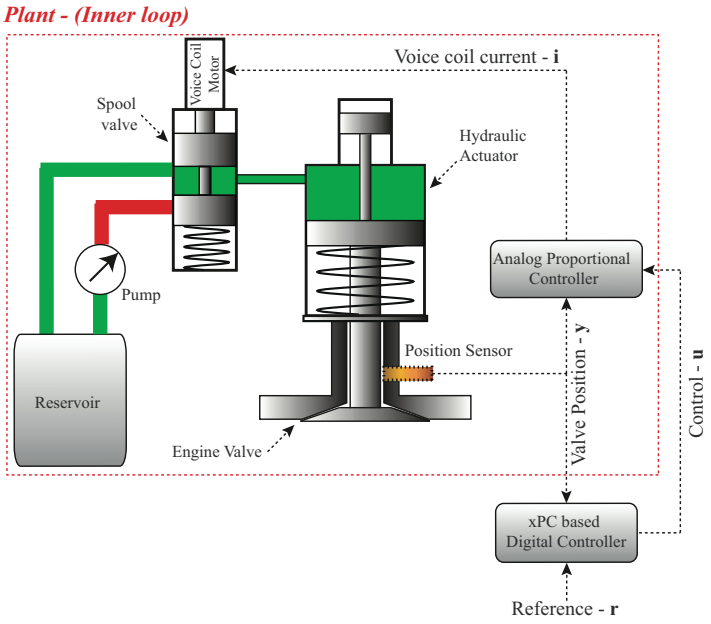

(a)

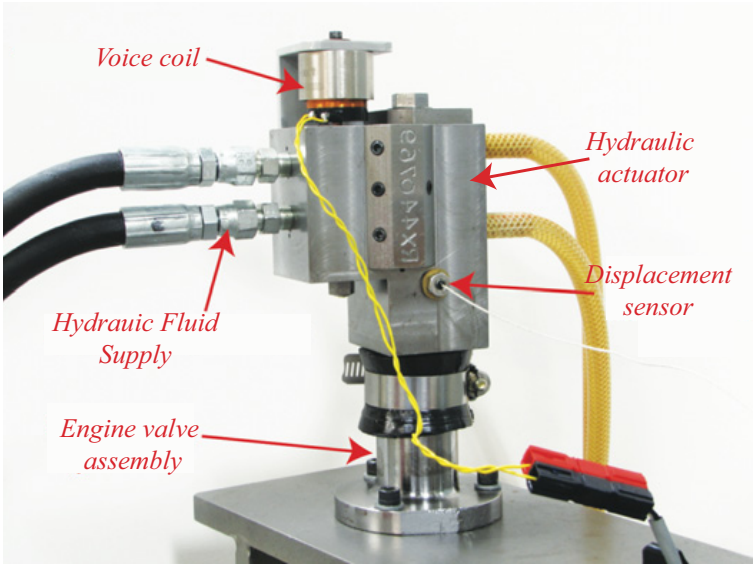

(b)

Figure 5.7: The schematic (a) and a picture (b) of the prototype camless valve actuation system

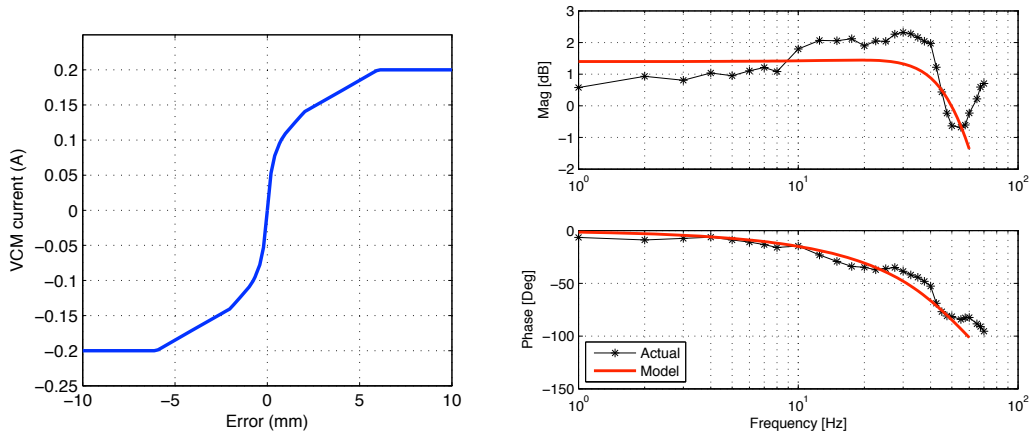

(a) (b)

Figure 5.8: (a) Static map used as the gain for the inner-loop control (b) Frequency response of the experimental system and the model used for control design

with a 2.6 GHz CPU and 2GB of RAM. The DAQ card is a Measurement Computing PCI-DAS1602-16 with 16 channels of 16 bit A/D with 5μs conversion time and 2 channels of 16 bit D/A with 13μs settling time

Since this open loop system has boundary stable dynamics i.e., the input (voice-coil current) directly affects the derivative (velocity) of the output (position), it needs to be stabilized first. This is achieved by designing a feedback controller to vary the current in the voice coil of the spool valve based on the difference between the commanded valve position *(u)* and the actual position *(y)*. The components described above form the inner loop system which is plant that needs to be controlled using the advanced tracking algorithms developed in the previous sections. Due to the presence of stiction in the spool valve, there is a small range of coil currents for which there is no response from the valve. Using a small proportional gain leads to performance degradation since the system does not respond to voice coil currents smaller than a certain magnitude. However, increasing the proportional gain leads to instability of the entire loop. Hence instead of a scalar gain, a non-linear static map as shown in Fig. 5.8(a) was used in the feedback controller.

This along with the inherent characteristics of the actuator makes the dynamics of the entire inner loop to be non-linear. However, for small amplitudes of the command signals, the response of the inner-loop can be approximated using a linear time invariant model obtained based on the frequency response of the system as shown in Fig. 5.8 *(The lack of correlation between the amplitude and phase response indicates that the behavior of the inner-loop is not perfectly linear. The model was chosen to approximate the phase response better as it is more critical for the controller performance).*

The continuous-time transfer function of the model used for the control design is given by,

$$\frac{Y(s)}{U(s)} = \frac{9.65e1s + 1.563e5}{s^2 + 4.931e2 + 1.33e5} \tag{5.1}$$

This plant model obtained is then used for the design of the time-varying internal model based controllers to track 1, 2, 3, 4& 5 harmonic signals. For the higher order controllers, the amplitudes and phases of each of the harmonics in the reference signal are adjusted to represent an actual valve profile.

Hence the output from the internal model based controller i.e., u_p is the command signal for inner loop system which is automatically generated to ensure that the actual position *(y)* tracks the reference signal *(r)*.

The inner loop controller is also implemented on the same control hardware and was found to perform satisfactorily only when sampled at atleast 5 KHz i.e., as sample time of 0.2 ms. Increasing the sample times lead to performance degradation. However, it can be seen from Fig. 5.4 that even with the all the optimization i.e., with minimal online computations, the controllers took longer to execute for the 4& 5 harmonics cases. Since all the coefficients of the internal model unit are explicitly dependent on the trajectory of the engine speed, they are computed offline for each trial and loaded into the controller before the experiment. This allowed the controller to run at much higher sample rates and thus enabled the real-time implementation.

Another observation was that, as the number of harmonics increases, the synthesis procedure using Eq. 4.30 started to become infeasible for smaller values of γ. Adding the LMIs to constrain the gains corresponding to the dynamic compensator also made it difficult to obtain feasible solutions. Hence, with the constraint of not saturating the inner loop, it was possible to synthesize controllers for the first method for signals up to 5 harmonics.

The following pages show sample tracking results for all the controllers described previously. The reference signals with amplitude between 2 mm and 3 mm were chosen for all cases to ensure that the system operation is within the linear approximation. The reference signal and the tracking error for the entire experiment are shown in the first two rows. A zoomed in portion of the signals where the tracking performance is good is also shown along with the corresponding control signal.

It can be seen that, for the lower order harmonics, the controller is able to maintain the desired tracking performance even during aggressive variation in the signal's frequency. Also, for all the cases, even when the performance deteriorates due to the unmodeled dynamics or the controller is able to maintain the stability of the overall system.

Fig. 5.10, Fig. 5.11, Fig. 5.12 and Fig. 5.13 show the tracking of a signal resembling the actual

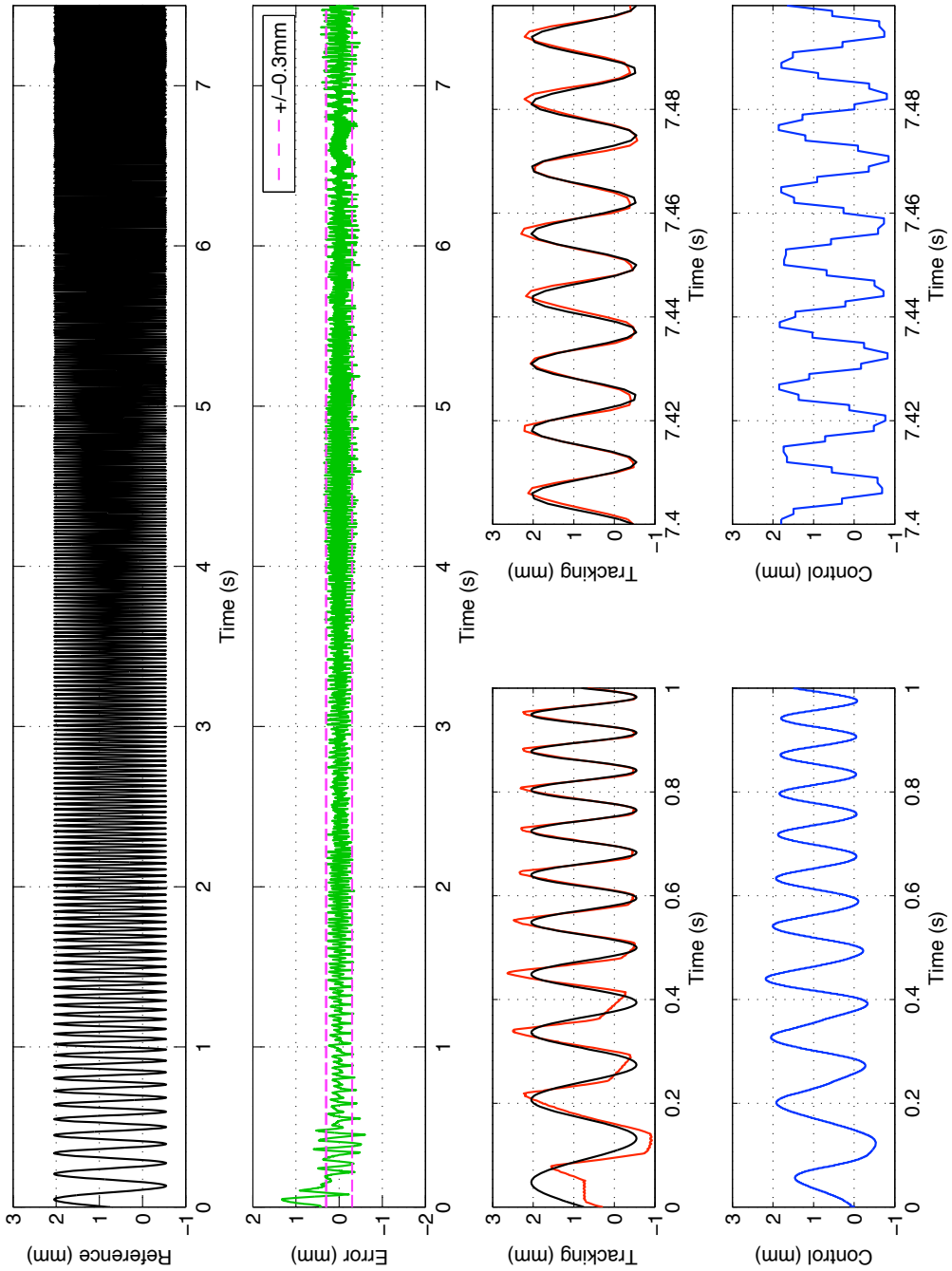

Figure 5.9: Experimental tracking results for a 1-harmonic sinusoid (5 Hz → 80 Hz @ 10Hz/s)

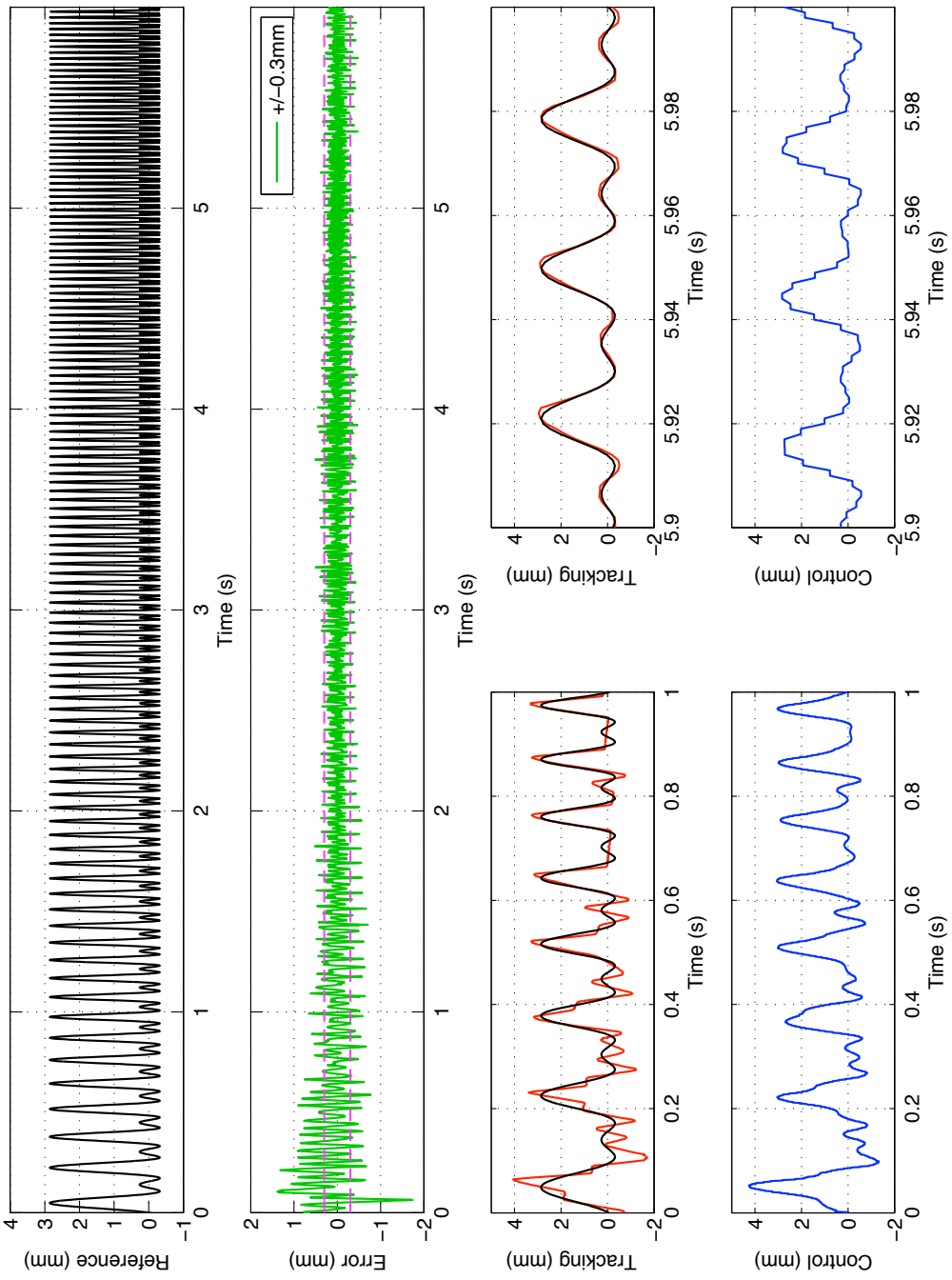

Figure 5.10: Experimental tracking results for the valve profile using a 2-harmonic sinusoid based controller (5 Hz → 35 Hz @ 5Hz/s)

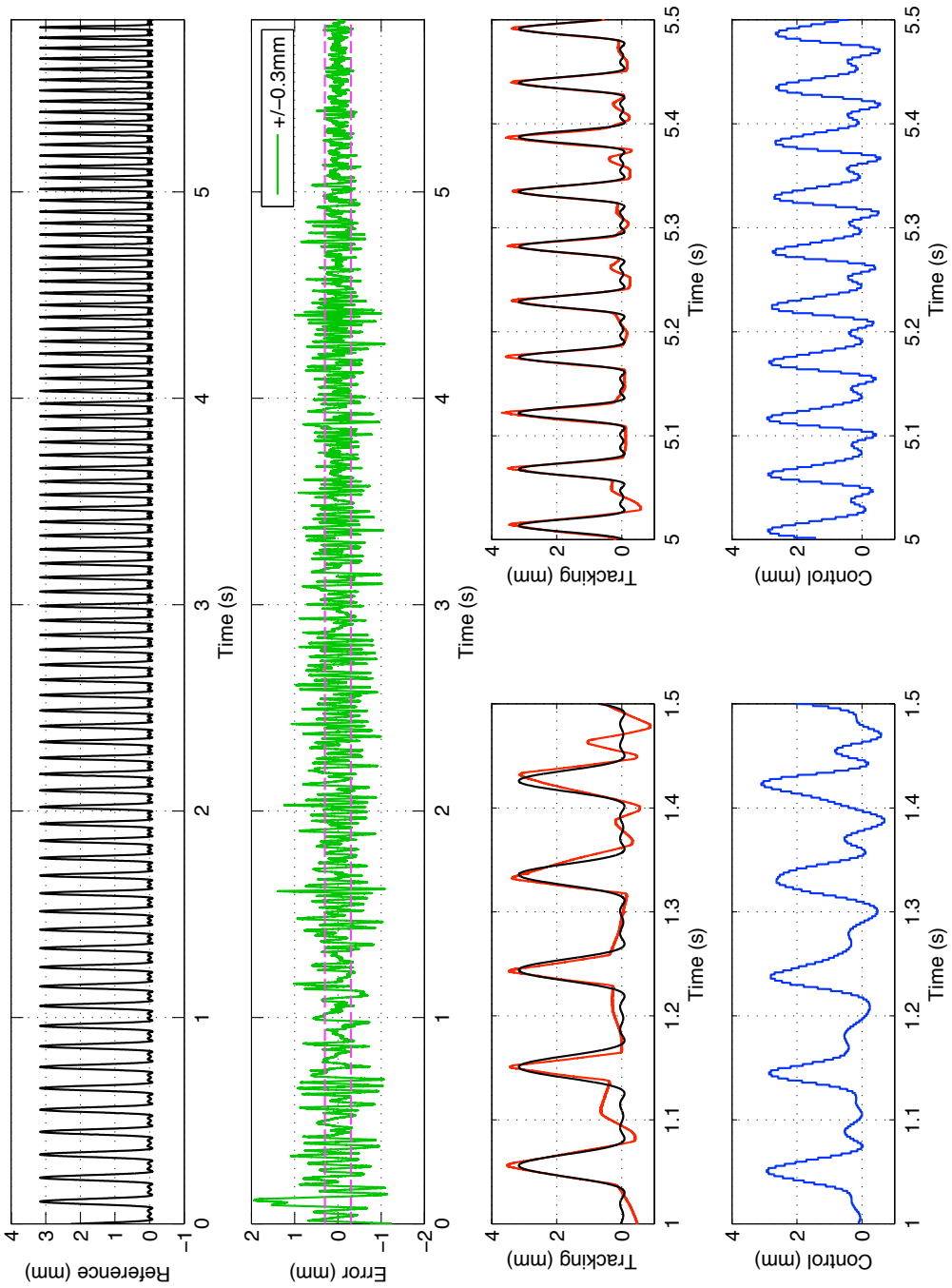

Figure 5.11: Experimental tracking results for the valve profile using a 3-harmonic sinusoid based controller (8 Hz → 20 Hz @ 2Hz/s)

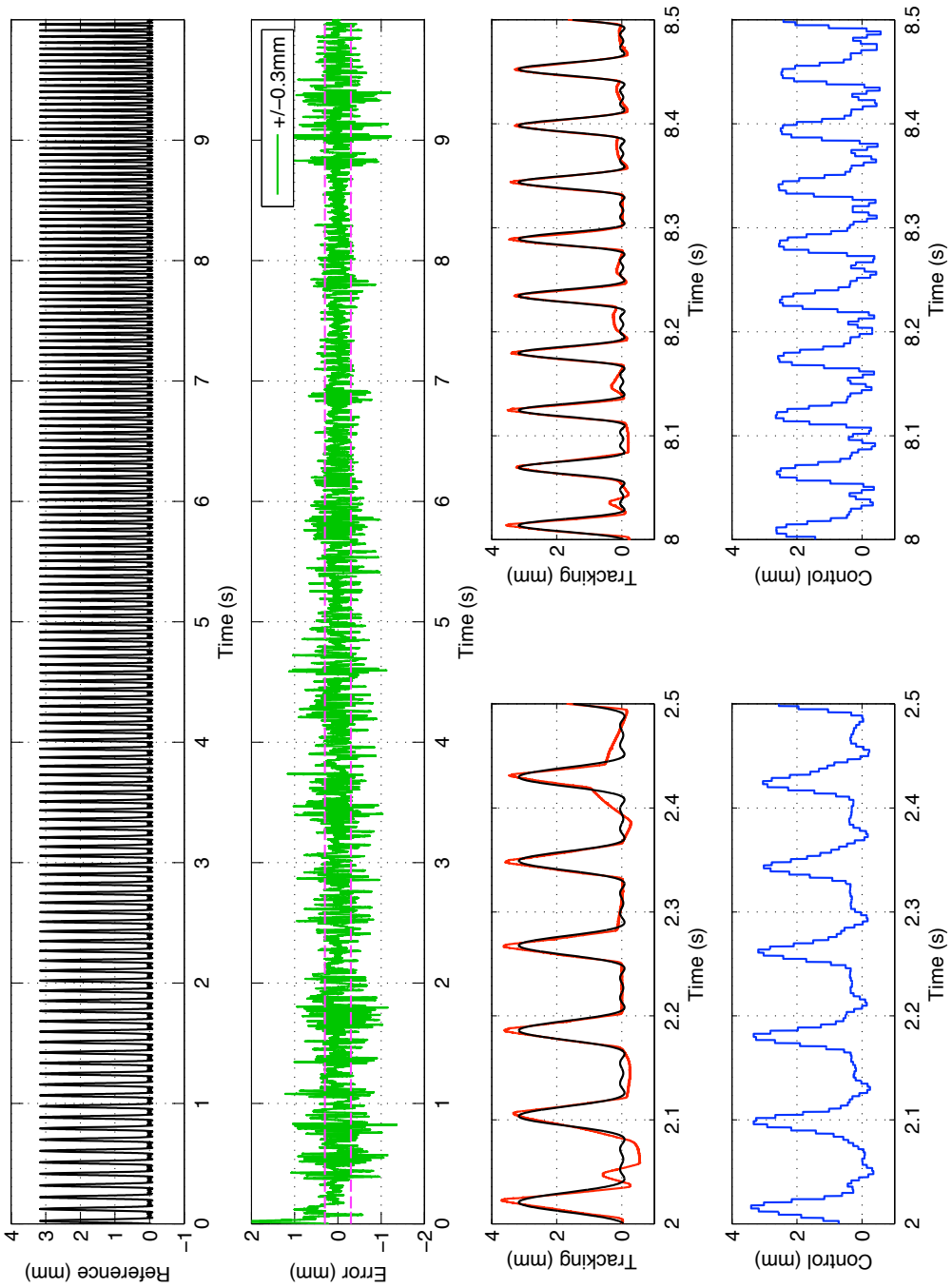

Figure 5.12: Experimental tracking results for the valve profile using a 4-harmonic sinusoid based controller (10 Hz → 20 Hz @ 1Hz/s)

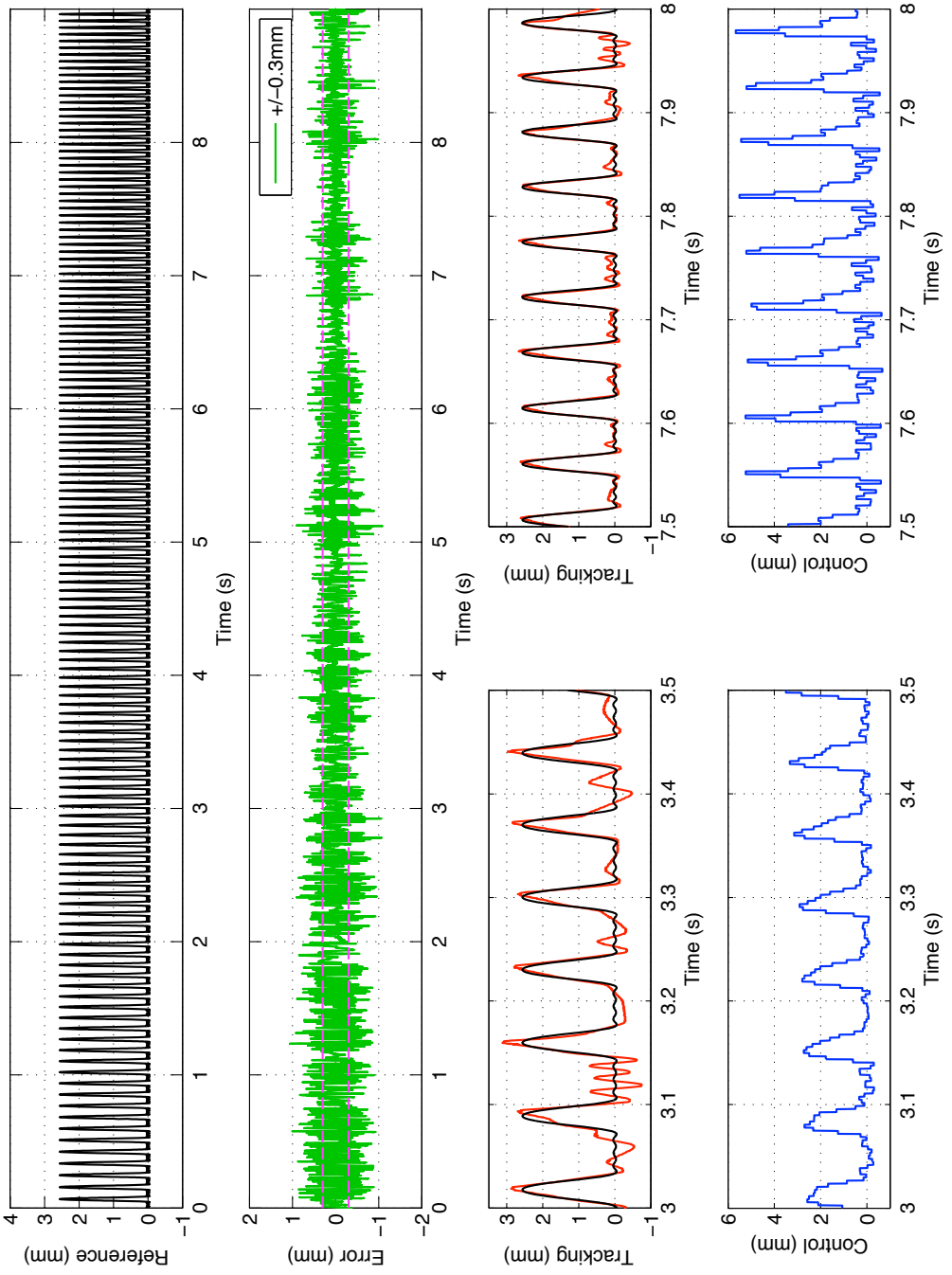

Figure 5.13: Experimental tracking results for the valve profile using a 5-harmonic sinusoid based controller (10 Hz → 20 Hz @ 1Hz/s)

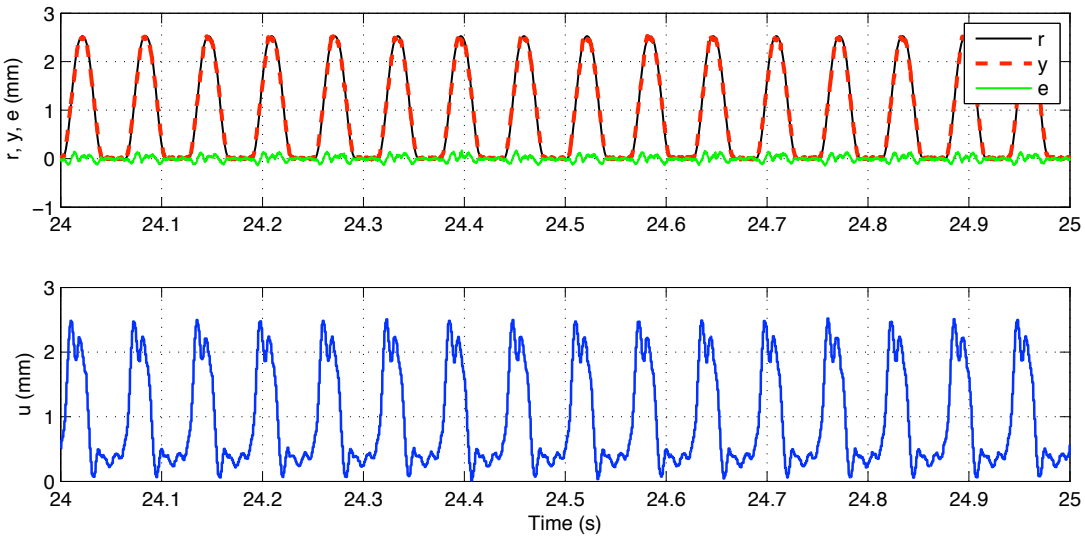

Figure 5.14: Experimental results from tracking a periodic signal (16 Hz) using an LTI Repetitive controller

valve profile using controller of higher order. It can be observed that, during a major portion of the experiment, the tracking error remains within the ± 0.3 mm bound. In the zoomed in portion corresponding to the best tracking performance, even though the overall shape of the reference and the actual output match well, there is still some persistent error at specific portions of the valve profile (especially, when the motion reverses direction) tracking error is larger.

This can be attributed to the fact that, the internal model unit is capable of generating signals with only the frequency content it is designed for. However, the slight deviations from the linear behavior of the plant could make it necessary to have a control signal with additional dynamics to ensure the required tracking performance. To illustrate this argument, Fig. 5.14 shows the results from implementing an LTI controller using $N = 128$ to track a periodic signal corresponding to a similar valve profile. The control required to minimize the tracking error is more complex than the output from the internal model controller based on several harmonics.

This suggests the use of more harmonics or Approach 2 i.e., sampling the system in the crank angle domain to improve the tracking performance. Both the alternatives require the increase in N, which motivates addressing the issues with the robust stabilizer for very high order systems. This is precisely the focus of the ongoing research effort.

5.6 Controller Simulations

5.6.1 Angle Domain Implementation

The design of the robust stabilizer based on the parameter dependent gain injection becomes challenging for higher order systems due to the dimensionality of the LMIs and the difficulty in tuning the various constraints to obtain feasible solutions i.e., gains which are robust and avoid control saturation. Hence, with the current formulation, it was possible to design controllers for generating dynamics with order at most 10. As explained in the earlier section 5.2, this is not sufficient to enable experimental investigations with the angle domain control. However simulations can used to validate some of the proposed ideas since it allows the relaxation of the design requirements (robustness - assume perfect model,control saturations - assume linear behavior even during control saturation etc).

Fig. 5.15 shows the simulation results for tracking the valve profile using a rotational angle domain controller with generating dynamics of order 10 (fixed interval sampling). It can be seen that the sparse sampling of the system leads a persistent tracking error even after the initial transients settle down and the characteristics of the control signal are also undesirable (rapid change in direction and large magnitudes). To verify if increasing the order of the generating dynamics increases the controller performance, the pole-placement based stabilizer was implemented using the variable interval sampling technique. As a comparison the results from the controller based on the time-domain sampling (harmonic approximation) for the exact same operating conditions. The frequency variation is also identical for both cases. It is interesting to note that, although the design methods for the two approaches are fundamentally different, the resulting control signals after the transients have settled down are very similar to each other.

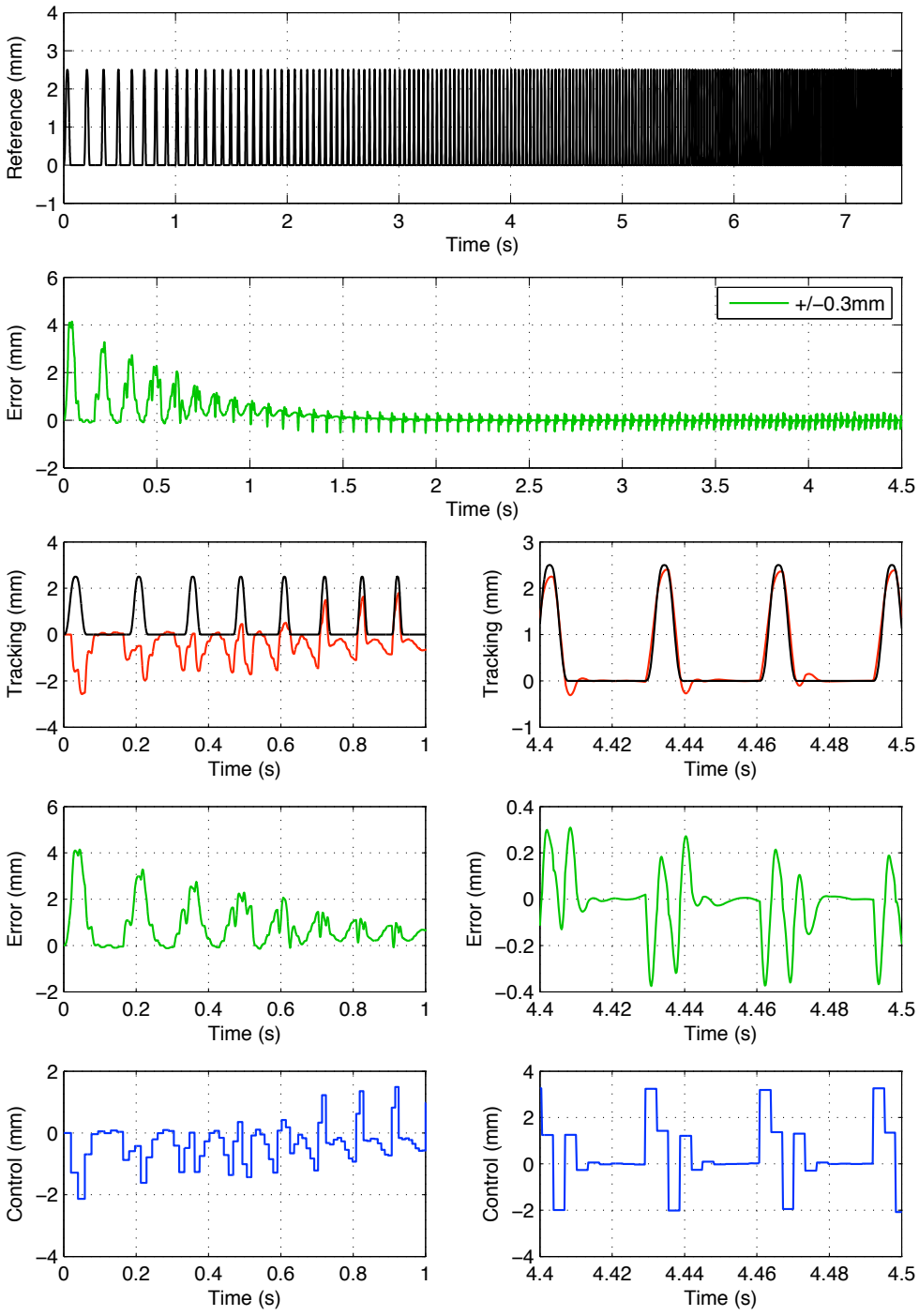

Figure 5.15: Simulations results for tracking the valve profile using 10 sample rotational angle domain controller

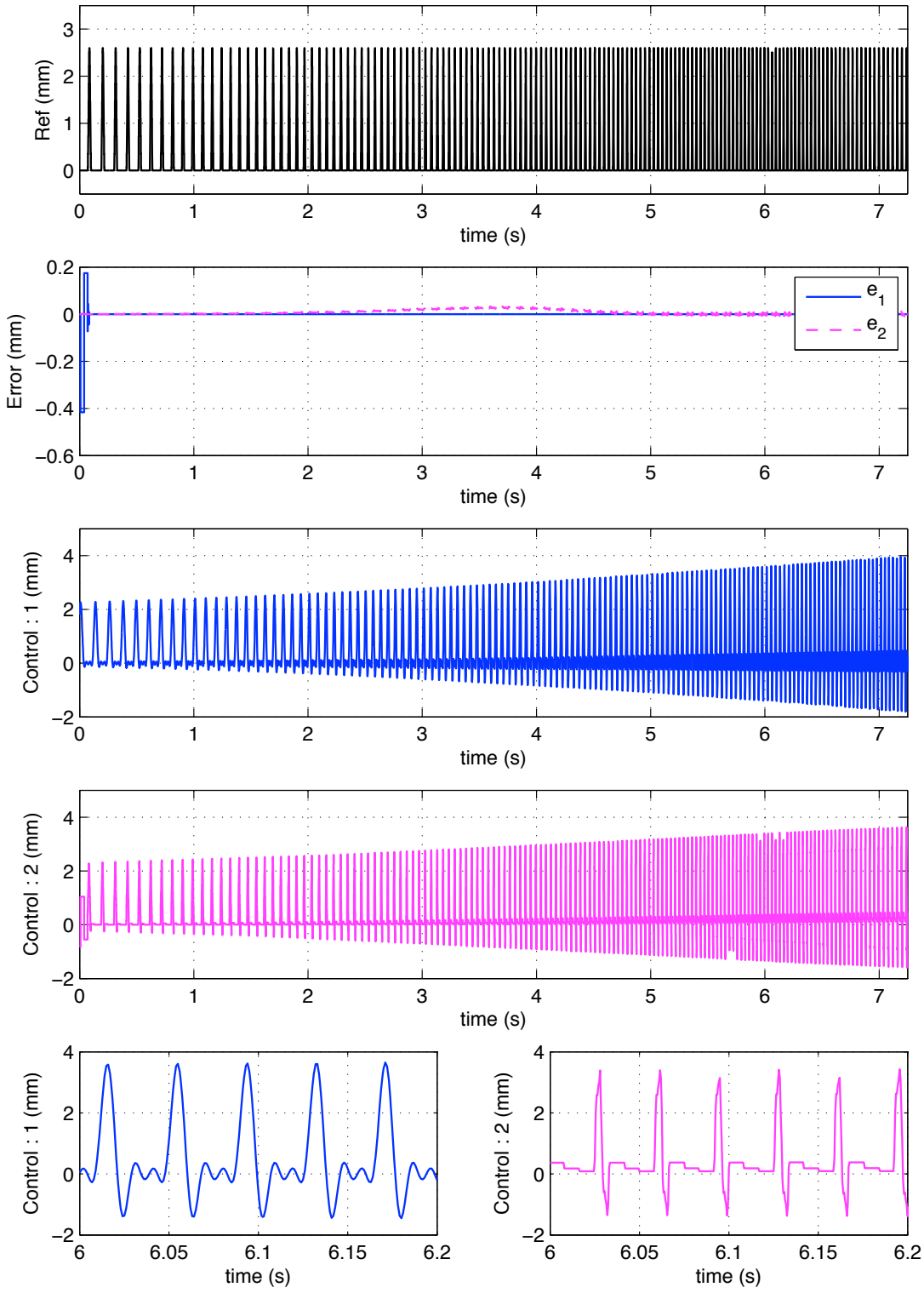

Figure 5.16: Simulation results comparing both the approaches for tracking the same signal (1 : time domain, 2 : angle domain)

5.6.2 Valve Event Transients

The performance of the controllers during valve event transients is also of interest since it is also one of the requirements of a camless actuation system. As observed previously, since the characteristics of the physical system make it difficult to reduce the tracking error bound below 0.3 mm, it is difficult to evaluate the transient performance in the experiments and thus simulation studies will be used to assess the characteristics of the controller during valve event transients. The 5 harmonics based controller is used for these investigations. Fig. 5.17 shows the performance corresponding to a step change in lift and Fig. 5.18 shows the transients during a duration change. For both the figures, the error is shown in the log scale to highlight the exponential convergence properties of the controller and it can also be seen that the control signal is also within the acceptable limits during the entire simulation.

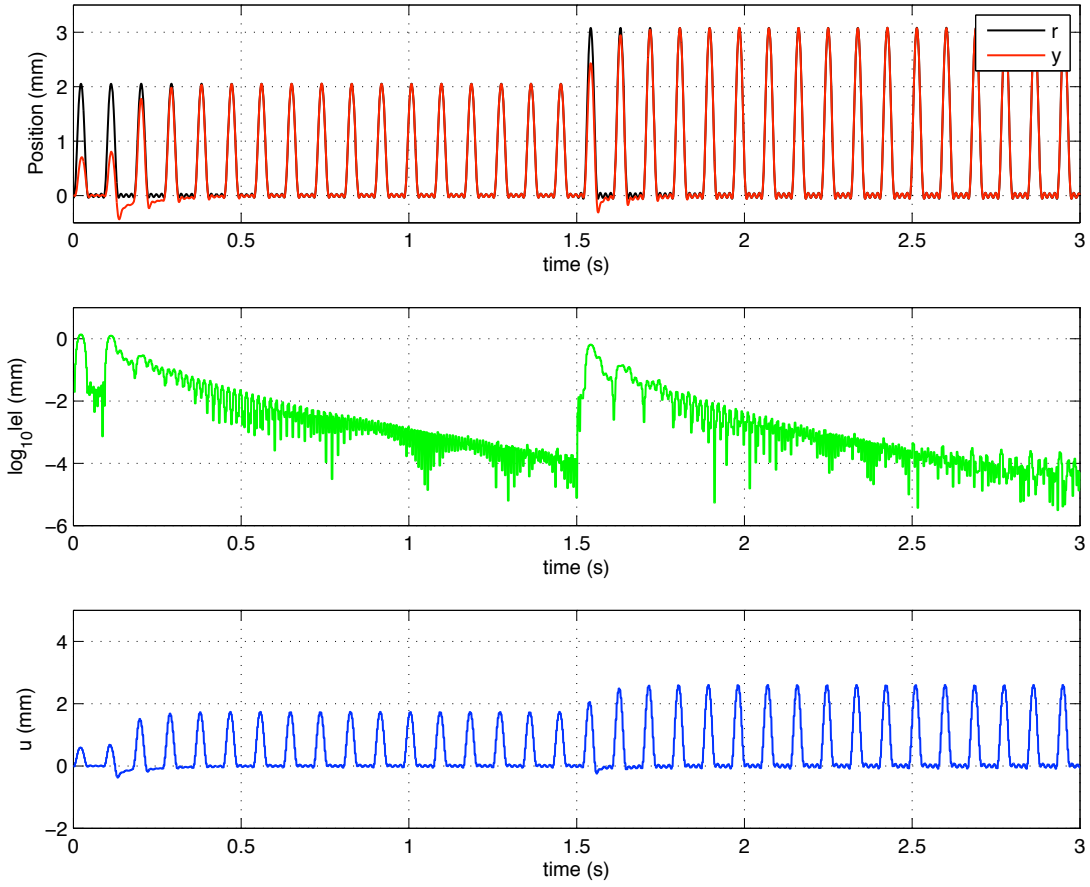

Figure 5.17: Performance of the controller during a step change in lift (2mm to 3mm) and fixed duration (360 CAD)

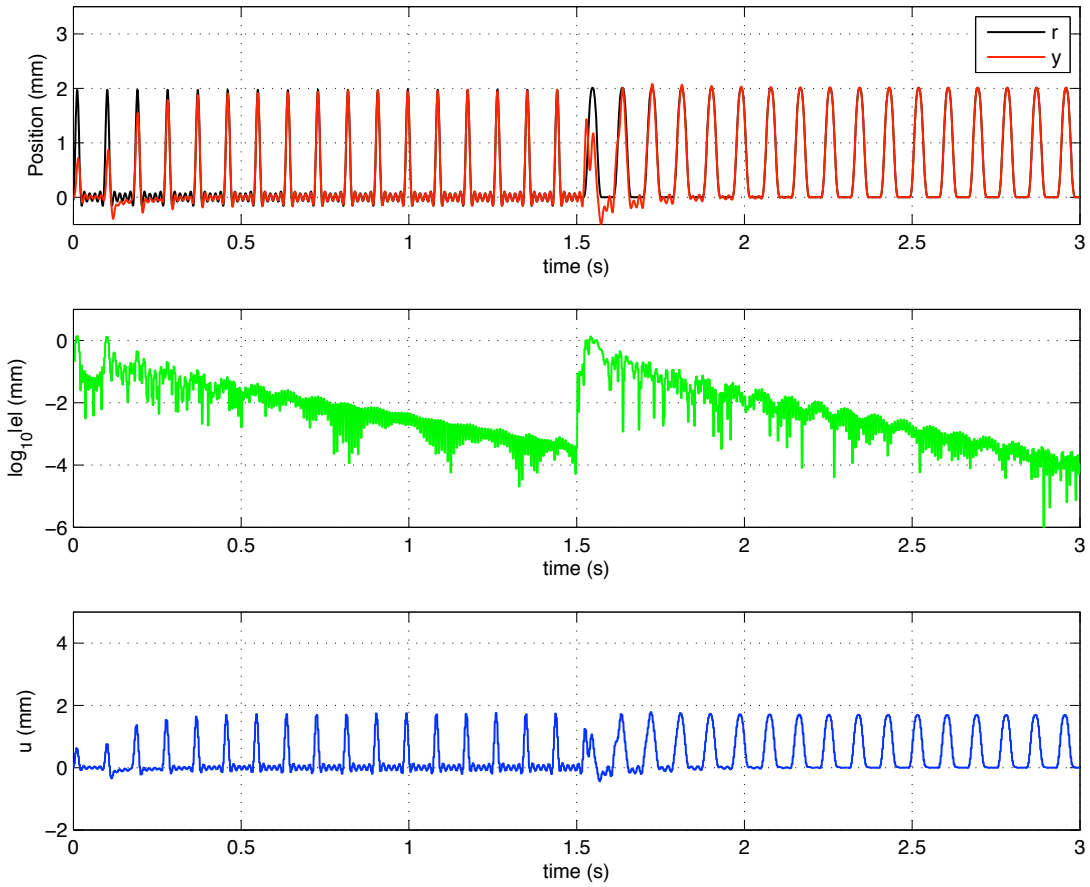

Figure 5.18: Performance of the controller during a step change in duration (180 CAD to 450 CAD) and fixed lift (2 mm)

5.7 Summary

This work explored the implementation aspects of applying the time-varying internal model based controller for camless engine valve actuation. A comparison of various implementation strategies i.e., the continuous-time vs discrete domain, time vs crank angle domain sampling has been performed and the relative merits of each approach has been documented. The current state of the art in the control design has enabled one particular realization of the controller to be implemented on the experimental hardware and helps validate the choice of this framework while motivating the requirement for higher order controllers. The future research thrust is on the theoretical developments required to extend the robust stabilizer design for very higher order systems and thus enable the experimental implementation of alternate realizations of the controller which promise to further improve the tracking performance.

References

[1] Pischinger, M., Salber, W., der Staay, F. V., Baumgarten, H., and Kemper, H., 2000. "Benefits of the electromechanical valve train in vehicle operation". *SAE Technical Paper Series*(2000-01-1223), Mar, pp. 1–13.

[2] Turner, J. W. G., Bassett, M. D., Pearson, R. J., Pitcher, G., and Douglas, K. J.", 2004.". *SAE Technical Paper Series*(2004-01-1386).

[3] Kreuter, P., Heuser, P., and Schebitz, M. "Strategies to improve si-engine performance by means of variable intake lift, timing and duration". *SAE Technical Paper Series*.

[4] Schechter, M. M., and Levin, M. B., 1996. "Camless engine". *SAE Technical Paper Series*(960581), pp. 17–31.

[5] Moriya, Y., Watanabe, A., Uda, H., Kawamura, H., and Yoshioka, M. "A newly developed intelligent variable valve timing system – continuously controlled cam phasing as applied to a new 3 liter inline 6 engine". *SAE Technical Paper Series*.

[6] Hosaka, T., and Hamazaki, M., 1991. "Development of the variable valve timing and lift (vtec) engine for the honda nsx". *SAE Technical Paper Series*(910008), Dec, pp. 1–7.

[7] Donitz, C., Vasile, I., Onder, C., and Guzzella, L., 2009. "Dynamic programming for hybrid pneumatic vehicles". *Proceedings of the 2009 American Control Conference*, Apr, pp. 3956–3963.

[8] He, X., Durrett, R. P., and Sun, Z., 2009. "Late intake valve closing as an emissions control strategy at tier 2 bin 5 engine-out nox level". *SAE Technical Paper Series*(2008-01-0637), Feb, pp. 427–443.

[9] Tai, C., Tsao, T.-C., Levin, M. B., Barta, G., and Schechter, M. M., 2003. "Using camless valvetrain for air hybrid optimization". *SAE Technical Paper Series*(2003-01-0038), Jan.

[10] Titolo, A., 1991. "The variable valve timing system - application on a v8 engine". *SAE Technical Paper Series*(910009), Oct, pp. 1–8.

[11] Steinberg, R., Lenz, I., Köehnlein, G., Scheidt, M. E., Saupe, T., and Buchinger, W., 1998. "A fully continuous variable cam timing concept for intake and exhaust phasing". *SAE Technical Paper Series*(980767), Jul, pp. 1–11.

[12] Hannibal, W., and Bertsch, A., 1998. "Vast: A new variable valve timing system for vehicle engines". *SAE Technical Paper Series*(980769), Mar, pp. 1–9.

[13] Brüstle, C., and Schwarzenthal, D., 2001. "Variocam plus – a highlight of the porsche 911 turbo engine". *SAE Technical Paper Series*(2001-01-0245), Dec.

[14] Sellnau, M., and Rask, E., 2003. "Two-step variable valve actuation for fuel economy, emissions, and performance". *SAE Technical Paper Series*(2003-01-0029), Jan.

[15] Flierl, R., and Klüting, M., 2000. "The third generation of valvetrains - new fully variable valvetrains for throttle-free load control". *SAE Technical Paper Series*(2000-01-1227), Jan, pp. 1–13.

[16] Pierik, R. J., and Burkhard, J. F., 2000. "Design and development of a mechanical variable valve actuation system". *SAE Technical Paper Series*(2000-01-1221), Feb, pp. 1–10.

[17] Fujita, T., Onogawa, K., Kiga, S., Mae, Y., Akasaka, Y., and Tomogane, K., 2008. "Development of innovative variable valve event and lift (vvel) system". *SAE Technical Paper Series*, Feb, pp. 1–11.

[18] Sun, Z., 2009. "Electrohydraulic fully flexible valve actuation system with internal feedback". *ASME Journal of Dynamic Systems, Measurement and Control,* **131**, Feb, pp. 024502 (1–8).

[19] di Gaeta, A., Glielmo, L., Giglio, V., and Police, G., 2008. "Modeling of an electromechanical engine valve actuator based on a hybrid analytical–fem approach". *IEEE/ASME Transactions on Mechatronics,* **13**(6), Nov, pp. 625–637.

[20] Hoffmann, W., Peterson, K., and Stefanopoulou, A. G., 2003. "Iterative learning control for soft landing of electromechanical valve actuator in camless engines". *IEEE Transactions on Control System Technology,* **11**(2), pp. 174–184.

[21] Picron, V., Postel, Y., Nicot, E., and Durrieu, D., 2008. "Electro-magnetic valve actuation system: First steps toward mass production". *SAE Technical Paper Series,* **Variable Valve Optimization, 2008**(2008-01-1360), Feb, pp. 1–17.

[22] Henry, R. R., 2001. "Single-cylinder engine tests of a motor-driven, variable-valve actuator". *SAE Technical Paper Series*(2001-01-0241).

[23] Parlikar, T. A., Chang, W. S., Qiu, Y. H., Seeman, M. D., Perreault, D. J., Kassakian, J. G., and Keim, T. A., 2005. "Design and experimental implementation of an electromagnetic engine valve drive". *IEEE/ASME Transactions on Mechatronics,* **10**(5), Oct, pp. 482–294.

[24] Turner, C. W., Babbitt, G. R., Balton, C. S., Raimao, M. A., and Giordano, D. D., 2004. "Design and control of a two-stage electro-hydraulic valve actuation system". *SAE Technical Paper Series*(2004-01-1265), Dec, pp. 1–14.

[25] Allen, J., and Law, D., 2002. "Production electro-hydraulic variable valve-train for a new generation of i.c. engines". *SAE Technical Paper Series*(2002-01-1109), Nov.

[26] Battistoni, M., Cristiani, M., Foschini, L., and Postrioti, L., 2007. "Development of an electro-hydraulic camless vva system". *SAE Technical Paper Series*(2007-24-0088), Jul, pp. 1–15.

[27] Denger, D., and Mischker, K., 2005. "The electro-hydraulic valvetrain system ehvs - system and potential". *2005 SAE World Congress*(2005-01-0774), Feb.

[28] Sun, Z., and He, X., 2007. "Development and control of electro-hydraulic fully flexible valve actuation system for diesel combustion research". *SAE Technical Paper Series*(2007-01-4021), Aug.

[29] Watson, J. P., and Wakeman, R. J., 2005. "Simulation of a pneumatic valve actuation system for internal combustion engine". *SAE Technical Paper Series,* **Variable Valve Actuation 2005**(2005-01-0771), Jan.

[30] Ma, J., Stuecken, T., Schock, H., Zhu, G., and Winkelman, J., 2007. "Model reference adaptive control of a pneumatic valve actuator for infinitely variable valve timing and lift". *SAE Technical Paper Series*(2007-01-1297), Feb, pp. 1–19.

[31] Ma, J., Zhu, G., Hartsig, A., and Schock, H., 2008. "Model-based predictive control of an electro-pneumatic exhaust valve for internal combustion engines". *Proceedings of the 2008 American Control Conference*, May, pp. 298–305.

[32] Trajkovic, S., Milosavljevic, A., Tunestål, P., and Johansson, B., 2006. "Fpga controlled pneumatic variable valve actuation". *SAE Technical Paper Series*(2006-01-0041), Jan.

[33] Sun, Z., 2005. "Engine valve actuator assembly with dual automatic regulation". *United States Patent,* **6959673**.

[34] Gillella, P., and Sun, Z., 2011. "Design, modeling, and control of a camless valve actuation system with internal feedback". *IEEE/ASME Transactions on Mechatronics,* **16**(3), Apr, pp. 527–539.

[35] Peterson, K. S., Grizzle, J. W., and Stefanopoulou, A. G., 2006. "Nonlinear control for magnetic levitation of automotive engine valves". *IEEE Transactions on Control System Technology,* **14**(2), Feb, pp. 346–354.

[36] Anderson, M. D., Tsao, T.-C., and Levin, M. B., 1998. "Adaptive lift control for a camless electrohydraulic valvetrain". *SAE Technical Paper Series*(981029), Jun, pp. 1–10.

[37] Sun, Z., and Kuo, T.-W., 2010. "Transient control of electro-hydraulic fully flexible engine valve actuation system". *IEEE Transactions on Control System Technology,* **18**(3), pp. 613–621.

[38] Sun, Z., Zhang, Z., and Tsao, T.-C., 2009. "Trajectory tracking and disturbance rejection for linear time-varying systems: Input/output representation". *Systems & Control Letters,* **58**(6), pp. 452 – 460.

[39] Bellman, R., and Dreyfus, S., 1962. *Applied dynamic programming.* No. v. 4.

[40] Luus, R., 1993. "Application of iterative dynamic programming to very high dimensional systems". *Hungarian Journal of Industrial Chemistry*, Oct, pp. 243–250.

[41] Luus, R., 1990. "Application of dynamic programming to high-dimensional non-linear optimal control problems". *Int. J. Control (UK),* **52**(1), pp. 239 – 250.

[42] Luus, R., 2000. *Iterative dynamic programming.*

[43] Gillella, P., and Sun, Z., 2009. "Modeling and control design of a camless valve actuation system". pp. 2696 – 2701.

[44] Amirante, R., Vescovo, G. D., and Lippolis, A., 2006. "Flow forces analysis of an open center hydraulic directional control valve sliding spool". *Energy Conversion & Management,* **47**, pp. 114 – 131.

[45] Amirante, R., Vescovo, G. D., and Lippolis, A., 2006. "Evaluation of the flow forces on an open centre directional control valve by means of a computational fluid dynamic analysis". *Energy Conversion & Management,* **47**, pp. 1748 – 1760.

[46] Amirante, R., Moscatelli, P. G., and Catalano, L. A., 2007. "Evaluation of the flow forces on a direct (single stage) proportional valve by means of a computation fluid dynamic analysis". *Energy Conversion & Management,* **48**, pp. 942–953.

[47] Yuan, Q., and Li, P. Y., 2005. "Using steady flow force for unstable valve design: Modeling and experiments". *ASME Journal of Dynamic Systems, Measurement and Control,* **127**(3), pp. 451–462.

[48] Yuan, Q., and Li, P. Y., 2007. "Robust optimal design of unstable valves". *IEEE Transactions on Control System Technology,* **15**(6), Oct, pp. 1065–1074.

[49] Manring, N. D., and Zhang, S., 2012. "Pressure transient flow forces for hydraulic spool valves". *J. Dyn. Sys., Meas., Control,* **134**(3), Jan, pp. 034501 (1–5).

[50] Viall, E. N., and Zhang, Q., 2000. "Determining the discharge coefficient of a spool valve". *Proceedings of the 2000 American Control Conference*, Mar, pp. 3600–3604.

[51] Yang, R., 2003. "Hydraulic spool valve metering notch characterization using cfd". *Proceedings of the 2003 ASME International Mechanical Engineering Congress*, Mar, pp. 11–17.

[52] Cao, M., Wang, K. W., DeVries, L., Fujii, Y., Tobler, W. E., and Pietron, G. M., 2006. "Experimental characterization and gray-box modeling of spool-type automotive variable-force-solenoid valves with circular flow ports and notches". *ASME Journal of Dynamic Systems, Measurement and Control,* **128**(3), Mar, pp. 636–654.

[53] Pan, X., Wang, G., and Lu, Z., 2011. "Flow field simulation and a flow model of servo-valve spool valve orifice". *Energy Conversion and Management,* **52**, Sep, pp. 3249–3256.

[54] Postrioti, L., Foschini, L., Battistoni, M., and Cristiani, M., 2008. "Experimental and numerical study of an electro-hydraulic camless vva system". *SAE Technical Paper Series*(2008-01-1355), Feb.

[55] Hoffmann, W., Peterson, K., and Stefanopoulou, A. G., 2003. "Iterative learning control for soft landing of electromechanical valve actuator in camless engines". *IEEE Transactions on Control System Technology,* **11**(2), Jul, pp. 174–184.

[56] Heinzen, A., Gillella, P., and Sun, Z., 2011. "Iterative learning control of a fully flexible valve actuation system for non-throttled engine load control". *Control Engineering Practice,* **19**, Oct, pp. 1490–1505.

[57] Wang, J., and Tsao, T.-C., 2004. "Repetitive control of linear time varying systems with application to electronic cam motion control". *Proceedings of the 2004 American Control Conference*, pp. 3794–3799.

[58] Liao, H.-H., Roelle, M. J., Chen, J.-S., Park, S., and Gerdes, J. C., 2011. "Implementation and analysis of a repetitive controller for an electro-hydraulic engine valve system". *IEEE Transactions on Control System Technology,* **19**(5), pp. 1102–1113.

[59] Chen, C.-L., and Chiu, G. T., 2008. "Spatially periodic disturbance rejection with spatially sampled robust repetitive control". *ASME Journal of Dynamic Systems, Measurement and Control,* **130**, pp. 021002 (1–11).

[60] Davison, E. J., 1976. "The robust control of a servomechanism problem for linear time-invariant multivariable systems". *IEEE Transactions on Automatic Control,* **21**(1), pp. 25–34.

[61] Francis, B. A., and Wonham, W. M., 1976. "The internal model principle of control theory". *Automatica,* **12**, pp. 457–465.

[62] Serrani, A., Isidori, A., and Marconi, L., 2001. "Semiglobal nonlinear output regulation with adaptive internal model". *IEEE Transactions on Automatic Control,* **46**(8), pp. 1178–1194.

[63] Zhang, Z., and Serrani, A., 2006. "The linear periodic output regulation problem". *Systems & Control Letters,* **55**(7), pp. 518 – 529.

[64] Gillella, P., and Sun, Z., 2010. "Transient control of a camless valve actuation system using a time-varying repetitive controller". *Proceedings of the 2010 ASME Dynamic Systems and Control Conference*(DSCC2010-4149), pp. 1–8.

[65] Tsakalis, K. S., and Ioannou, P. A., 1993. "Linear time varying systems : Control and adaptation". *Prentice Hall, Englewood Cliffs, NJ.*

[66] Kamen, E., Khargonekar, P. P., and Poolla, K. R., 1985. "A transfer-function approach to linear time-varying discrete-time systems". *SIAM Journal of Control and Optimization,* **23**(4), Dec, pp. 550–565.

[67] Sun, Z., 2004. "Tracking or rejecting rotational-angle dependent signals using time varying repetitive control". *Proceedings of the 2004 American Control Conference*, pp. 144–149.

[68] Song, X., Wang, Y., and Sun, Z., 2012. "Robust stabilizer design for linear time varying internal model based control". *Proceedings of the 2012 American Control Conference*, pp. 6727–6732.

[69] Song, X., Gillella, P., and Sun, Z., 2012. "Robust stabilization of discrete linear time varying internal model based system". *Proceedings of the 2012 ASME Dynamic Systems and Control Conference.*

[70] Song, X., Gillella, P., and Sun, Z. "A new stabilizer for ltv internal model based system and its application to camless engine valve actuation". *2013 American Control Conference (Submitted)*.

[71] Daafouz, J., and Bernussou, J., 2001. "Parameter dependent lyapunov functions for discrete time systems with time varying parametric uncertainties". *Systems & Control Letters,* **43**, Jul, pp. 355–359.

[72] Silverman, L. M., 1966. "Transformation of time-variable systems to canonical (phase-variable) form". *IEEE Transactions on Automatic Control,* **11**, Apr, pp. 300–303.

[73] Ramaswami, B., and Ramar, K., 1969. "On the transformation of time-variable systems to the phase-variable canonical form". *IEEE Transactions on Automatic Control,* **14**, Aug, pp. 417–419.

Appendix A

Input/Output Representations (Time-varying systems)

This section presents the details of the procedure required for transforming general time-varying systems to certain specific observer canonical forms as required for the implementation of the time-varying internal model based controller. A method for converting continuous linear time-varying systems to the controllable canonical form was first presented in [72] and later simplified in [73]. In this section, the procedure is modified and adapted to convert a system in a general linear time varying state space form to the observable canonical forms which can then be used to obtain the required I/O representations.

A.1 Continuous-time domain

Given a continuous linear time-varying system in the general state space representation as shown below,

$$\begin{aligned} \dot{x}(t) &= A(t)x(t) + B(t)u(t) \\ y(t) &= Cx(t) \end{aligned} \tag{A.1}$$

where,

$$A(t) = \begin{bmatrix} a_{11}(t) & a_{12}(t) & ... & a_{1n}(t) \\ a_{21}(t) & a_{22}(t) & ... & a_{2n}(t) \\ : & : & ... & : \\ a_{n1}(t) & a_{n2}(t) & ... & a_{nn}(t) \end{bmatrix}, B(t) = \begin{bmatrix} b_1(t) \\ b_2(t) \\ : \\ b_n(t) \end{bmatrix}$$

$$C(t) = \begin{bmatrix} c_1(t), & c_2(t), & ... & , c_n(t) \end{bmatrix}$$

We need to find a matrix $P(t)$ in order to transform the system into the observer canonical form as shown in Eq. A.3.

$$\tilde{x}(t) = P(t)x(t) \tag{A.2}$$

$$\begin{aligned} \dot{\tilde{x}}(t) &= A_o(t)\tilde{x}(t) + B_o(t) \\ y(t) &= C_o\tilde{x}(t) \end{aligned} \tag{A.3}$$

where,

$$A_o(t) = \begin{bmatrix} -\tilde{a}_{n-1}(t) & 1 & 0 & ... & 0 & 0 \\ -\tilde{a}_{n-2}(t) & 0 & 1 & ... & 0 & 0 \\ : & : & : & ... & : & : \\ -\tilde{a}_1(t) & 0 & 0 & ... & 1 & 0 \\ -\tilde{a}_0(t) & 0 & 0 & ... & 0 & 0 \end{bmatrix}$$

$$B_o(t) = \begin{bmatrix} \tilde{b}_{n-1}(t) \\ : \\ : \\ \tilde{b}_1(t) \\ \tilde{b}_0(t) \end{bmatrix}, C_o(t) = \begin{bmatrix} 1 & 0 & ... & 0 \end{bmatrix}$$

To derive the relationship between the two systems and the transformation matrix, we start with Eq. A.2. Since all the matrices are time-varying, we drop the trailing "(t)" for all the matrices for

the sake of clarity.

$$\begin{aligned}
\tilde{x}(t) &= Px(t) \\
\dot{\tilde{x}}(t) &= \dot{P}x(t) + P\dot{x}(t) \\
\dot{\tilde{x}}(t) &= \dot{P}x(t) + P\left[Ax(t) + Bu(t)\right] \\
\dot{\tilde{x}}(t) &= \dot{P}P^{-1}\tilde{x}(t) + P\left[AP^{-1}\tilde{x}(t) + B(t)u(t)\right]
\end{aligned}$$

$$\begin{aligned}
\dot{\tilde{x}}(t) &= \underbrace{\left[PA + \dot{P}\right]P^{-1}}_{A_o}\tilde{x}(t) + \underbrace{PB}_{B_o}u(t) \\
y(t) &= \underbrace{CP^{-1}}_{C_o}\tilde{x}(t)
\end{aligned} \tag{A.4}$$

Hence, $A_o = (PA + \dot{P})P^{-1}$, $B_o = PB$, $C_o = CP^{-1}$. By defining $Q = P^{-1}$, we have

$$\begin{aligned}
A_o &= (Q^{-1}A + \dot{Q}^{-1})Q \\
&= Q^{-1}AQ + \dot{Q}^{-1}Q
\end{aligned} \tag{A.5}$$

To proceed further, we make use of the following identity,

$$\begin{aligned}
Q^{-1}Q &= I \\
\frac{d}{dt}\left(Q^{-1}Q\right) &= \frac{d}{dt}\left(I\right) \\
Q^{-1}\dot{Q} + \dot{Q}^{-1}Q &= 0 \\
\Rightarrow Q^{-1}\dot{Q} &= -\dot{Q}^{-1}Q
\end{aligned} \tag{A.6}$$

Hence combining Eq. A.5 and Eq. A.6, we get

$$\begin{aligned}
A_o &= Q^{-1}AQ - Q^{-1}\dot{Q} \\
&= Q^{-1}\left[AQ - \dot{Q}\right] \\
\Rightarrow QA_o &= AQ - \dot{Q}
\end{aligned} \tag{A.7}$$

Utilizing the special structure of the matrix A_o, and defining q_1, q_2, ... etc as the columns of Q,

Eq. A.7 can be written as,

$$\begin{aligned} q_1 &= Aq_2 - \dot{q}_2 \\ q_2 &= Aq_3 - \dot{q}_3 \\ &\vdots \\ &\vdots \\ q_{n-1} &= Aq_n - \dot{q}_n \end{aligned} \tag{A.8}$$

Hence, it can be seen that, with the knowledge of the last column of Q i.e., q_n, the remaining columns can be computed recursively using the expressions shown above. Next, we introduce the steps necessary for calculating q_n. From Eq. A.3 and Eq. A.4, we get

$$\begin{aligned} C_o &= \begin{pmatrix} 1 & 0 & ... & 0 & 0 \end{pmatrix} \\ &= CP^{-1} \\ &= CQ \end{aligned} \tag{A.9}$$

Using $Cq_n = 0$ and letting $\eta_n = C$, we get

$$\eta_n q_n = 0$$

Using $Cq_{n-1} = 0$, Eq. A.8 and an identity similar to A.6, we get

$$\begin{aligned} C\left[Aq_n - \dot{q}_n\right] &= CAq_n - C\dot{q}_n \\ &= CAq_n + \dot{C}q_n \\ \Rightarrow &= \underbrace{\left[\eta_n A + \dot{\eta}_n\right]}_{\eta_{n-1}} q_n = 0 \end{aligned}$$

Using $Cq_{n-2} = 0$ and assigning $\eta_{n-2} = \eta_{n-1}A + \dot{\eta}_{n-1}$, we get $\eta_{n-2}q_n = 0$. Proceeding in a similar fashion, we finally obtain $\eta_1 q_n = 1$. Combining all the above equations, we obtain an expression

which can be used to calculate q_n i.e., the last column of matrix Q.

$$q_n = \begin{bmatrix} \eta_1(t) \\ \eta_2(t) \\ : \\ \eta_{n-1}(t) \\ \eta_n(t) \end{bmatrix}^{-1} \begin{bmatrix} 1 \\ 0 \\ : \\ 0 \\ 0 \end{bmatrix} \tag{A.10}$$

where, each of the ηs are calculated using the recursive relation, $\eta_{m-1} = \eta_m A + \dot{\eta}_m$ starting with $\eta_n = C$. The q_n obtained can be used along with Eq. A.8 to compute all the entries in the matrix Q which can then be used to obtain the require transformation matrix $P = Q^{-1}$. The transformation matrix can then be used along with the expressions in Eq. A.4 to obtain state space representation of the system in the observer canonical form.

A.2 Discrete domain

Consider a discrete linear time varying system as shown in (4.10) where,

$$A(k) = \begin{bmatrix} a_{11}(k) & a_{12}(k) & .... & a_{1n}(k) \\ a_{21}(k) & a_{22}(k) & .... & a_{2n}(k) \\ : & : & .... & : \\ a_{n1}(k) & a_{n2}(k) & .... & a_{nn}(k) \end{bmatrix}, B(k) = \begin{bmatrix} b_1(k) \\ b_2(k) \\ : \\ b_n(k) \end{bmatrix} \tag{A.11}$$

$$C(k) = \begin{bmatrix} c_1(k), & c_2(k), & .... & c_n(k) \end{bmatrix}$$

We need to find a transformation $\tilde{x}(k) = P(k)x(k)$ to represent the system in the observable canonical form,

$$\begin{aligned} \tilde{x}(k+1) &= A_o(k)\tilde{x}(k) + B_o(k)u(k) \\ y(k) &= C_o(k)\tilde{x}(k) \end{aligned} \tag{A.12}$$

$$A_o(k) = \begin{bmatrix} -\alpha_1(k) & 1 & 0 & .... & 0 & 0 \\ -\alpha_2(k) & 0 & 1 & .... & 0 & 0 \\ : & : & : & .... & : & 1 \\ -\alpha_n(k) & 0 & 0 & .... & 0 & 0 \end{bmatrix}, B_o(k) = \begin{bmatrix} \beta_1(k) \\ \beta_2(k) \\ : \\ \beta_n(k) \end{bmatrix} \tag{A.13}$$

$$C_o(k) = \begin{bmatrix} 1, & 0, & 0, & .... & 0 \end{bmatrix}$$

To find the relationship between A, B, C and A_o, B_o, C_o, note that

$$x(k) = P^{-1}(k)\tilde{x}(k)$$
$$x(k+1) = P^{-1}(k+1)\tilde{x}(k+1)$$

Substituting this into (4.10), we get

$$\begin{aligned} P^{-1}(k+1)\tilde{x}(k+1) &= A(k)P^{-1}(k)\tilde{x}(k) + B(k)u(k) \\ \tilde{x}(k+1) &= \underbrace{P(k+1)A(k)P^{-1}(k)}_{A_o(k)}\tilde{x}(k) + \underbrace{P(k+1)B(k)}_{B_o(k)}u(k) \\ y(k) &= \underbrace{C(k)P^{-1}(k)}_{C_o(k)}\tilde{x}(k) \end{aligned} \tag{A.14}$$

We need to find $P(*)$ such that it satisfies all the above conditions. Let $Q(*) = P^{-1}(*)$ and let $Q_1, Q_2, ...Q_n$ be the columns of Q. Substituting this into (A.14), we get

$$\begin{aligned} C(k)Q(k) &= C_o(k) \\ C(k)\begin{bmatrix} Q_1(k) & Q_2(k) & .... & Q_n(k) \end{bmatrix} &= \begin{bmatrix} 1, & 0, & .... & 0 \end{bmatrix} \\ &\Downarrow \\ C(k)Q_1(k) &= 1 \\ C(k)Q_2(k) &= 0 \\ &: \\ C(k)Q_n(k) &= 0 \end{aligned} \tag{A.15}$$

Again from (A.14), we have

$$\begin{aligned} A_o(k) &= P(k+1)A(k)P^{-1}(k) \\ A_o(k)P(k) &= P(k+1)A(k) \\ [A_o(k)P(k)]^{-1} &= [P(k+1)A(k)]^{-1} \\ P^{-1}(k)A_o^{-1}(k) &= A^{-1}(k)P^{-1}(k+1) \\ Q(k)A_o^{-1}(k) &= A^{-1}(k)Q(k+1) \end{aligned} \tag{A.16}$$

Substituting the value of $A_o(k)$ from (A.13), we get

$$Q(k)\begin{bmatrix} 0 & 0 & 0 & .... & 0 & -(1/\alpha_n(k)) \\ 1 & 0 & 0 & .... & 0 & -(\alpha_1(k)/\alpha_n(k)) \\ : & : & : & .... & : & : \\ : & : & : & .... & : & -(\alpha_{n-2}(k)/\alpha_n(k)) \\ 0 & 0 & 0 & .... & 1 & -(\alpha_{n-1}(k)/\alpha_n(k)) \end{bmatrix} = A^{-1}(k)Q(k+1) \tag{A.17}$$

Using the above equation and the definitions of $Q_1, Q_2, ...Q_n$, we get

$$\begin{aligned} Q_2(k) &= A^{-1}(k)Q_1(k+1) \\ Q_3(k) &= A^{-1}(k)Q_2(k+1) \\ &= A^{-1}(k)A^{-1}(k+1)Q_1(k+2) \\ Q_4(k) &= A^{-1}(k)Q_3(k+1) \\ &= A^{-1}(k)A^{-1}(k+1)A^{-1}(k+2)Q_1(k+3) \\ &: \\ Q_n(k) &= A^{-1}(k)A^{-1}(k+1)...A^{-1}(k+n-2)Q_1(k+n-1) \end{aligned} \tag{A.18}$$

shifting the indices, we get

$$\begin{aligned} Q_2(k-1) &= A^{-1}(k-1)Q_1(k) \\ Q_3(k-2) &= A^{-1}(k-2)A^{-1}(k-1)Q_1(k) \\ Q_4(k-3) &= A^{-1}(k-3)A^{-1}(k-2)A^{-1}(k-1)Q_1(k) \\ &: \\ Q_n(k-n+1) &= A^{-1}(k-n+1)...A^{-1}(k-2)A^{-1}(k-1)Q_1(k) \end{aligned} \tag{A.19}$$

Using (A.15), we can rewrite the above equation as,

$$\begin{aligned}
1 &= C(k)Q_1(k) \\
0 &= C(k-1)A^{-1}(k-1)Q_1(k) \\
0 &= C(k-2)A^{-1}(k-2)A^{-1}(k-1)Q_1(k) \\
0 &= C(k-3)A^{-1}(k-3)A^{-1}(k-2)A^{-1}(k-1)Q_1(k) \\
&\vdots \\
0 &= C(k-n+1)A^{-1}(k-n+1)...A^{-1}(k-2)A^{-1}(k-1)Q_1(k)
\end{aligned} \tag{A.20}$$

The above equation can be compactly written in matrix form as follows,

$$Q_1(k) = \underbrace{\begin{bmatrix} C(k) \\ C(k-1)A^{-1}(k-1) \\ C(k-2)A^{-1}(k-2)A^{-1}(k-1) \\ C(k-3)A^{-1}(k-3)A^{-1}(k-2)A^{-1}(k-1) \\ \vdots \\ C(k-n+1)A^{-1}(k-n+1)...A^{-1}(k-2)A^{-1}(k-1) \end{bmatrix}}_{\mathcal{O}(k,k-n)}^{-1} \begin{bmatrix} 1 \\ 0 \\ 0 \\ 0 \\ \vdots \\ 0 \end{bmatrix} \tag{A.21}$$

Since A_c corresponds to a continuous time model of a physical system, $A^{-1}(k)$ exists for each time step. (A.21) has a unique solution if the matrix $\mathcal{O}(k, k-n)$ is non-singular. Using the above equation and by manipulating the indices, we can then calculate $Q_1(k+1), Q_1(k+2), ..., Q_1(k+n-1)$, which together with (A.18) can be used to calculate $Q_2(k), Q_3(k), ..., Q_n(k)$. The required transformation matrix $P(k)$ is as follows,

$$P(k) = \begin{bmatrix} Q_1(k), & Q_2(k), & Q_3(k), & ..... & Q_n(k) \end{bmatrix}^{-1}$$

Similarly, by manipulating the indices, we can calculate $P(k+1)$ which can then be used in (A.14) to calculate the system matrices in the observable canonical form.